THE ASTROPHYSICAL JOURNAL, 463:26–59, 1996 May 20

THE EXTRAGALACTIC DISTANCE SCALE KEY PROJECT. III. THE DISCOVERY OF CEPHEIDS AND A NEW DISTANCE TO M101 USING THE *HUBBLE SPACE TELESCOPE*

DANIEL D. KELSON,[1] GARTH D. ILLINGWORTH,[1] WENDY F. FREEDMAN,[2] JOHN A. GRAHAM,[3] ROBERT HILL,[2] BARRY F. MADORE,[4] ABHIJIT SAHA,[5] PETER B. STETSON,[6] ROBERT C. KENNICUTT JR.,[7] JEREMY R. MOULD,[8] SHAUN M. HUGHES,[9] LAURA FERRARESE,[5,10] RANDY PHELPS,[2] ANNE TURNER,[7] KEM H. COOK,[11] HOLLAND FORD,[5,10] JOHN G. HOESSEL,[12] AND JOHN HUCHRA[13]

Received 1995 January 13; accepted 1995 December 4

ABSTRACT

We report on the discovery of 29 Cepheid variables in the galaxy M101 using the original Wide Field Camera (WFC) and the new Wide Field and Planetary Camera 2 (WFPC2) on the *Hubble Space Telescope*. We observed a field in M101 at 17 independent epochs in V (F555W), five epochs in I (F785LP/F814W), and one epoch in B (F439W), with a time interval baseline of 381 days. We have found Cepheids with periods ranging from 10 to 60 days. The data have been calibrated using WFPC2 observations with zero points derived from ω Cen, Pal 4, and NGC 2419 observations. This calibration has been verified by using the Medium Deep Survey (MDS) WFC photometric zero points, and ground-based secondary standards in V and I. The V calibrations agree to ± 0.06 mag, and the I calibrations agree to ± 0.04 mag. We have constructed V and I period-luminosity (PL) relations and have derived apparent distance moduli based on a distance modulus for the Large Magellanic Cloud (LMC) of 18.50 mag and a reddening of $E(B-V) = 0.10$ mag to the LMC Cepheids. Period-residual minimization was used to minimize the effects of Malmquist bias on the period-luminosity relation fitting process. Using a Galactic extinction law and the apparent V and I distance moduli, we have found a mean reddening for the M101 sample of $E(B-V) = 0.03$ mag and a true distance modulus to M101 of 29.34 ± 0.17 mag, corresponding to a distance of 7.4 ± 0.6 Mpc. The sources of error have been rigorously tracked through an error budget; systematic and random errors contribute roughly equally to the quoted error. The mean gas-phase metal abundances in the LMC and in the M101 outer field are similar so we expect metallicity effects to be minimal. These Cepheids will be used in conjunction with results from a Key Project search for Cepheids in an inner field, where the metallicity is larger by a factor of 5, to probe the effects of abundance on the Cepheid period-luminosity relation.

Subject headings: Cepheids — distance scale — galaxies: distances and redshifts — galaxies: individual (M101)

1. INTRODUCTION

The goal of the *Hubble Space Telescope* (*HST*) Key Project on the Extragalactic Distance Scale is to provide a global value of the Hubble constant accurate to 10% (Kennicutt, Freedman, & Mould 1995).

Since much of the controversy over the Hubble constant (H_0) arises from disagreements over distance indicators (see, for example, Jacoby et al. 1992; Sandage 1993; Fukugita, Hogan, & Peebles 1993; and other reviews), a concerted effort is required to define zero points for a number of independent secondary distance indicators. These include the Tully-Fisher relation, the planetary-nebula luminosity function, surface brightness fluctuations, and methods based on supernovae. By calibrating these distance indicators, and understanding their systematic differences, the Key Project can then measure distances out to where the Hubble flow is expected to dominate over local velocity perturbations. Results from M81, the first galaxy to be studied with the original Wide Field Planetary Camera (WF/PC), have already been published (Freedman et al. 1994a; Hughes et al. 1994). M101 was the second and final galaxy to be observed for our program with the original Wide Field Camera (WFC). Results from M100, the first galaxy studied with the new Wide Field and Planetary Camera (WFPC2), have now been published (Freedman et al. 1994b), as has a discussion of the implications of these results for H_0 (Mould et al. 1995). The more distant galaxies in the *HST* Key Project sample that were deferred due to the primary mirror's spherical aberration are now being studied.

[1] UCO/Lick Observatory, University of California, Santa Cruz, CA 95064.
[2] Carnegie Observatories, 813 Santa Barbara Street, Pasadena, CA 91101.
[3] Department of Terrestrial Magnetism, Carnegie Institution of Washington, 5241 Broad Branch Road NW, Washington, DC 20015.
[4] NASA/IPAC Extragalactic Database, Infrared Processing and Analysis Center, Jet Propulsion Laboratory, California Institute of Technology, Pasadena, CA 91125.
[5] Space Telescope Institute, Homewood Campus, Baltimore, MD 21218.
[6] Dominion Astrophysical Observatory, National Research Council, 5071 West Saanich Road, Victoria, BC, Canada V8X 4M6.
[7] Steward Observatory, University of Arizona, Tucson, AZ 85721.
[8] Mt. Stromlo and Siding Springs Observatories, Private Bag, Weston Creek Post Office ACT 2611, Australia.
[9] Royal Greenwich Observatory, Madingley Road, Cambridge, UK CB3 0EZ.
[10] Department of Physics and Astronomy, Bloomberg 501, Johns Hopkins University, 3400 North Charles Street, Baltimore, MD 21218.
[11] Lawrence Livermore National Laboratory, MS L-401, P.O. Box 808, Livermore, CA 94550.
[12] Department of Astronomy, University of Wisconsin, 475 North Charter Street, Madison, WI 53706.
[13] Harvard-Smithsonian, Center for Astrophysics, 60 Garden Street, Cambridge, MA 02138.

Further discussion of the results and goals of the program can be found in the review by Kennicutt et al. (1995).

M101 is located at $\alpha_{2000} = 14^h03^m$, $\delta_{2000} = 54°21'$, ($l = 102°$, $b = 60°$). It is a luminous Sc spiral with morphological type SAB(rs)cd (de Vaucouleurs et al. 1991). As a face-on, grand-design spiral, M101 has been widely used for the study of spiral structure (Elmegreen, Elmegreen, & Montenegro 1992; and others). It also has a substantial metallicity gradient (see Shields & Searle 1978; Scowen, Dufour, & Hester 1992; Zaritsky, Elston, & Hill 1990; Zaritsky, Kennicutt, & Huchra 1994). Two fields have been observed in M101, one at a radius of 1'.7 using the WFPC2, and the one presented here, 7'.9 from the center. The goal is to establish the effects of metallicity on the period-luminosity relation. The metallicity difference is about a factor of 4–5, with the outer field H II regions comparable to those of the LMC [i.e., $(12 + \log O/H)_{M101} = 8.37 \pm 0.15$ and $(12 + \log O/H)_{LMC} = 8.30$; Zaritsky et al. 1994; Westerlund 1990]. Only the outer field was observed before the *HST* refurbishment mission, because crowding and the poor WFC point-spread function (PSF) would have seriously compromised photometry in the inner field.

Previously estimated distances to M101 range from roughly 5 to 8 Mpc, although these estimates largely fall into two extremes. Selected distances for M101 are listed in Table 1 (see also the review of distances to nearby galaxies by de Vaucouleurs 1993). The earliest determination, of 28.71 mag, is from (de Vaucouleurs 1975), based on an estimate to the distance of the M101 group itself. In contrast, Sandage & Tammann (1974) determined a distance modulus of 29.3 mag. Cook, Aaronson, & Illingworth (1986) discovered two Cepheids in M101 using *R*-band CCD images obtained at the KPNO 4 m telescope. They found a relative M101-LMC distance modulus of 10.8 mag Citing the debate over the LMC true distance modulus, they argued that a reasonable range for the M101 distance modulus is $29.0 \lesssim (m - M) \lesssim 29.5$ mag. More recently, those data have been extended and include two more Cepheids, and several Mira variables (Alves & Cook 1995); using a distance modulus of 18.4 mag for the LMC, they claim a distance modulus to M101 of 29.08 ± 0.13 mag (we discuss this result in more detail in § 8). Cohen (1993) discovered two more Cepheids in Thuan-Gunn g CCD images taken at the Hale 200 inch (5.08 m) telescope.

The Type II supernova 1970G, in M101, has been used by Schmidt, Kirshner, & Eastman (1992) to derive a distance of $7.6^{+1.0}_{-2.2}$ Mpc, or $(m - M) \approx 29.4$ mag from the expanding photosphere method (EPM). Schmidt et al. (1994) quoted a revised distance of $7.4^{+1.0}_{-1.5}$ Mpc, or $(m - M) \approx 29.3$ mag, based on further analysis by Eastman, Schmidt, & Kirshner (1994). Pierce (1994) reported a mean *BRI* Tully-Fisher distance modulus of 29.2 ± 0.5 mag in a recent comparison of EPM and luminosity-line width distances to local galaxies. These EPM distances seem to favor the long distance scale measurements of Sandage & Tammann (1974) and others, which typically gave $(m - M) \approx 29.2$ mag.

Using the *Hubble Space Telescope*, we have observed Cepheid variables in M101 at 14 independent epochs in *V* (three additional observations with WFPC2 were used for calibration purposes), and 5 independent epochs in *I*. We have constructed *V* and *I* period-luminosity (PL) relations based on 29 Cepheid variables in the outer field, and have used the resulting *V* and *I* apparent distance moduli to derive a reddening-corrected distance estimate for M101.

In § 2 we discuss the observations and preprocessing of the data. Section 3 covers the instrumental photometry and data reduction. Section 4 briefly highlights the results from the calibration (discussed in more detail in Appendix A). In § 5, we detail the variable star search and period finding analysis. In § 6, we describe our procedures for determining mean magnitudes. We derive apparent period-luminosity relations, as well as the reddening and distance to M101, in § 7 and discuss systematic effects arising from incompleteness and flat fielding. Appendix A describes the calibration of the *HST* photometry. Appendix B contains the tabulation of magnitudes and positions of the Cepheids for every epoch used in the distance analysis. Lastly, Appendix C lists several apparently variable stars that could not easily be classified.

2. THE OBSERVATIONS

The M101 outer field is shown in Figure 1 (Plate 3), which was taken from an image obtained at the Canada-France-Hawaii Telescope (CFHT).

The outer field in M101 (7'.9 from the nucleus) was observed with the WFC at 13 independent epochs with the F555W filter ($\sim V$) and at 1 epoch with the F785LP filter ($\sim I$). Most of the WFC observations were cosmic-ray split (i.e., a pair of exposures taken one immediately after the other to facilitate the identification, and removal, of cosmic ray events). As a consequence of telescope scheduling constraints, the WFC observations were grouped into three sets: spring, summer, and late fall of 1993, each observation at a different roll angle, with the exception of the summer observations, which were at constant roll angle with small pixel offsets. These observations spanned 260 days, beginning on 1993 March 2. Total exposure times for the split

TABLE 1

A SELECTION OF PREVIOUSLY PUBLISHED DISTANCES TO M101

Method	Distance Modulus	Distance (Mpc)	Reference
Group Membership	28.71	5.5	de Vaucouleurs (1973)
Group Membership	29.30 ± 0.3	7.2	Sandage & Tammann (1974)
Group Membership	29.08 ± 0.3	6.5	Sandage & Tammann (1976)
Revision of ST (1976)	28.56	5.2	Jaakkola & Le Denmat (1976)
Brightest Stars	29.2	6.9	Sandage (1983)
B-Band Tully-Fisher	28.4	4.8	Bottinelli (1985)
R-Band Cepheids (2)	29.5	7.9	Cook *et al.* (1986)
M Supergiants	28.4 (upper limit)	4.8	Humphreys *et al.* (1986)
BRI-Band Tully-Fisher	29.2 ± 0.5	6.9	Pierce (1994)
EPM (SN 1970G)	29.35	$7.4^{+1.0}_{-1.5}$	Schmidt *et al.* (1994)
Four Cepheids & Five Miras	29.08 ± 0.13	6.5	Alves & Cook (1995)
VI-Band Cepheids	29.34 ± 0.17	7.4 ± 0.6	This Paper

NOTE.—Cook et al. 1986 value corrected for LMC distance modulus and reddening, consistent with this paper.

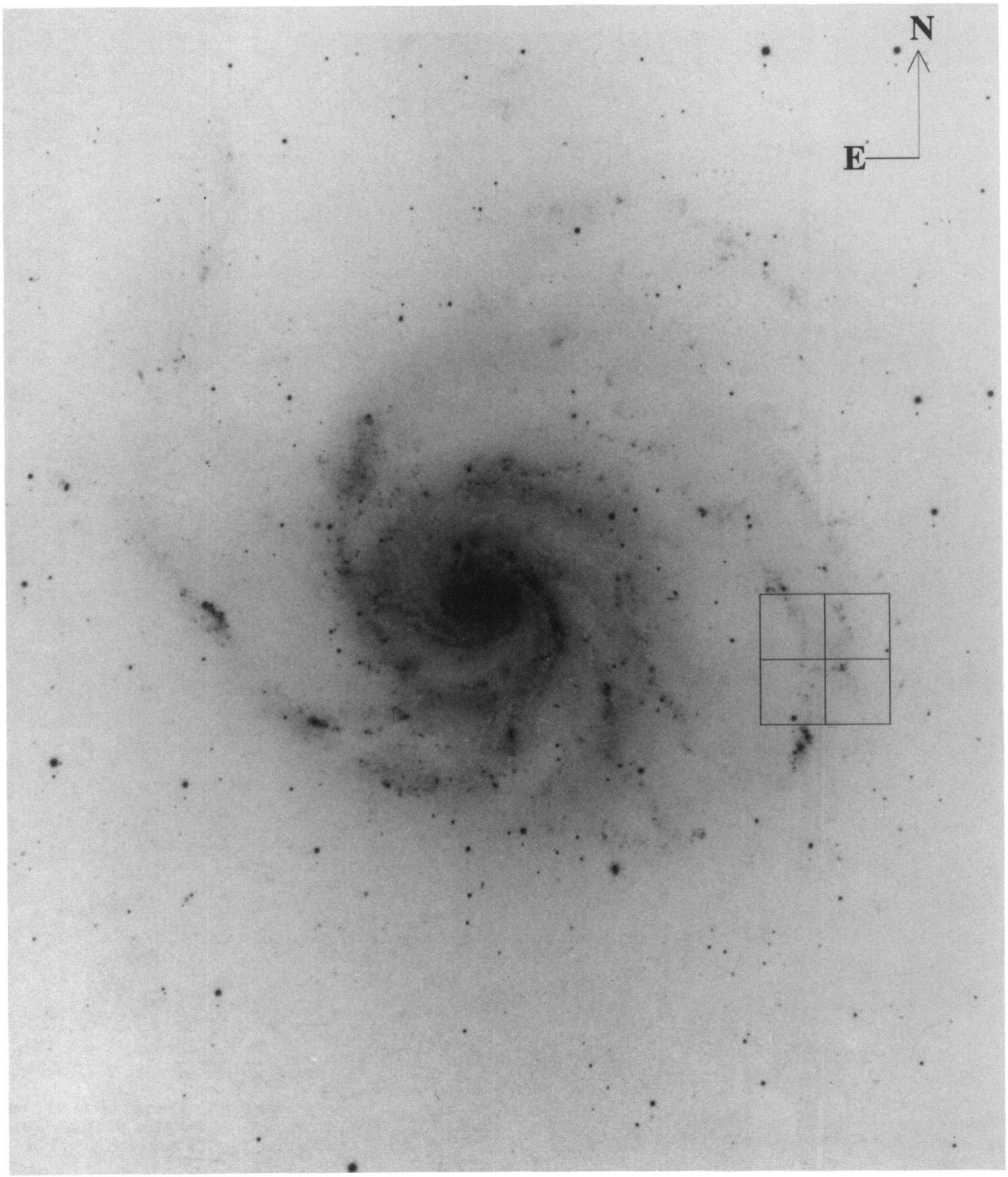

FIG. 1.—Image of M101 taken by WLF at the Canada-France-Hawaii Telescope. The WFC field of view is shown, 160″ on a side. North is to the top and east is to the left.

pairs were 3800 seconds in the spring, and 4200 seconds in the summer and fall. The F785LP total exposure time was 4200 seconds.

Our WFC observations were originally scheduled in an optimal power-law time series in order to minimize period aliasing, as detailed in Freedman et al. (1994a) and Madore & Freedman (1991). However, some of our visits were lost to *HST* safe-mode and other technical problems. Two epochs were partially lost; the second epoch was a single on-target exposure and the third epoch contained a short exposure member in the pair. These epochs thus have less reliable photometry because of shortened exposure times, so they frequently appeared as spurious points. The aliasing problems that were introduced by these phase coverage gaps are discussed in § 4.

To address some of these problems, a short series of observations with WFPC2 were obtained shortly after the refurbishment mission. These included one F555W observation, four F814W observations, and one cosmic-ray split F439W observation. Exposure times for these WFPC2 observations were about 1200 seconds apiece. These WFPC2 observations were made between 1994 February 21 and 1994 April 4. The F555W epoch was taken on 1994 March 18, yielding a total baseline for the Cepheid period search of 381 days. The F439W exposure was split into an 800 second frame and a 1300 second frame. These 1994 exposures were all taken when the instrument was at an operating temperature of $-76°$ C (known as the "warm" temperature).

Three more epochs were observed in F555W in March and April of 1995. These data were cosmic-ray split, 1000 second exposures, and have been used to aid in calibration of the earlier epochs. The "charge-transfer effect" is expected to be significantly reduced in these exposures, due to the reduced operating temperature ($-88°$ C—"cold") of the detectors.

The WFC observations were processed by the pipeline system at the Space Telescope Science Institute (see Lauer 1989 for details). Four calibration steps were performed, namely, correction of small analog-to-digital conversion (A/D) errors, bias subtraction, dark subtraction, and flat-field division. The flat fields used were made from observations of the bright Earth. Corrections using the Medium Deep Survey (MDS) correction flats (Phillips et al. 1994) were applied after the WFC photometry reduction. Epoch-to-epoch magnitude offsets were applied to register all photometry to the first epoch, taken about halfway between two decontaminations (1992 August and 1993 August).

The WFPC2 observations were processed by the pipeline, as outlined in the WFPC2 Status Report (Holtzman et al. 1995a), and involved correction of small A/D errors, bias subtraction, superbias subtraction, superdark subtraction, and flat-field division. The flat fields before 1994 mid-March were constructed from the thermal-vacuum (TV) flat fields and a model for the on-orbit illumination pattern. At the warmer operating temperature, the detectors suffered from enhanced charge transfer inefficiency; observed magnitudes were subject to errors correlated with position on a CCD, in that counts were suppressed with increasing distance from the readout amplifier. We discuss this below in the context of the calibration.

3. INSTRUMENTAL PHOTOMETRY

Most of the independent epochs were cosmic-ray split, facilitating recognition of genuine stars in each frame. Coordinate transformations relating the positional systems of the various observations were derived from comparison of preliminary object lists from each image (discussed below). Instead of reducing the images in four distinct sets (as was the case for M81; see Freedman et al. 1994a; Hughes et al. 1994), the large relative rotations of our frames required us to place the images from all four CCDs onto a single coordinate system. Using these coordinate transformations on the cosmic-ray split exposures, all 108 WFC 800×800 images (100 in F555W, 8 in F785LP) were reduced *simultaneously* using the ALLFRAME photometry package (Stetson 1994a). This WFC ALLFRAME reduction took about *four weeks* to complete on a Sun Sparc 2 workstation!

ALLFRAME simultaneously solves for the magnitudes and positions of all of the stars in all of the frames. The WFC PSFs were originally derived from WFC frames of the globular cluster NGC 1850 (see Stetson 1994a). The PSF structure varied quadratically across each CCD, as determined empirically from the stars in NGC 1850. As discussed in Freedman et al. (1994a), the ALLFRAME magnitudes are representative of stellar core magnitudes. Mischaracterization of the structure in the outer parts of the PSF does not directly affect the measurement of the core photometry, and so relative photometry across the field is preserved. While the profile fitting was restricted to a radius of 2.5 pixels, the final ALLFRAME magnitudes were determined by integration of the PSF out to 25 pixels (2".5). Mischaracterization of the PSF, however, may affect the determination of total magnitudes, and is the reason that external calibrations were used for the ALLFRAME photometry.

The large WFC star list input to ALLFRAME was generated in several steps. First, individual epoch star lists were generated from averages of the cosmic-ray split image pairs. The STSDAS.WFPC.COMBINE routine was used to reject cosmic rays in the averaging process. A master star list was generated from the individual lists by comparing star positions in the coordinate transformation derivation. Any object found in a single image was included in the master list. During the reduction process, ALLFRAME discarded many unusable objects (because they were peaks in unresolved associations or background galaxies, or because they were high signal features in the wings of bright stars). Had these objects been kept, their poorly determined magnitudes and positions would have hindered the variable star search. By the final iteration, the final star list contained more than 23,000 stars. The total number of stars found in *at least* 16 exposures was nearly 11,000.

Corrections to the WFC ALLFRAME magnitudes, based on the MDS correction flats (Phillips et al. 1994), were applied, and the two different sets of ALLFRAME magnitudes were analyzed (i.e., the uncorrected and the MDS-corrected magnitudes).

After the WFPC2 exposures were obtained, coordinate transformations were derived to incorporate the new data into the WFC dataset. ALLFRAME was run on the 56 new 800×800 images (28 in F555W, 20 in F814W, and 8 in F439W); one WFC exposure (4 images in F555W) was included to facilitate incorporation of the new data into the WFC coordinate system. The WFPC2 PSFs were derived from public-domain observations of ω Cen, and from images of the outer halo globular clusters Palomar 4 and NGC 2419 (Stetson 1994b).

A parallel effort for photometry and detection of variable

stars was done using a variant of the DoPHOT program (Schechter, Mateo, & Saha 1993). The essentials of the variant, its rationale, and details of the procedure to obtain photometry are described in Saha et al. (1994). The DoPHOT WFC photometry was used primarily to discover variable candidates and was not zero-point calibrated. In a single WFC epoch comparison between DoPHOT and ALLFRAME magnitudes (this comparison was done with an arbitrary zero-point offset between the two data sets), there were no magnitude-dependent trends to ± 0.02 mag over the range $21.5 \lesssim V \lesssim 24.5$. A limited set of WFPC2 frames were also processed by DoPHOT as a check on the calibration procedures; these results are discussed below in that section (§ 4).

4. CALIBRATION

The photometric calibration is a crucial step in establishing the distance modulus. The calibration of WFC data is complicated by the *HST* spherical aberration problem (Hughes et al. 1994) and potential flat-fielding problems (Phillips et al. 1994). We therefore utilized several different calibration sources. The primary calibration was derived from comparisons with WFPC2 images. Ground-based data and the Medium Deep Survey WFC calibration both aided as checks of the calibration of our WFPC2 observations. The full details of these independent sources of the calibration are discussed in Appendix A, and a brief summary is given below.

The adopted calibration.—We calibrated our WFC F555W photometry using secondary standards in the WFPC2 exposures. We calibrated our WFPC2 photometry using Stetson (1994c) instrument zero points. The other calibrations provide a cross-check and an estimate of external systematic errors. For example, the ground-based calibration may be affected by systematic effects arising from incompleteness and improper sky determinations. Furthermore, the simple interpretation of the ALLFRAME PSF magnitudes as true representations of the observed counts may be seriously affected by a poor fit to the PSF. External calibrations bypass the resulting systematic effects. The globular cluster-based transformations have been derived from nearly identical WFPC2 ALLFRAME reductions of ω Cen, Pal 4, and NGC 2419 exposures, with a variety of exposure times.

These WFPC2 zero points have all been derived from data acquired at the cold operating temperature ($-88°$ C). Most of our WFPC2 observations in F555W were also taken with the instrument at the cold temperature. However, our F814W observations were taken when the WFPC2 was at an operating temperature of $-76°$ C. In Appendix A, we discuss the impact of this change on the F814W instrument zero point. To summarize, the "cold" F814W zero point appears to be essentially unchanged, to within ± 0.02 mag, from the "warm" state of the detector, in an average of the two CCDs that were used in the comparison. We therefore treat any residual F814W zero-point change as a ± 0.02 mag *uncertainty* in the F814W calibration.

The WFPC2 calibration.—Briefly, there are several steps involved in calibrating the WFPC2 ALLFRAME magnitudes, and then in calibrating the WFC ALLFRAME magnitudes. These steps are more thoroughly discussed below and in the first appendix.

1. Measure and apply aperture corrections, to correct WFPC2 ALLFRAME magnitudes to the system of 0.″5 radius aperture magnitudes.
2. Correct ALLFRAME magnitudes for the charge-transfer effect.
3. Add offsets for exposure time, amplifier gain ratio.
4. Correct magnitudes using the long-exposure set of zero points.
5. Iterate the magnitudes using the color terms listed in the WFPC2 Status Report (Holtzman et al. 1995b).
6. Choose secondary standards in common between the WFPC2 and WFC exposures.
7. Verify nonvariability of secondary standards and find the mean offset between the WFC ALLFRAME magnitudes and the calibrated WFPC2 photometry.

Stetson (1994c) has used WFPC2 observations of ω Cen, Pal 4, and NGC 2419 to derive transformations of the ALLFRAME magnitudes to the standard system. This direct transformation was first applied with the assumption that there is a constant correction from ALLFRAME PSF magnitudes to aperture magnitudes with a 0.″5 radius, i.e., that the correction in the M101 frames is identically the same as that in the globular cluster frames. Those globular cluster-based zero points have been themselves adjusted to incorporate differences in the correction from ALLFRAME magnitudes to 0.″5 aperture instrumental magnitudes, differences due to telescope jitter or focus changes. We then derived new aperture corrections from the F555W and F814W WFPC2 frames themselves, using results from growth curve analysis with the Stetson (1990) program DAOGROW. This calibration avoids uncertainties introduced by poorly fit profile wings. ALLFRAME magnitudes are derived from least-squares fits of the PSF *scaled* to the observed stellar profile. This scale factor is treated as the number of counts required to minimize the residuals *within a fitting radius*. The ALLFRAME magnitude is computed by multiplying the integral of the PSF by this scale factor. The WFPC2 charge-transfer effect is a problem, since it can diminish the counts in stellar wings, and result in an incorrect integrated PSF magnitude. Along with crowding and cosmic rays, the wing depletion can make it difficult to directly establish the correction from ALLFRAME counts to "true" counts.

An additional effect has also been unearthed. The Stetson (1994c) zero points agree very well with the Holtzman et al. (1995b) zero points in the short-exposure regime (< 100 s). However, long exposures (> 1000 s) of Pal 4 and NGC 2419 show a systematic difference in zero points from those of the short exposures of the same stars; the effect has been measured to be $+0.050 \pm 0.007$ mag (instrumental magnitudes from long-exposure frames are brighter than magnitudes measured in an identical way on short-exposure frames; Stetson 1994c). This factor is not understood at this point, and so there is not a clear rationale for choosing between the long- or short-exposure zero point. However, since our M101 integrations are long, we have adopted the "long" calibration. We have also included the difference above in the error budget (§ 7.3). Although small, the offset is applicable in both F555W and F814W, and remains as a systematic uncertainty in the final distance modulus.

The Stetson (1994c) transformations also include the individual chip gain ratios (which are not identically 2.00;

see Burrows et al. 1994). Table A1 in Appendix A lists the components of the WFPC2 calibration.

Our WFPC2 observations were used to define secondary standards that were measured in the WFC images. These WFPC2 observations were calibrated using a combination of zero points from Holtzman et al. (1995b) and Stetson (1994c). These secondary standards were also screened for variability in the WFC data. The relevant instrumental and aperture corrections are discussed in Appendix A. The cross-calibration of WFPC2 and WFC magnitudes was performed using 38 secondary standards in the PC CCD, plus 114, 236, and 160 secondary standards in the three WF CCDs. The difference in the *mean* WFPC2 calibrations for the MDS-corrected and uncorrected WFC ALLFRAME photometry was small ($\lesssim 0.01$ mag), indicating that WFC flat-fielding errors were not a significant problem in the zero-point calibration. Hughes et al. (1994) also determined that flat-fielding errors were not a serious issue in the case of M81.

The Medium Deep Survey WFC calibration.—An internal calibration of the WFC F555W ALLFRAME magnitudes was derived from the WFC photometric zero points from the Medium Deep Survey (MDS) project (Phillips et al. 1994). Converting the MDS zero points to our instrumental scale required corrections to the ALLFRAME PSF zero point and a small aperture correction (see Table A2 in Appendix A). An estimate of the contamination at the reference epoch was also applied (as noted, the reference epoch was six months after the previous decontamination, corresponding to a correction of -0.05 mag). Our single epoch observation in F785LP was calibrated in similar fashion, except that a color term was added to bring the Cepheid data in the same system as the F814W WFPC2 data, as described in Appendix A.

The ground-based calibration.—A third calibration of the F555W observations utilized ground-based V and I photometry from the KPNO 4 m CCD images taken as part of the Cook et al. (1986) Cepheid search (see also Alves & Cook 1995). Image crowding prevented accurate ground-based photometry of individual stars, but with many *groups* of stars used as secondary standards, we found a mean difference of $+0.01$ mag between the ground-based calibration and the WFC calibration. An additional $(V-\mathrm{F555W})$ color term of $+0.02$ mag was applied for the mean $(B-V)$ colors of Cepheids, well within the uncertainty of the ground-based calibration. The detailed use of groups as secondary standards is explained in Appendix A3. Ground-based I secondary standard magnitudes were converted to WFPC2 F814W magnitudes (Holtzman et al. 1995b), so no additional color term is expected for the (Ground − ALLFRAME) magnitude offsets.

A DoPHOT consistency check.—DoPHOT was also used as a check on the calibration for one of the WFPC2 CCDs. Wide Field CCD No. 4 was chosen as the test quadrant using two exposures, one in F555W (500 s) and the other in F814W (1200 s). For ~ 600 stars, calibrated DoPHOT magnitudes were found to be systematically fainter than the mean calibrated ALLFRAME magnitudes (derived from all of the WFPC2 exposures) by 0.049 ± 0.022 in F555W, and 0.039 ± 0.010 in F814W. The origin of these discrepancies appears to be uncertainties in aperture corrections determined in separate routines from the DoPHOT algorithm. These differences could be specific to the particular chip-filter-exposure combinations that were chosen, from either contamination, focus variations, or a combination of both. If the discrepancy was common to all four chips, and we adopted the DoPHOT calibration, our final distance modulus would change by ~ -0.02 mag. If the differences are purely random between the CCDs, this would require the addition of a fourth error of ± 0.03 mag to the V and I apparent distance moduli, for an error in the final distance modulus of up to ± 0.06 mag. These errors are included in the error budget, discussed in § 7.3.

The uncertainties in the final calibration.—A more comprehensive discussion of all our sources of error can be found in § 7.3 on the error budget. The sources of error inherent in the calibration of WFC and WFPC2 data are summarized below.

The final PL relation zero points are based on the accurate calibration of the magnitude system defined by a set of ALLFRAME PSF magnitudes. Several problems, inherent to the WFPC2 instrument, complicate the calibration, most notably CCD nonlinearities and changes in telescope focus. The former set of uncertainties consists of charge-transfer losses (Holtzman et al. 1995a), the dependence of the CCD zero point on exposure time (Stetson 1994c), and, for F814W, the change in the instrument zero point with operating temperature. These sources of error are poorly understood and their magnitudes are known only approximately.

The charge-transfer effect can be roughly compensated for by applying a correction, proportional to distance from readout, to the instrumental magnitudes. The correction is only an approximation, and therefore carries with it a source of error. In our case, the error is approximately ± 0.02 mag.

The Stetson (1994c) exposure-time effect is also poorly understood. The effect, as explained earlier, causes stars on long exposures (1000 s) to have magnitudes offset from short exposures (100 s) by -0.050 ± 0.007 mag. Unfortunately, this effect has only been observed in WFPC2 observations of the globular clusters NGC 2419 and Pal 4. The ω Cen data were also taken with a different gain ($14e^-$/ADU).

At this time, it is not clear whether the Stetson correction should be applied to our data, but it seems reasonable to do so since out data are also long exposures. The impact on the final distance is 2.5%. Unfortunately, the ω Cen data that define the zero points in the WFPC2 Status Report (Holtzman et al. 1995b) have a limited range of exposure times for each filter so there was no measurable dependence of zero point on exposure time. The effect appears to occur somewhere between exposure times of 60 s and 1200 s.

By comparing our calibration sources, we estimate the random and systematic sources of error associated with the secondary standards themselves. Seeing effects and poor sky determinations impact the ground-based calibration. Zero-point errors in *both* the WFPC2 and ground-based calibration also appear in the comparison. For example, crowding is likely to be the cause of the calibration discrepancy in the F555W images of WFC CCD No. 1. The ground-based data suffer from poor seeing, yet so do the WFC images also suffer from the aberrated PSF. That region of the spiral arms is densely packed with bright groups and H II regions. The WFPC2 F814W observations use the PC to resolve the region into the individual bright stars, and the ALLFRAME star list is much more complex than the original WFC star list.

Together, all these effects lead to total F555W and

F814W/F785LP calibration uncertainties of ± 0.06 and ± 0.04 mag, respectively (see, also, § 7.3, the error budget).

5. VARIABLE STAR SEARCH

Two search criteria were used to select variable star candidates in the ALLFRAME photometry. The first was the Welch & Stetson (1993) variability test. The cosmic-ray split pairs provide an ideal data set for this technique. The test utilizes the paired variations from a star's mean magnitude to compute a variability index based on the principle that the magnitude deviations for pairs of images taken "simultaneously" will be correlated for variables whose periods are much longer than the epoch's exposure time. The variability index is a sum of the pairwise products of deviations from a star's mean magnitude across all epochs:

$$I = \frac{1}{\sqrt{N_{\rm pairs}(N_{\rm pairs}-1)}} \sum_{i}^{N_{\rm pairs}} \frac{(m_{i,1}-\bar{m})}{\sigma_{i,1}} \frac{(m_{i,2}-\bar{m})}{\sigma_{i,2}} . \quad (1)$$

For nonvariable stars, the uncorrelated magnitude residuals in the paired exposures should give a random scatter with a mean variability index near zero. For variable stars, the index will have a large positive value. One should use a threshold of $I = 1$ for a sample of stars with a Gaussian error distribution and well-determined errors.

The second method by which variable star candidates were selected was simply to identify those stars with a large dispersion in their measured magnitudes. The approach adopted here was to generate histograms of magnitude dispersion for several magnitude bins. A tentative set of candidates was then selected from those in the high-dispersion tails of the histograms. This second method was supplementary to the Welch & Stetson (1993) technique. The Welch & Stetson index is a much more efficient means of selecting variable stars. However, its efficiency is diminished if the magnitude errors are overestimated. A few of our Cepheid candidates, found by the supplemental search, had variability indices around $I \approx 0.9$.

Candidate period search.—The light curves for the candidates identified by these two methods were inspected so that spurious ones could be eliminated; some candidates were flagged solely because of strong cosmic-ray events, multiple cosmic-ray events, etc. For real variables, spurious observations were also identified (due to, e.g., cosmic rays or bad pixels). For promising candidates, the data were searched for best-fitting periods, then phased and plotted. Periods were determined using a generalized Lafler & Kinman (1965) phase dispersion minimization method (PDM), as described by Stellingwerf (1978). Two versions of the PDM algorithm were run simultaneously: one which weighted the individual points by their magnitude uncertainties, and another which did not. The listed potential periods were identical, but the estimated signal-to-noise ratio (S/N) would differ slightly, because estimated total dispersions for trial periods would contain different normalizations (the weights assigned to trial *phase* points are what matters, even though these weights are constant for any given epoch). That both methods gave essentially the same results is not surprising. The dispersion about the mean light curve at the correct period should still reflect the *typical* measurement errors. The individual magnitudes within cosmic-ray split pairs were averaged prior to the final period determinations.

The period search range was 2–400 days, in steps of 0.1 days. Typically, from 4 to 10 periods were inspected for each candidate. In the final tests V and I data were phased and plotted together to ensure that periods were consistent between the two bandpasses. Inconsistencies for candidate periods between V and I did not occur within the ALLFRAME data set itself, but occasionally arose when the ALLFRAME data were phased with periods derived from DoPHOT photometry. In the final stages, period phasing of both the DoPHOT and ALLFRAME magnitudes simultaneously would settle disagreements, because even the relative photometry between epochs should be mostly conserved for both programs (within measurement errors). These inconsistencies are discussed below. Special care was taken to avoid aliasing problems, which were introduced by missing epochs in our original observing schedule (see § 2).

An independent variable search using DoPHOT.—An independent list of variable stars was generated using the relative DoPHOT photometry (for searching only—mean magnitudes and distance moduli were not derived from the DoPHOT photometry). This search used the stars' observed dispersions in mean DoPHOT magnitude, Lafler-Kinman periodicity, and image blinking to generate an independent candidate list. Periods for the variables that were found in common (about 75%) were then compared between the DoPHOT and ALLFRAME searches. Variables found by only one of the two methods were scrutinized to see if they were valid detections (e.g., were spurious cosmic-ray hits causing stars to appear variable?). Because the DoPHOT data set contained single magnitude measurements at each epoch (the cosmic-ray split pairs were combined with a cosmic-ray rejection scheme prior to reduction), spurious cosmic-ray hits could effectively remove whole epochs, for individual stars, from the variable search. The ALLFRAME-based and DoPHOT-based variable searches both set a minimum to the number of exposures in which a star was detected as a rejection criterion to ensure that aliasing would not seriously interfere with the period search. For the ALLFRAME search, a star had to be found in at least 16 exposures (which could potentially be a minimum of 8 cosmic-ray split epochs). For variables to be recovered in the DoPHOT scheme, a star had to be measured in at least 9 epochs. Stars not found in the overlap of the two candidate lists had typically been excluded by one search or the other simply by the rejection of too many spurious observations (these could differ since different reduction and rejection approaches were used with the two programs).

To ensure that biases were minimized, the variable star and period searches were cross-checked by several team members. The cross-check was done for both the DoPHOT and ALLFRAME photometry. Agreement, in most cases, was quite good, with occasional period disagreements between DoPHOT and ALLFRAME only for the alternate periods. Discrepancies between *period* determinations generally arose from differences over which spurious observations had been rejected in the initial analysis. These disagreements were resolved by close inspection of discrepant observations, and by simultaneously inspecting the phased V and I observations. Occasionally, an ALLFRAME variable candidate would show inconsistencies between the V and I light curves, when phased at a period derived from DoPHOT V photometry. In such cases, the V light curve appeared Cepheid-like, but the derived $(V-I)$

colors would be significantly too blue or too red for it to be a bona fide Cepheid.

Our final list of Cepheids and other possible variables was made after this cross-comparison. This final list was agreed upon after blinking images. Visual inspection was the final discriminant for those stars not common to both lists. Image blinking experiments convinced us in some cases that an object was indeed variable, but the inconsistencies in the color and differences between the V and I light curves led to the creation of a category of unclassified variables. These objects are listed in Appendix C. We are confident that the final periods are largely free from aliases because the alternate periods from the DoPHOT and ALLFRAME data sets were invariably different and because we had good phase coverage (see Fig. 2).

Incompleteness in the Cepheid sample.—The nonoptimum spacing of the observations, the partially lost epochs, and the crowding problems in the data led to substantial incompleteness in what would normally be considered a rich field for Cepheids. We estimate below that only about 50% of the Cepheids were detected. Figure 2 shows a Monte Carlo estimate of the phase coverage completeness for a period range of 5–100 days. The simulation used the timing of the observations to effectively sample a random distribution of phases and periods, with an ad hoc threshold for period detection (i.e., a level of measured fluctuation in the *observed* light curve that is required before being called variable). Integrating this curve indicates that our completeness from sampling effects alone is ~70% over the period range of 10–70 days. This does not include incompleteness due to magnitude cutoffs in the measurement process. Given the slope and intrinsic width of the period-luminosity relation, there would naturally be greater incompleteness at short periods (faint magnitudes).

The remainder of the Cepheids may have been lost because of crowding, contamination by neighbors (which decreases the observed amplitude of variation), or because they were too faint for high S/N measurement of the light variation. The incompleteness from crowding and magnitude selection effects can be estimated a few different ways. One way, for example, is based on the assumption that the LMC sample is fairly complete (i.e., the full intrinsic width of the PL relation is well populated) over the period range of interest; we can simply compare the M101 Cepheid sample, binned by period, to the LMC sample. The derived apparent distance moduli (see § 7) for the long- and short-period Cepheids differ by up to +0.25 mag in V (up to +0.2 mag in I). These discrepancies are appreciable fractions of the PL relations' intrinsic widths in V and I, 0.29 mag and 0.26 mag, respectively, and can be blamed on a dearth of faint Cepheids in the short-period subset. To account for such a large discrepancy, we estimate that the short-period subset is approximately a third incomplete. If the mean sampling completeness is about $\frac{2}{3}$ to $\frac{3}{4}$, as can be seen in Figure 2, then we estimate the incompleteness, from *all* effects, is about 50% over the period range of 10–70 days.

We stress, however, that incompleteness is only important when the full intrinsic width of the PL relation is undersampled. Our program is designed to provide a diverse sample of quality Cepheids, which populate the full width of the PL relation. As part of our ongoing error analysis, the Key Project is studying the effects of incompleteness and other sample biases through artificial star experiments and Monte Carlo simulations.

The normalized Cepheid period distribution of M101, shown as the filled histogram in Figure 2, has been plotted over the normalized LMCC Cepheid period distribution (for the 22 Cepheids in the same period range, $1 < \log P < 1.8$). Exceopt for a small difference between 25 and 50 days, the two distributions are comparable (the M101 sample cuts off at about 12 days, presumably due to magnitude selection effects).

The final Cepheid list.—After all cross-checks have been applied, a total of 29 Cepheids have been reliably recovered in the outer field of M101. The finder charts for the 29 Cepheids are shown in Figures 3*a*–3*d* (Plates 4–7), with magnified image subsections shown in Figure 4 (Plates 8–9). Corresponding positions are listed in Table 2. Some candidates remained unclassified but are clearly variable, as noted; these are discussed in Appendix C. The two

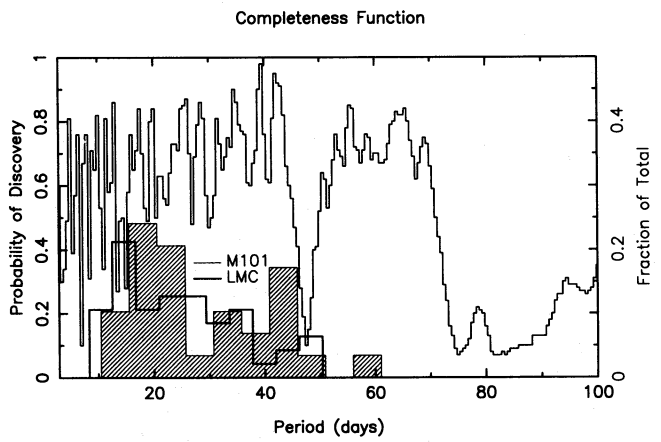

FIG. 2.—Phase-detection incompleteness function for a Monte Carlo simulation, based on the M101 outer field observation dates. No other selection effects have been included for this plot. In particular, no magnitude limit effects are included. The Cepheid period distributions for the detected Cepheids in M101 (*hashed*) and the LMC (*solid line*) have been overlayed as well.

TABLE 2

M101 CEPHEID COORDINATES

ID	P (days)	CCD	x	y
C1	58.54	2	82.1	133.9
C5	47.10	3	712.0	233.5
C6	45.80	3	179.3	271.9
C7	43.00	3	329.1	670.1
C19	43.00	1	517.3	783.3
C20	42.50	1	148.4	205.9
C8	41.00	3	284.0	211.7
C9	38.00	3	326.8	72.4
C10	37.60	3	302.0	754.3
C21	33.50	1	272.5	727.9
C12	33.50	4	343.9	235.6
C13	32.00	4	205.0	497.7
C22	27.30	1	300.2	469.7
C23	25.60	1	178.0	509.4
C14	25.00	4	619.3	451.3
C11	23.70	3	389.1	202.2
C24	23.50	1	81.1	242.1
C15	23.40	4	306.5	218.8
C16	22.80	4	710.4	662.8
C25	19.35	1	294.4	517.6
C2	18.20	2	194.2	334.2
C26	17.70	1	35.6	300.3
C27	17.20	1	454.5	62.2
C28	16.70	1	519.1	604.0
C3	16.67	2	327.7	457.5
C17	16.45	4	371.5	302.3
C4	14.27	2	411.8	134.9
C29	14.00	1	73.8	182.6
C18	13.00	4	69.7	141.7

NOTE.—Coordinates applicable for epochs shown in finder charts.

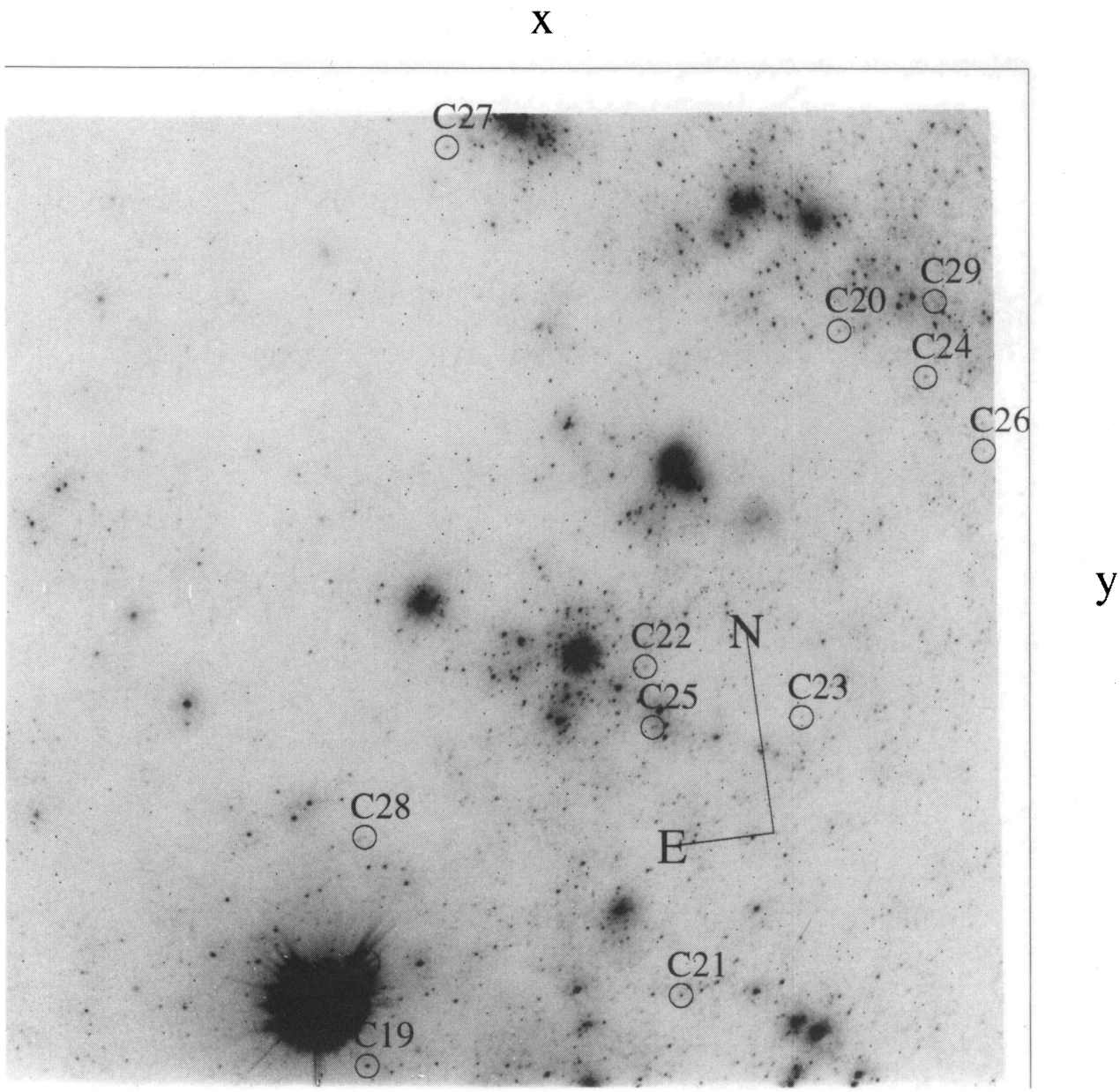

FIG. 3*a*

FIG. 3.—(*a–d*) Finder charts made from median WFC F555W images of the M101 outer field observations, taken from JD 2,449,131 to JD 2,449,163, have been rotated and aligned with CCD No. 3 so that north is approximately toward the top of the page. The original *x*-, *y*-axes of the CCDs are rotated with the images. The outer field Cepheids are circled and labeled. Each 800 × 800 image is 80″ on a side.

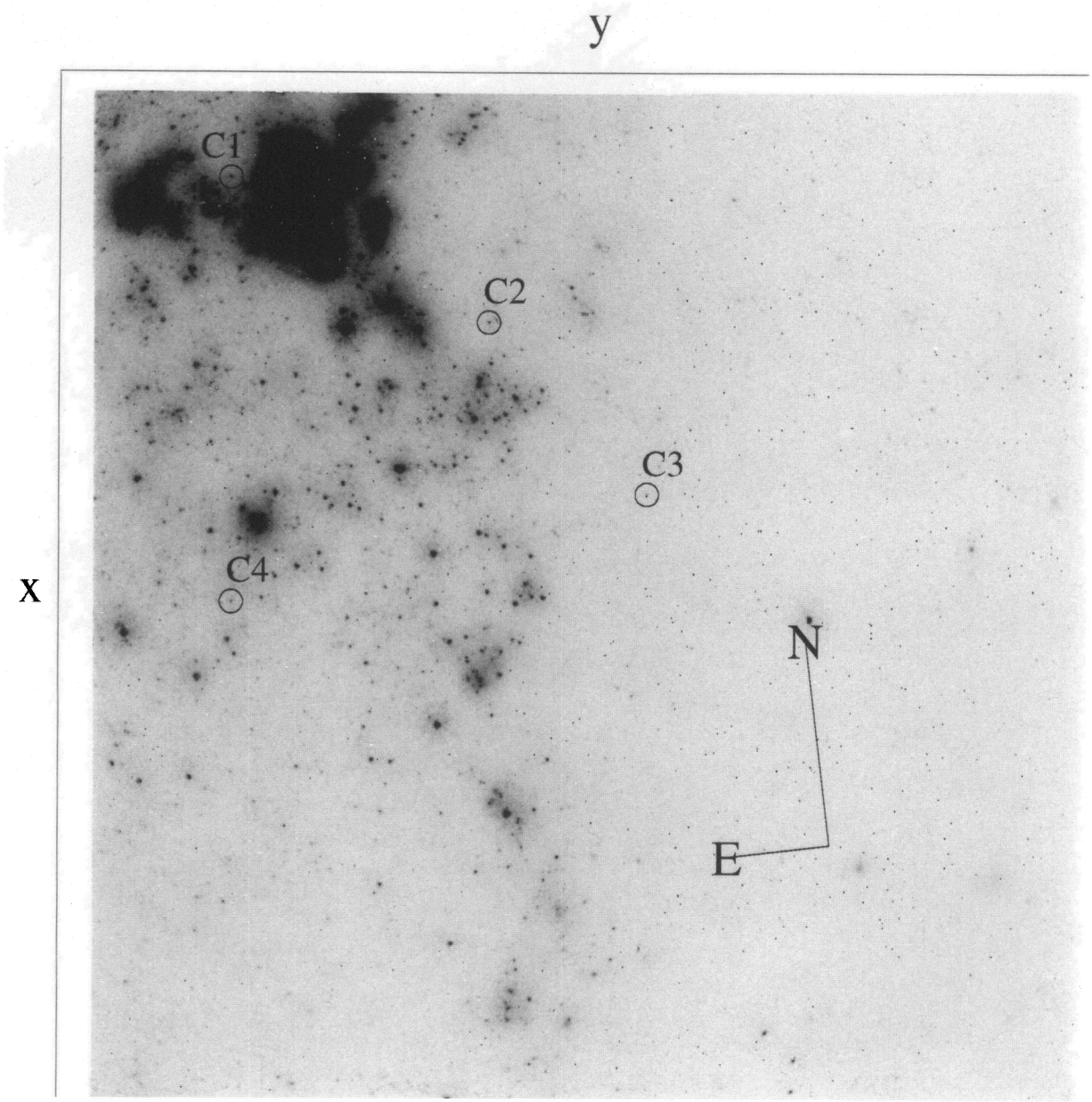

FIG. 3*b*

KELSON et al. (see 463, 32)

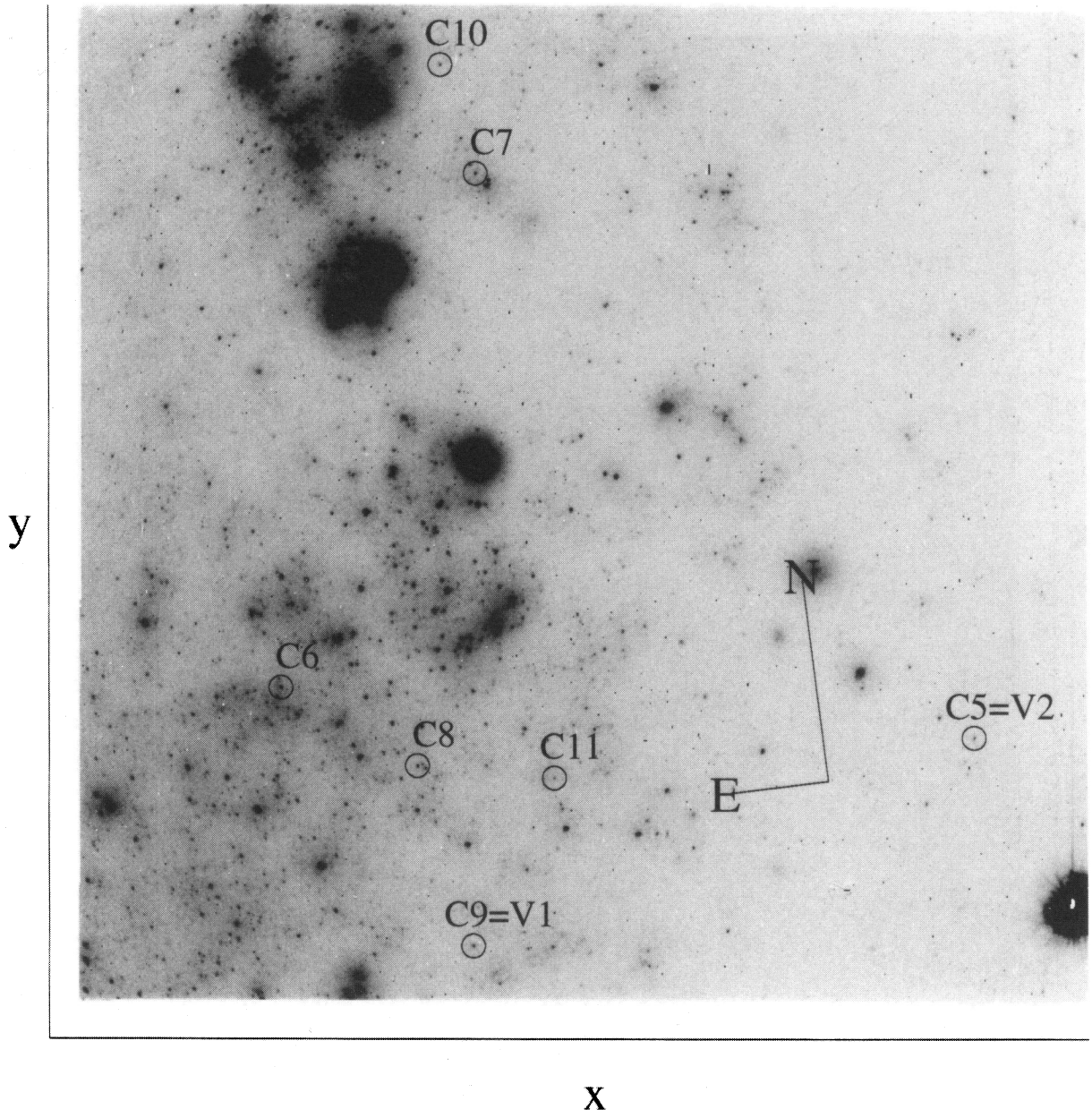

FIG. 3*c*

KELSON et al. (see 463, 32)

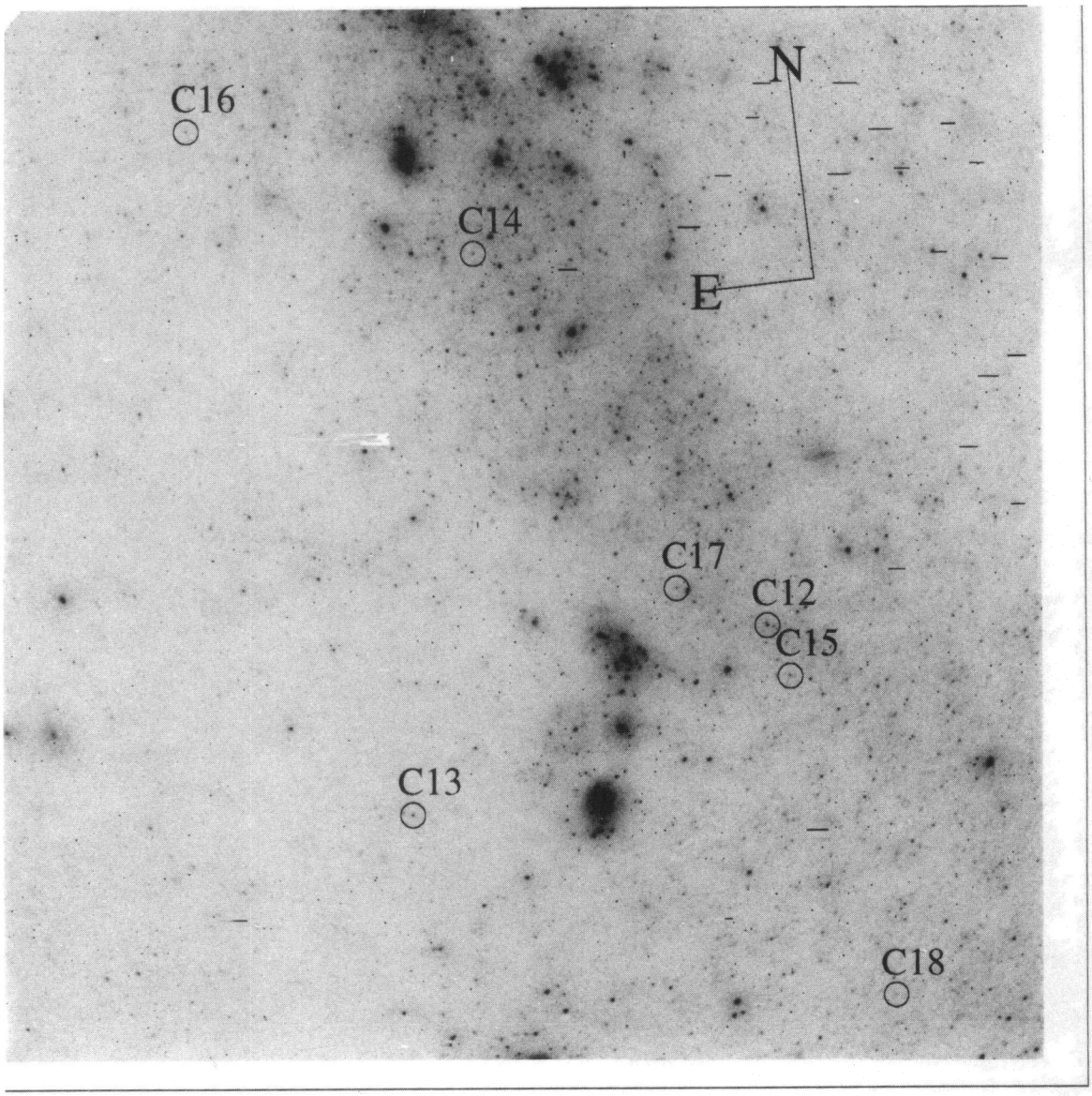

FIG. 3*d*

KELSON et al. (see 463, 32)

1996ApJ...463...26K

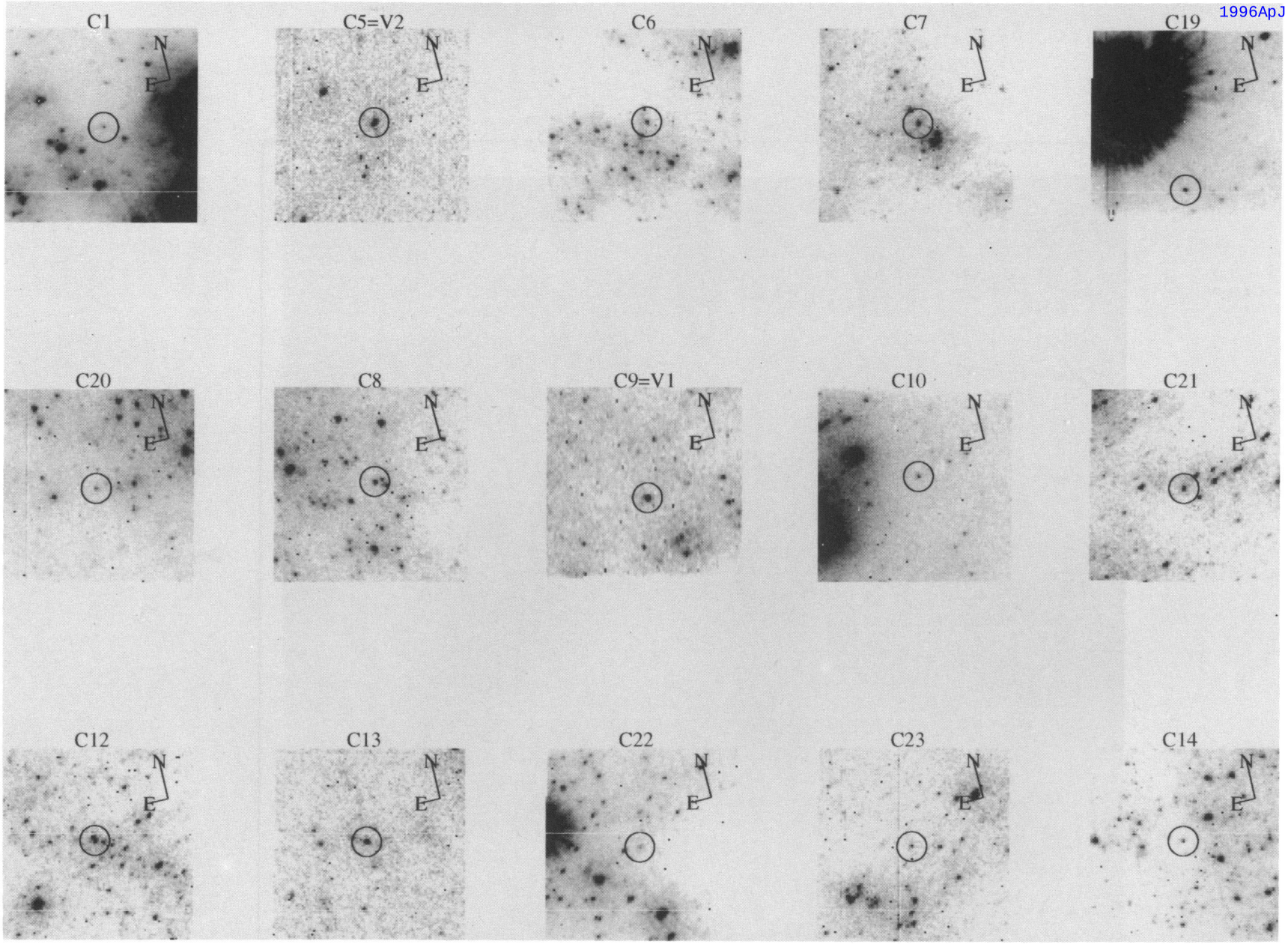

FIG. 4.—F555W finder chart subsections 10″ on a side are shown with the M101 outer field Cepheids circled. The gray scales have been adjusted in each subsection to illustrate Cepheid positions and to minimize crowding effects in the images.

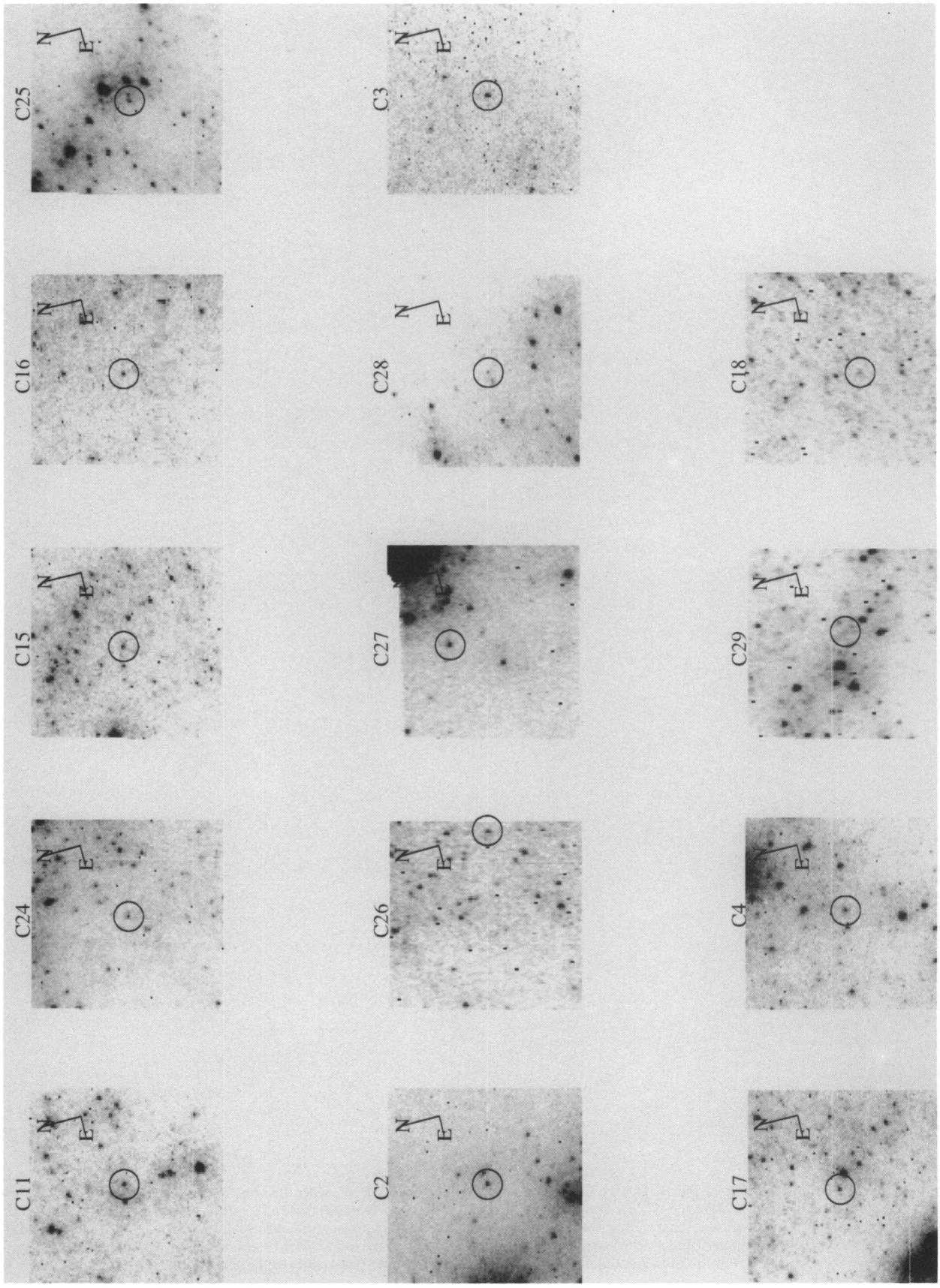

FIG. 4—*Continued*

Cepheids of Cook et al. (1986) were recovered. Cepheid V1 (=C9) was recovered with a revised period of 38 days (compared to the original determination of 37 days) and Cepheid V2 (=C5) was recovered with a revised period of 47.1 days (compared to 47 days). The additional Cepheids in Cohen (1993) and Alves & Cook (1995) were not in our field.

6. LIGHT CURVES AND MEAN MAGNITUDES

Each cosmic-ray split pair samples a single phase point in the light curve of a Cepheid. Therefore, pairs were averaged prior to generating the light curves and computing final mean magnitudes, excluding members whose observations were found to be contaminated by cosmic rays. The phase-wrapped light curves for the Cepheids are shown in Figure 5. The Cepheid V and I magnitudes and (x, y) positions for each exposure are tabulated in Tables B1 and B2, in Appendix B.

6.1. *Mean F555W Magnitudes*

The phase sampling in F555W was very uniform, as these light curves (Fig. 5) clearly indicate. In calculating mean V

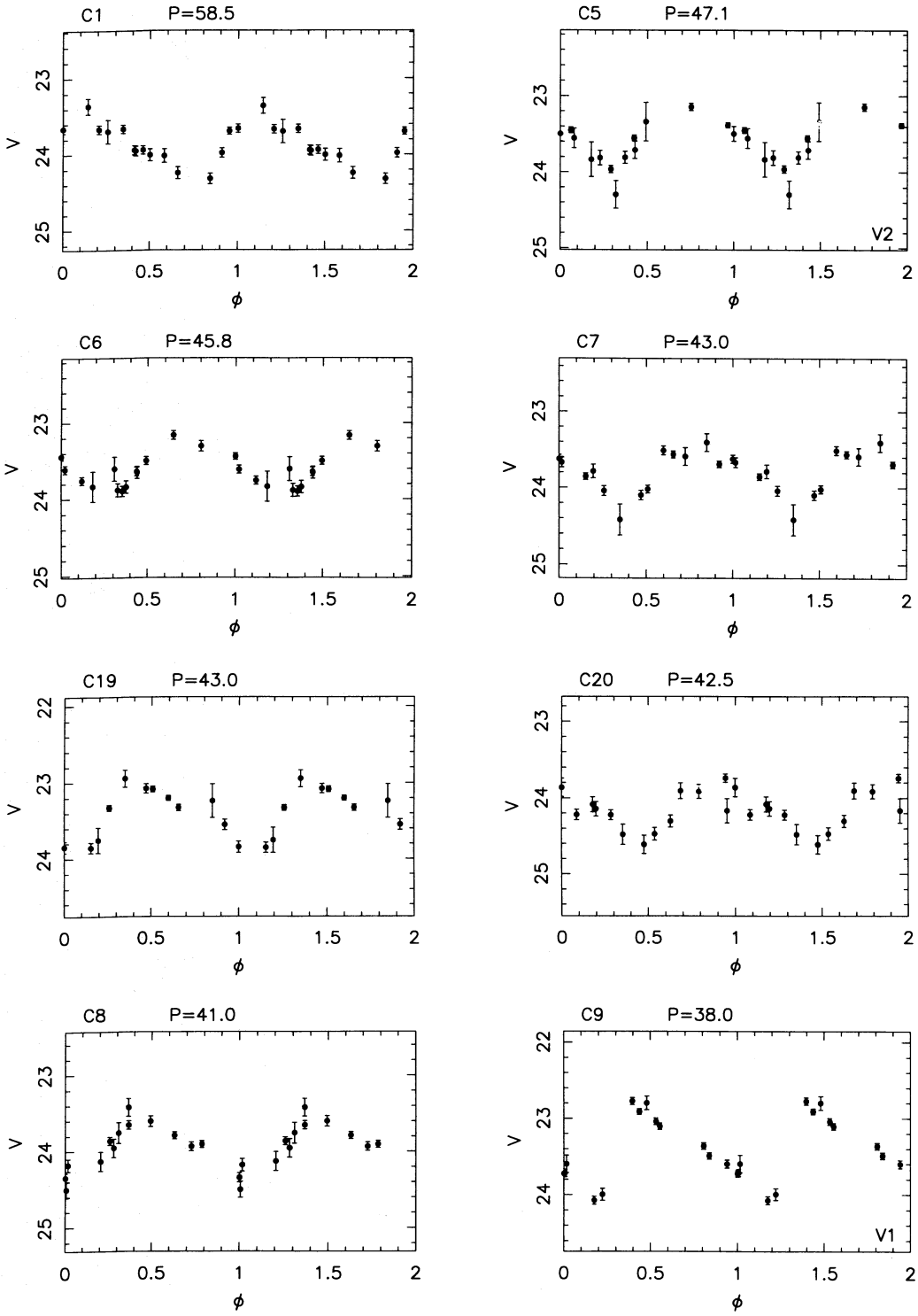

FIG. 5.—Phase-wrapped V light curves for the M101 outer field Cepheids, in order of decreasing period

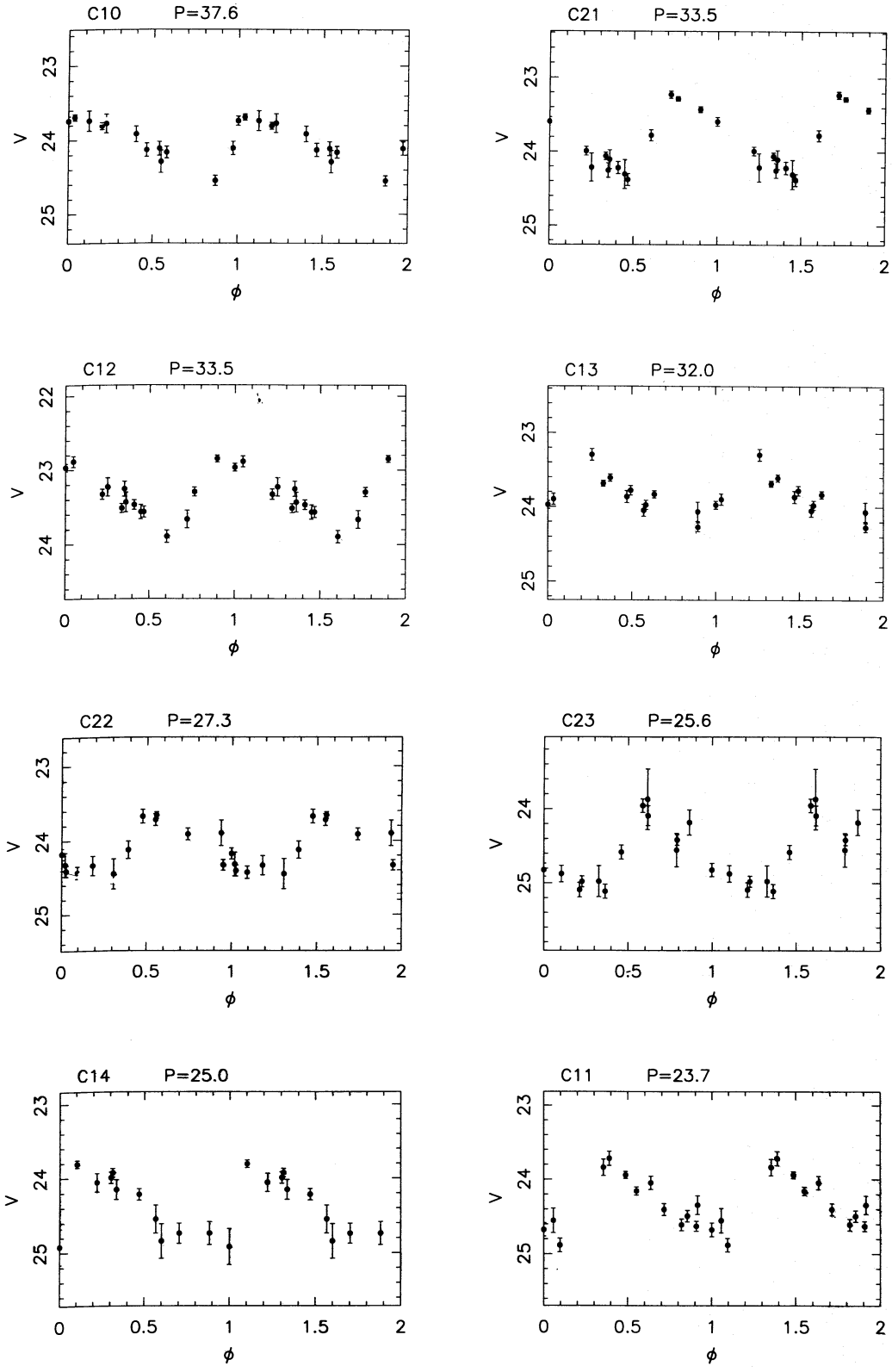

FIG. 5—*Continued*

magnitudes for these Cepheids, we computed means of intensity values for all the data points, except those rejected as spurious from investigation of the light curves. Both unweighted as well as phase-weighted mean intensity magnitudes were computed. They were then used in separate PL analyses to assess the impact of differences in the way the light curves were sampled for different Cepheids. Phase-weighted mean photometry is defined by the mean intensity, as integrated over an entire cycle ($0 \leq \phi \leq 1$), such that

$$\langle m \rangle \equiv -2.5 \log \sum_{i}^{N} \tfrac{1}{2}(\phi_{i+1} - \phi_{i-1}) 10^{-0.4 m_i} . \quad (2)$$

Saha & Hoessel (1990) use phase-weighting to determine the mean flux from a star, averaged over an entire phase, as

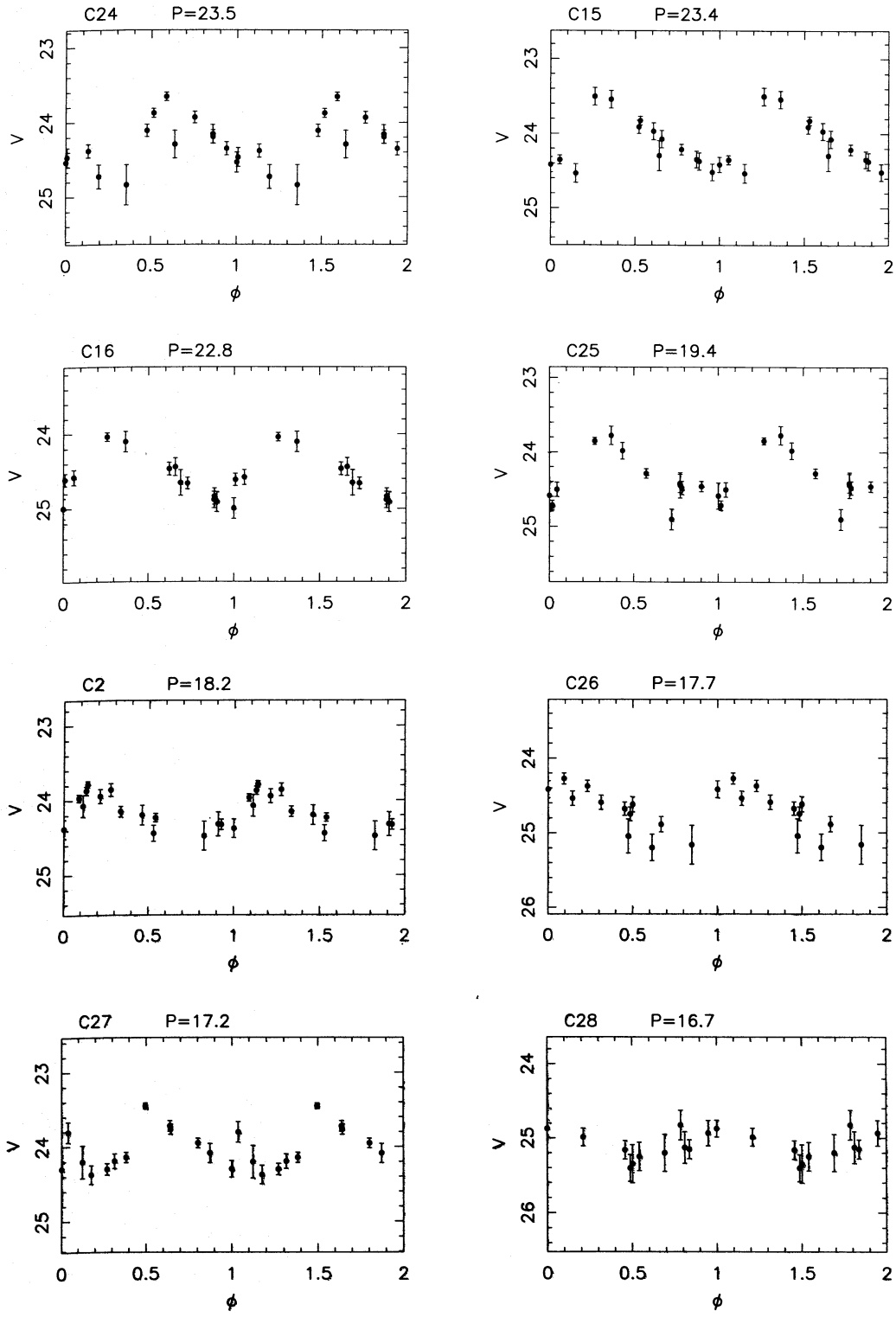

FIG. 5—*Continued*

a measure of the mean intensity which is more accurate when the light curves are irregularly sampled.

The mean difference between the unweighted and phase-weighted mean F555W magnitudes was +0.02 mag, with an rms scatter of ±0.06 mag.

6.2. *Mean F814W Magnitudes*

The much smaller number of F814W epochs meant that we did not sample the light variation as uniformly as in F555W, and we needed to determine our mean $\langle I \rangle$ magnitudes quite carefully. Compensation for the poor sampling of the light variation was done by determining corrections from the well-sampled V data. By selecting different subsets of Cepheids whose I data satisfied certain constraints (based on the quality of the data), we probed the effects of the sampling on the final distance estimates. The effects of the constraints on the final distance estimates are discussed below and tabulated later.

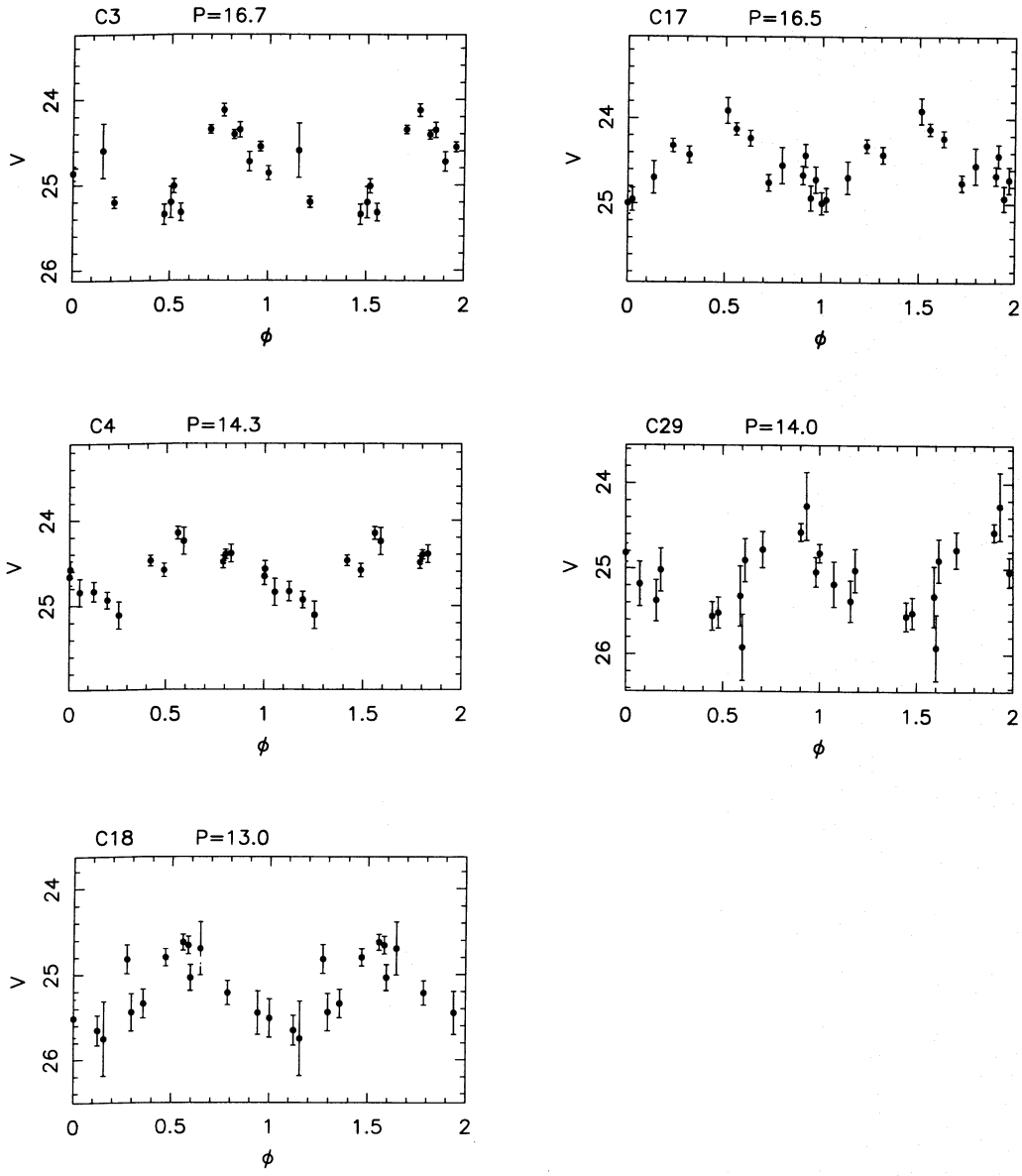

FIG. 5—*Continued*

Definitions of magnitude uncertainty constraints.—1. The first constraint is based solely on the uncertainties reported by ALLFRAME. The poor sampling of the light curve makes it difficult to detect outliers and discrepant points, in a statistically meaningful way. Only those F814W values with estimated uncertainties ($\sigma_{\rm ALLFRAME}$) *less than* some upper limit were used in the computations. Upper limits of 0.4, 0.3, and 0.2 magnitudes were imposed in separate reductions to yield information on the sensitivity of the derived relative distance moduli to the adopted upper limit. This restriction deals with the question, "Which of the *I* observations are reasonably good?"

2. The second quality constraint was based on an overall ability of ALLFRAME to derive photometric results for a given star. To continue computing a Cepheid's mean *I* photometry, the reported error of the *least* uncertain (best determined) observation was required to be smaller than some value (we used $\sigma_{\rm min,ALLFRAME} < 0.4$ mag, 0.2 mag, and 0.1 mag). Since the Cepheids also had to satisfy the first constraint, we grouped the constraints and discuss these grouped restrictions below. This second restriction implies the question, "How good is the best determined measurement?"

3. The third, and most important, constraint was related to the required number of *I* frames in which a Cepheid had to be found. For each Cepheid, we counted the number of F814W observations *with* associated F555W phase points (where the phase difference, $\Delta\phi \leq 0.1$) that had F814W magnitude uncertainties less than the previously defined tolerance levels. Strong constraints would require nearly all (e.g., at least 4) *I* observations to satisfy the criteria. Weak constraints (e.g., allowing Cepheids with a single observation) would allow many more Cepheids to be included in the PL analysis. We chose the two extremes for this constraint. Requiring at least 4 observations imposes a strong selection effect. Including Cepheids with only a single *I* detection (that still satisfies that previous two restrictions) allows us to study the faint-end population of the PL in more detail. This third criterion is equivalent to the question, "How many observations are required, which satisfy the previous conditions, before we can reliably determine a mean intensity?"

The effects of magnitude uncertainty constraints.—These restrictions are clearly flux-dependent and are discussed later in the context of their effect on the derived slopes for the PL relations and on the final distance estimates. To better understand the resulting systematic effects, three sets of these three constraints were used: strong restrictions (0.2, 0.1, 4), moderate restrictions (0.3, 0.2, 4), and weak restrictions (0.4, 0.4, 1) in generating unweighted and phase-weighted mean intensity magnitudes.

To overcome the poor sampling of the light curve by the small number of F814W epochs, mean I magnitudes were computed by deriving corrections based on the V empirical light curve. For a given period, the closest F555W *phase points* to those observed in F814W (or the old F785LP) were used to calculate a correction to the computed I magnitude. Only F555W phase points within $\Delta\phi \leq 0.1$ were used. Any F814W observation without such an associated F555W phase point was excluded. For a given Cepheid, we used the set of matching F555W phase points to compute a mean $\langle$F555W$\rangle$ magnitude. Using its offset from the mean of all F555W epochs, scaled by the I to V amplitude ratio (0.5:1) as reported in Freedman (1988), we corrected the computed intensity mean in F814W. This procedure is similar to the procedure used for M81 (Freedman et al. 1994a).

Overall, the results from the F555W data were encouraging. The mean correction was close to zero for the mean magnitudes determined from both the unweighted and phase-weighted averages. The *mean* correction to the unweighted mean $\langle$F814W$\rangle$ magnitudes was -0.003 mag. The rms of the corrections was ± 0.062 mag, with corrections ranging from -0.18 to $+0.12$ mag. The *mean* correction to the phase-weighted mean $\langle$F814W$\rangle$ magnitudes was -0.011 mag. The rms correction was ± 0.062 mag, with corrections ranging from -0.24 to $+0.10$ mag. The largest corrections were typically only found in the weak restriction case, when the detection threshold affects the phase coverage. These offsets are reasonable since the typical light curve amplitudes (peak-to-peak) are approximately ~ 1.0 mag over our period range.

In I, the decreased light curve amplitude brought the rms scatter in the difference between the unweighted and phase-weighted mean magnitude determinations down to ± 0.04 mag, with a mean zero-point difference of $+0.01$ mag.

6.3. *Transformation to Standard BVI*

The mean F555W Cepheid magnitudes were transformed to Johnson V as prescribed by Harris et al. (1991):

$$V = \text{F555W} - 0.0768(B-V) + 0.0254(B-V)^2 . \quad (3)$$

The WFPC2 epochs, using the Stetson (1994c) calibration, had been transformed to Johnson V and Kron-Cousins I already. Hence, the Harris transformations were required to calibrate the WFC photometry. A mean Cepheid $(B-V) = 0.80$ was used to transform F555W to V. Because of the slight period dependence on color and the slope of the instability strip in the color-magnitude diagram, the largest incurred errors in V for our sample should be $\sim +0.02$ mag for the long-period Cepheids and ~ -0.02 mag for the short-period Cepheids. These small errors could potentially change the derived slope of the V PL relation and flatten it by $+0.04$ mag over the period range $0 \leq \log P \leq 2$. However, the PL zero-point difference should be negligible in the mean.

For the 22 Cepheids with F439W magnitude uncertainties less than 0.6 mag, only 3 had associated V phase points, and so amplitude-based mean magnitude corrections could not be derived for the bulk of our sample, as was done for the I data. Even by allowing for F439W uncertainties up to 0.8 mag, there are only 7 Cepheids with associated V phase points. The mean F439W uncertainty was also 0.4 mag. Therefore, we used the mean V photometry to transform the single F439W phase points to B with the transformation from Harris et al. (1991):

$$B = \text{F439W} + 0.0915(B-V) - 0.0168(B-V)^2 . \quad (4)$$

As the B data are only being used as a consistency check, and not to derive the true distance modulus, they are not included here but are available from the first author.

The M101 outer field color-magnitude diagram.—A color-magnitude diagram (V vs. $V-I$) is shown in Figure 6 with the Cepheids marked with filled circles. The Cepheid sample spans a range of $(V-I)$ colors of 0.5–1.6, appropriate for our range of periods, although there are a few blue outliers. Only those stars with mean V errors $\leq \pm 0.2$ mag and mean I errors $\leq \pm 0.3$ mag are plotted in the CM diagram (about 20% of the total). The typical errors are ± 0.12 mag and 0.25 mag in F555W and F814W, respectively.

Table 3 lists the Cepheid periods with unweighted and phase-weighted mean V and I magnitudes, respectively. The mean differences between the two mean photometry sets resulted in slightly different slopes and relative distance moduli for the apparent period-luminosity relations derived below (see Tables 4A–4C and 5A–5C, where deeper samples lead to slightly flatter slopes).

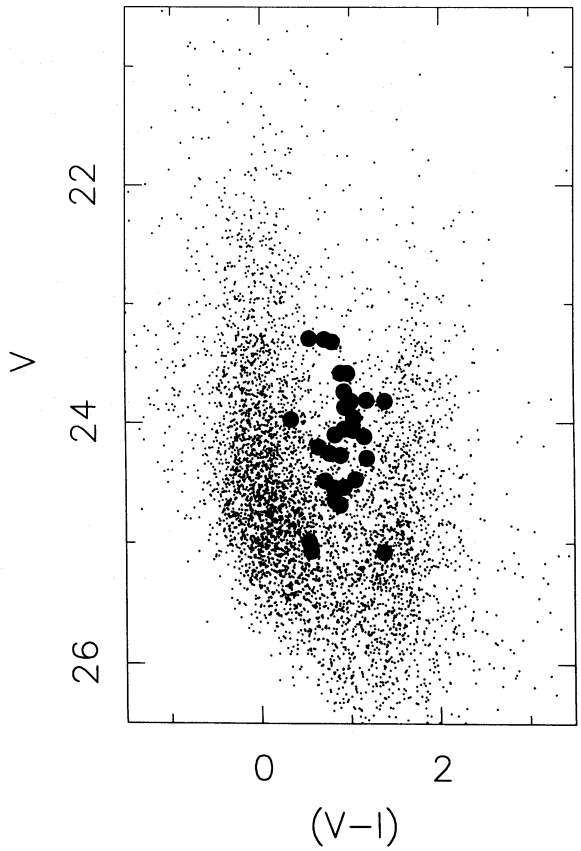

FIG. 6.—Color-magnitude diagram for the outer field of M101 showing V vs. $(V-I)$. The positions of the 29 M101 Cepheids are shown as filled circles.

TABLE 3

MEAN PHOTOMETRY OF M101 OUTER FIELD CEPHEIDS

		Unweighted Mean Photometry									Phase-Weighted Mean Photometry								
ID	P (days)	$\langle V\rangle$	σ_V	$\langle I\rangle^a$	σ_I	$\langle I\rangle^b$	σ_I	$\langle I\rangle^c$	σ_I	Δ^d	$\langle V\rangle$	σ_V	$\langle I\rangle^a$	σ_I	$\langle I\rangle^b$	σ_I	$\langle I\rangle^c$	σ_I	Δ^d
C1	58.54	23.82	0.07	22.42	0.08	22.42	0.08	22.42	0.08	0.02	23.83	0.07	22.42	0.09	22.42	0.09	22.42	0.09	−0.02
C5	47.10	23.58	0.09	22.61	0.15	22.61	0.15	22.61	0.15	0.01	23.44	0.10	22.52	0.16	22.52	0.16	22.52	0.16	0.05
C6	45.80	23.58	0.06	22.68	0.13	22.68	0.13	22.68	0.13	−0.07	23.47	0.07	22.62	0.13	22.62	0.13	22.62	0.13	−0.04
C7	43.00	23.74	0.08	22.80	0.08	22.80	0.08	22.80	0.08	−0.03	23.75	0.08	22.84	0.08	22.84	0.08	22.84	0.08	−0.04
C19	43.00	23.32	0.10	22.51	0.06	22.51	0.06	22.51	0.06	−0.01	23.32	0.10	22.54	0.06	22.54	0.06	22.54	0.06	−0.01
C20	42.50	24.11	0.07	23.00	0.09	22.95	0.08	22.95	0.08	0.10	24.11	0.07	22.96	0.10	22.93	0.08	22.93	0.08	0.08
C8	41.00	23.87	0.08	22.92	0.09	22.92	0.09	22.92	0.09	−0.02	23.88	0.08	23.00	0.09	23.00	0.09	23.00	0.09	−0.02
C9	38.00	23.30	0.12	22.58	0.11	22.58	0.11	22.58	0.11	−0.02	23.31	0.12	22.56	0.11	22.56	0.11	22.56	0.11	−0.02
C10	37.60	23.95	0.08	22.91	0.16	22.91	0.16	22.91	0.16	−0.03	24.01	0.08	22.94	0.16	22.94	0.16	22.94	0.16	−0.02
C21	33.50	23.82	0.11	22.80	0.16	22.80	0.16	22.80	0.16	0.07	23.70	0.12	22.72	0.17	22.72	0.17	22.72	0.17	0.05
C12	33.50	23.29	0.08	22.74	0.07	22.74	0.07	22.74	0.07	0.02	23.26	0.08	22.84	0.07	22.84	0.07	22.84	0.07	−0.03
C13	32.00	23.81	0.07	22.62	0.10	22.62	0.10	22.62	0.10	0.00	23.76	0.08	22.64	0.10	22.64	0.10	22.64	0.10	0.03
C22	27.30	24.05	0.08	23.11	0.06	23.11	0.06	23.11	0.06	0.02	24.01	0.09	23.12	0.07	23.12	0.07	23.12	0.07	−0.05
C23	25.60	24.47	0.12	23.41	0.18	23.41	0.18	23.41	0.18	0.02	24.52	0.12	23.46	0.18	23.46	0.18	23.46	0.18	0.01
C14	25.00	24.27	0.12	23.38	0.11	23.38	0.11	23.38	0.11	−0.03	24.34	0.12	23.45	0.11	23.45	0.11	23.45	0.11	−0.02
C11	23.70	24.25	0.10	23.48	0.11	23.48	0.11	23.48	0.11	0.05	24.22	0.10	23.58	0.11	23.58	0.11	23.58	0.11	0.00
C24	23.50	24.20	0.09	23.55	0.09	23.55	0.09	23.55	0.09	0.09	24.25	0.09	23.55	0.09	23.55	0.09	23.55	0.09	0.04
C15	23.40	24.06	0.09	...	...	23.02	0.19	23.02	0.19	−0.01	23.99	0.10	...	...	23.06	0.19	23.06	0.19	0.02
C16	22.80	24.54	0.09	...	...	23.60	0.08	23.60	0.08	0.00	24.40	0.10	...	...	23.57	0.08	23.57	0.08	0.02
C25	19.35	24.30	0.10	...	...	23.11	0.08	23.11	0.08	0.00	24.22	0.11	...	...	23.14	0.08	23.14	0.08	−0.03
C2	18.20	24.10	0.06	23.26	0.04	23.27	0.03	23.27	0.03	0.00	24.17	0.06	23.30	0.04	23.30	0.03	23.30	0.03	−0.03
C26	17.70	24.65	0.09	...	...	23.82	0.09	23.82	0.09	−0.02	24.66	0.09	...	...	23.82	0.09	23.82	0.09	−0.01
C27	17.20	23.97	0.08	...	...	23.63	0.06	23.63	0.06	−0.04	23.93	0.09	...	...	23.62	0.06	23.62	0.06	−0.01
C28	16.70	25.08	0.06	23.70	0.06	23.70	0.06	23.70	0.06	−0.08	25.04	0.06	23.66	0.06	23.66	0.06	23.66	0.06	−0.03
C3	16.67	24.68	0.12	...	...	...	...	23.80	0.13	−0.18	24.76	0.11	...	...	...	...	23.83	0.28	−0.21
C17	16.45	24.48	0.09	...	...	23.76	0.14	23.76	0.14	−0.07	24.41	0.09	...	...	23.74	0.14	23.74	0.14	−0.04
C4	14.27	24.54	0.08	...	...	...	...	23.72	0.10	−0.08	24.55	0.08	...	...	...	...	23.73	0.15	−0.09
C29	14.00	24.99	0.13	...	...	24.45	0.18	24.45	0.18	0.23	24.98	0.13	...	...	24.32	0.21	24.32	0.21	0.22
C18	13.00	25.07	0.11	...	...	24.50	0.10	24.50	0.10	−0.14	25.11	0.11	...	...	24.54	0.10	24.54	0.10	−0.16

Notes:

[a] Strong photometry restrictions (0.2, 0.1, 4).

[b] Moderate photometry restrictions (0.3, 0.2, 4).

[c] Weak photometry restrictions (0.4, 0.4, 1).

[d] Mean I magnitude correction.

7. THE DISTANCE TO M101

7.1. *Period-Luminosity Relations and Apparent Distance Moduli*

The V and I period-luminosity relations are shown in Figures 7*a* and 7*b*, where the M101 outer field Cepheids are displayed as filled circles. The LMC Cepheid PL data from Madore (1985) are superimposed as open circles. The solid lines are least-squares (unweighted) fits to the combined M101 and LMC data, shifted in relative moduli to give minimum dispersion. The LMC sample shown and used here is a sample of 22 Cepheids with both V and I photometry, with periods in the same range as the M101 outer field Cepheids ($1.0 < \log P < 1.8$). There are 25 more LMC Cepheids in this period range with V photometry. We have excluded these Cepheids from our primary sample in order to avoid imposing systematic errors, caused by differences between the two samples in V and I, on the distance determination for M101 (the effect of using these additional Cepheids is discussed below).

As was the case for M81 (Freedman et al. 1994a) and M100 (Freedman et al. 1994b), we adopted a true distance modulus to the LMC of 18.50 mag (Feast & Walker 1987), and a mean reddening for the LMC Cepheids of $E(B-V) = 0.10$ mag. Bessell (1991) gives a considerable range of values for the mean reddening for the LMC, essentially from 0.07 to 0.17 mag. Specifically for the Cepheids, he also cites values of 0.07 and 0.14 mag. However, the choice of this reddening is not crucial for the M101 distance determination, as will be shown below. We also assumed $A_V/E(B-V) = 3.30$ and the Galactic extinction law of Cardelli, Clayton, & Mathis (1989).

Inverse period-luminosity relation fitting.—In calculating the apparent distance moduli for M101, we fit the *inverse*

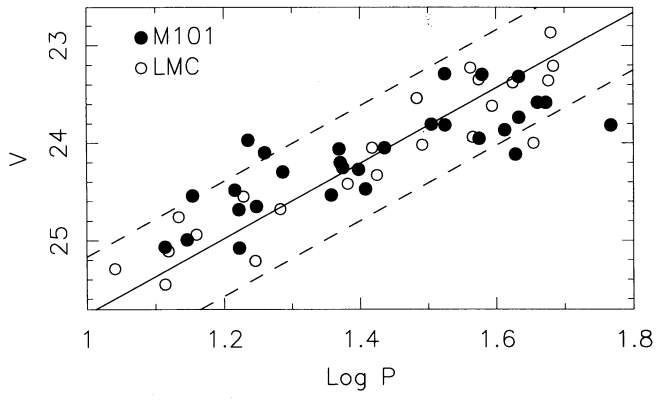

FIG. 7*a*

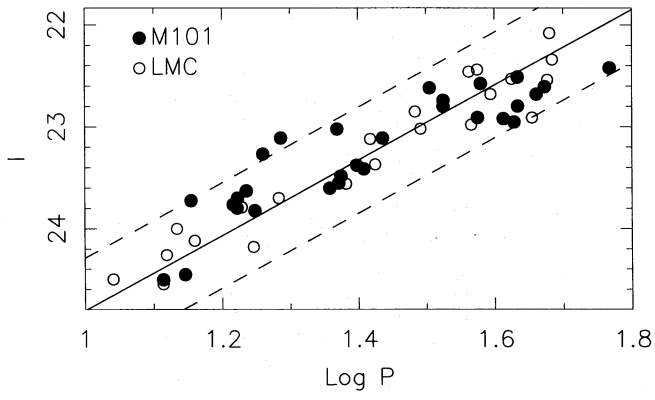

FIG. 7*b*

FIG. 7.—(*a*) and (*b*) Combined LMC and M101 V and I apparent period-luminosity relations

slope to the combined set of LMC and M101 Cepheid PL relations. The reason for this change is that traditional PL fitting of minimizing the *magnitude* residuals may be strongly affected by luminosity incompleteness. Simply put, for a given *period*, there is a dispersion in magnitude available for any star. Magnitude selection effects will cause an excess of brighter detections for any given period. Since there are no period selection effects at any given magnitude, once a star has been detected and found to be variable, there should be no consistent bias toward short or long periods. Sampling sets the window of available periods and is designed to be independent of magnitude, for a given period. While we were concerned about the bias in minimizing magnitude residuals, we did not, in fact, find a significant difference between the two different (period and magnitude residual) methods for our M101 data.

The LMC Cepheid period-luminosity relations.—For the present study, it is desirable to minimize the systematic effects in the LMC reference sample by using a common V and I set of LMC Cepheids. By using a different sample in V than in I, systematic differences between the two samples would propagate into reddening errors, possibly resulting in an erroneous distance determination. An example of the effect of using a different sample is explored below.

As was also the case for M81 and M100, we fixed the slopes of the period luminosity relations at the values derived from the LMC Cepheids. We find the following PL relations using *period* residual minimization. Over the range of periods and magnitudes, the LMC sample is assumed to be uniformly complete. For the 22 LMC Cepheids with *both* V and I magnitudes, the V and I apparent period-luminosity relations are

$$\langle V\rangle = -3.87\ (\log P - 1.4) + 13.62[\pm 0.08]\ , \quad (5)$$

$$\langle I\rangle = -3.70\ (\log P - 1.4) + 12.64[\pm 0.06]\ . \quad (6)$$

The rms scatter, *in* log P, is shown in brackets.

Using all 47 LMC Cepheids with measured V magnitudes, the V apparent period-luminosity relation is

$$\langle V\rangle = -3.87\ (\log P - 1.4) + 13.54[\pm 0.11]\ . \quad (7)$$

If the smaller set were affected by Malmquist bias, perhaps as a result of strong constraints on the LMC I data, then the smaller set should show a "brighter" PL relation zero point. However, the opposite is observed: the *larger* set of V Cepheids leads to a brighter PL relation zero point, though the difference is of marginal significance.

The choice of sets will therefore impact the determination of the V apparent distance modulus of M101 and hence the final distance. Using the larger LMC set, with its smaller zero point, leads to a longer V apparent distance modulus for M101. One might not, however, expect this difference to be a problem, except that by increasing the V apparent distance modulus, while keeping the I modulus constant, the derived M101 reddening-corrected distance modulus decreases, and the "measured" reddening greatly increases. Such a reddening determination would be erroneous and would largely be due to the systematic differences between the V and I reference samples.

Given our restricted period range in M101, one would ideally prefer to define the reference slope over a much broader range of periods. However, even if this sample of LMC Cepheids were extended down to shorter periods, contamination from overtone oscillators could complicate the comparison with M101 (Bohm-Vitense 1994). Furthermore, Cepheids with $P > 80$ days are excluded because of uncertainties in their evolutionary status and reddening (Gascoigne 1969; Martin, Warren, & Feast 1979). The importance of a longer period range is also diminished when the PL fitting is performed with period residual minimization, since magnitude bias effects are minimized.

In comparing the two V samples (those with I measurements and the complete V set), the larger sample contains more short period variables. The M101 sample is also better matched, in its period distribution, to the LMC sample with both V and I measurements. This subset, with V and I, is, again, more appropriate to use; the LMC and M101 PL relation residuals will have comparable weight over the entire period baseline.

The set of 22 does not appear to suffer from Malmquist bias as a result of the I magnitude restriction, and the set has consistent systematic biases in both filters. When the LMC Cepheid sample is expanded in the future, in both filters, the resulting systematic change in the apparent distance moduli of M101 will not have a large impact on the reddening, but primarily on the final distance, in a straightforward way. The Key Project team is engaged in an ongoing program to enlarge the LMC reference sample. As the sample grows, the team will update past distance determinations.

Period-residual minimization.—After fixing the slopes of the PL relations, we minimized the *period* residuals in the combined PL relations of the LMC and M101, weighting the individual Cepheids by a combination of their magnitude errors, period errors, and the intrinsic dispersion of the PL relation (converted to units of log P and independent of period). Magnitude errors, and the PL relation intrinsic width, increase the dispersion in period residuals for a given magnitude. The weight for a given Cepheid was defined as

$$1/\mathrm{wt}^2 = (\sigma_m^2 + \sigma_{\mathrm{PL}}^2)/b^2 + \sigma_{\log P}^2\ , \quad (8)$$

where σ_m is the star's magnitude uncertainty, σ_{PL} is the intrinsic magnitude width of the PL relation, and $\sigma_{\log P}$ is the star's period uncertainty. The magnitude errors and intrinsic width were transformed to equivalent period errors using the defined PL slope, b, determined from the above PL relations for the LMC Cepheids. The LMC Cepheids were assumed to have perfect magnitudes and periods (no errors)—i.e., in the fitting, their standard errors were set equal to the intrinsic dispersion in the PL relation. Period uncertainties for the M101 Cepheids were estimated from the widths of the appropriate period feature in the Lafler-Kinman periodicity statistic. They typically ranged from $\lesssim$0.1 days (at $P \approx$ 10–20 days) to $\lesssim$0.5 days (at $P \approx$ 50–60 days). The period uncertainties varied roughly linearly with period, so the errors in log P ($\delta \log P = \delta P/P$) were fairly constant (mean $\delta \log P \approx 0.05$). Of the three contributions to the weights, the intrinsic width of the PL relation was the largest.

Using the unweighted intensities, we find the PL relations for M101 are (for 29 M101 Cepheids in V, and 27 in I, using the "moderate" I uncertainty restrictions)

$$\langle V\rangle = -3.87(\log P - 1.4) + 24.21(\pm 0.10)[\pm 0.11]\ , \quad (9)$$

$$\langle I\rangle = -3.70(\log P - 1.4) + 23.33(\pm 0.07)[\pm 0.08]\ . \quad (10)$$

With apparent LMC moduli of 18.83 (V) and 18.65 (I), these PL relations imply apparent M101 moduli of 29.42

and 29.39 mag in V and I, respectively. The rms scatter, in log P, about the apparent PL relations in V and I are ± 0.11 and ± 0.08 mag and are values determined from the M101 Cepheids only. The excess scatter in the M101 Cepheids may come from several sources: different slopes inherent to the LMC and M101 Cepheid PL relations, errors in mean magnitude, which come from inadequate sampling of the light curve, magnitude selection effects, or even crowding for a few Cepheids. The rms scatter in units of magnitudes can be derived by multiplying the above values by the PL relation slopes. Using the phase-weighted mean magnitudes, the V and I apparent distance moduli, uncorrected for reddening, are $\mu_V = 29.40$ mag and $\mu_I = 29.40$ mag.

Magnitude-residual minimization.—The traditional slide-fitting using *magnitude* residual minimization, and, in this case, an unrestricted slope, yielded similar results. We derived the following apparent PL relations in V and I for the combined PL of the LMC Cepheids and the M101 outer field Cepheids (29 V and 27 I, based on the "moderate" magnitude uncertainty restrictions) using unweighted intensity mean magnitudes:

$$\langle V \rangle = -2.76(\pm 0.22)(\log P - 1.4) + 24.19(\pm 0.04)[\pm 0.31] , \quad (11)$$

$$\langle I \rangle = -3.12(\pm 0.18)(\log P - 1.4) + 23.31(\pm 0.03)[\pm 0.25] . \quad (12)$$

Using phase-weighted intensity mean magnitudes, we found

$$\langle V \rangle = -2.79(\pm 0.23)(\log P - 1.4) + 24.17(\pm 0.04)[\pm 0.32] , \quad (13)$$

$$\langle I \rangle = -3.11(\pm 0.17)(\log P - 1.4) + 23.31(\pm 0.03)[\pm 0.24] . \quad (14)$$

The rms scatter about these relations is given in brackets on the right. These values agree well with the rms scatter of ± 0.29 and ± 0.26 mag, reported in Madore & Freedman (1991). The unweighted intensity mean magnitudes, with the same assumptions about the LMC distance and reddening, give apparent distance moduli of $\mu_V = 29.41$ mag and $\mu_I = 29.37$ mag. The differences between the two fitting algorithms are within the uncertainties of the fits. The phase-weighted magnitudes lead to apparent distance moduli of $\mu_V = 29.39$ mag and $\mu_I = 29.37$ mag.

The B period-luminosity relation.—Unfortunately, the B data had a S/N too low to be of much use. We have determined an apparent B distance modulus and find consistency with the results from the V and I photometry; however, the scatter in the M101 PL relation is significantly larger than that for the LMC (see below).

A B band PL relation was constructed using the single phase-point observations in F439W, and the derived mean $\langle V \rangle$ photometry (for the Harris transformation to give B magnitudes). For most of the Cepheids, as noted previously, there were no closely associated V phase points, so corrections to determine mean B photometry could not be made. There were eight Cepheids with B magnitude uncertainties smaller than ± 0.3 mag. Using these eight B Cepheids, and the B-band slope of -3.14, we found

$$B = -3.14(\log P - 1.4) + 25.18(0.19)[\pm 0.59] , \quad (15)$$

which corresponds to an apparent B modulus of 29.58 mag. This B PL relation reflects a combination of the intrinsic width of the B PL (rms dispersion of 0.4 mag; Madore & Freedman 1991), *and* the random sampling of the ~ 1 mag amplitude of the light curve. Within the PL zero-point errors, this distance modulus is in agreement with the V and I moduli and the reddening curve, which is discussed below.

7.2. *Interstellar Extinction and the True Distance Modulus*

7.2.1. *Reddening*

One might expect our results to depend crucially on the adopted LMC distance and reddening, since we used the LMC Cepheid population *with* its intrinsic reddening. The derived *apparent* distance moduli do depend strongly on the assumed reddening, but fitting a Galactic extinction law to the apparent distance moduli removed the adopted LMC reddening and dereddened the M101 Cepheids at the same time.

Our approach involves finding the *relative* M101-LMC distance moduli, adding the adopted LMC distance and adopted LMC V and I extinctions, and then solving for a Galactic extinction law (Cardelli et al. 1989) at V ($\lambda^{-1} = 1.82\ \mu\mathrm{m}^{-1}$, for Johnson V) and I ($\lambda^{-1} = 1.23\ \mu\mathrm{m}^{-1}$, for Cousins I) to deduce the *difference* in reddening between the LMC and M101 Cepheid populations. One could also use B as well, but the lack of good photometry in B (and the greater potential impact of abundance effects in B; see Madore & Freedman 1991) led us to derive the reddening based on V and I.

The Cardelli et al. (1989) Galactic extinction law defines $A_I/A_V \equiv (0.77 - 0.59/R_V)$, where $R_V = A_V/E(B-V)$ (for stars of similar colors to Cepheids $R_V = 3.3$). If the apparent V and I distance moduli are μ_V and μ_I, then the true distance modulus is found as $\mu_{\mathrm{M101}} = (\mu_V - A_V)$ (also, by definition, equal to $\mu_I - A_I$). There are three known variables, μ_V, μ_I, and R_V, and two unknowns, the true distance modulus, μ_{M101}, and the visual extinction, A_V. Solving for the "true" distance modulus of M101 is a simple algebraic manipulation, because $A_V = (\mu_V - \mu_I)R_{VI}$, where $R_{VI} \equiv A_V/E(V-I) = 2.454$ (Cardelli et al. 1989).

In this process, the adopted LMC reddening and the mean M101 reddening are accounted for. This technique is insensitive to changes in the adopted LMC reddening, as long as the derived Galactic extinction law is appropriate for *both* galaxies. For the apparent distance moduli of $\mu_V = 29.42$ and $\mu_I = 29.39$, $E(B-V)_{\mathrm{LMC}} - E(B-V)_{\mathrm{M101}} = 0.07$ mag, and since we adopted $E(B-V)_{\mathrm{LMC}} = 0.10$ mag, $E(B-V) = 0.03$ mag for the M101 Cepheids. The unweighted V and I apparent distance moduli have been plotted in Figure 8, with the resulting extinction law superimposed. The true distance modulus we derived from the outer field Cepheids, based on unweighted mean intensity magnitudes, is 29.34 ± 0.17 mag, or a distance of 7.4 ± 0.6 Mpc (the exact nature of these errors are discussed below with the error budget).

This approach gives distances that are relatively independent of reddening effects. For example, we could have adopted $E(B-V) = 0.17$ mag for the LMC Cepheids, still within the range of observed total reddening for the LMC, based on polarization data (Bessell 1991). Since we solved for a Galactic extinction law, and found a reddening *difference* of 0.07 mag, the M101 reddening becomes $E(B-V) = 0.10$ mag, and the resulting true distance modulus *remains unaffected.* Only if *independent* estimates of

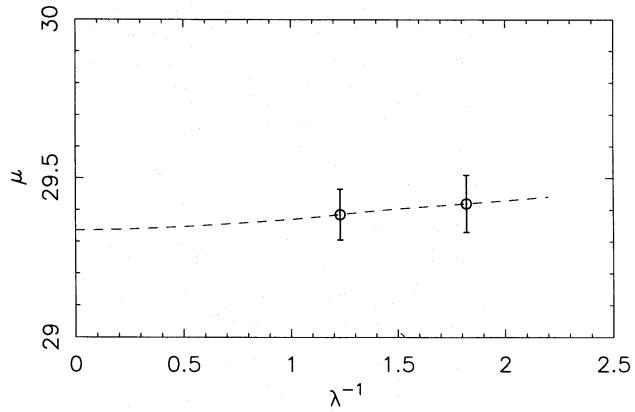

FIG. 8.—Galactic extinction law shown passing through V and I apparent distance moduli.

the reddening can be made can one be assured that the assumption of the Galactic extinction law is valid.

Other reddening estimates.—The colors of this Cepheid sample suggest that the reddening in M101 is indeed less than that for the LMC. Figure 9 shows the mean $\langle V-I\rangle$ color distributions for the LMC and M101 outer field Cepheids. The broader distribution in M101 probably reflects the large uncertainties in I. The mean LMC color is $\langle V-I\rangle_{\rm LMC} = 0.98$ mag. Using all 29 of the M101 outer field Cepheid variables, the mean color is $\langle V-I\rangle_{\rm M101} = 0.90$ mag. Comparing the two populations, using the Cardelli et al. (1989) extinction law, and adopting $E(B-V)_{\rm LMC} = 0.10$ mag, the difference in mean reddening for the two populations is 0.06 mag, leading to a mean color excess in M101 of $E(B-V)_{\rm M101} = 0.04$ mag. If we use the 23 Cepheids with the least uncertain I observations, the mean color of the M101 Cepheid population is $\langle V-I\rangle = 0.94$, leading to a mean color excess of $E(B-V)_{\rm M101} = 0.07$ mag. That is, in the mean, the M101 Cepheids are nearly as reddened as their LMC counterparts. Given the range of acceptable LMC Cepheid color excesses (up to 0.14 mag; see Bessell 1991), the reddening to the M101 Cepheids is $E(B-V)_{\rm M101} \lesssim 0.11$ mag $\approx E(B-V)_{\rm LMC}$.

The extinction for the outer field of M101 was expected to be quite low. Burstein & Heiles (1984) reported Galactic foreground reddening of $E(B-V) = -0.03$ mag (i.e., $E(B-V) \equiv 0$ mag). Because the disk itself is quite patchy, the range of M supergiant extinctions found by Humphreys et al. (1986), 0.17 mag $\leq A_V \lesssim 0.6$ mag, are consistent with our mean Cepheid color excess. However, the scatter in Tables 4A–4C and 5A–5C suggests an uncertainty in the M101 color excess of probably ± 0.05 mag.

Since the M101 distance modulus is referenced explicitly to the LMC distance modulus, any changes in the LMC distance modulus can easily be added as zero-point offsets. (This approach has been adopted for IC 1613 [Freedman 1988], M33 [Freedman, Wilson, and Madore 1991], M31 [Freedman & Madore 1990], NGC 300 [Freedman et al.

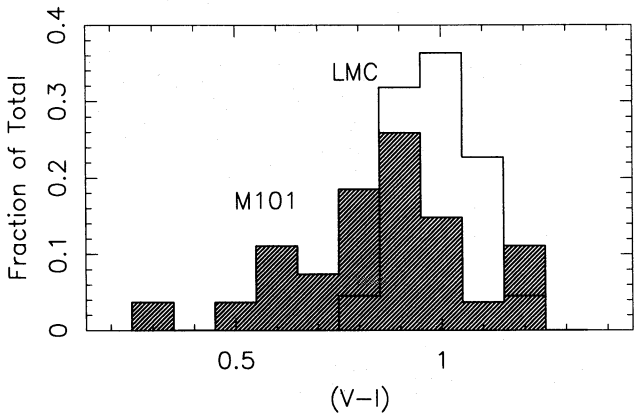

FIG. 9.—$(V-I)$ color distributions are shown for the LMC (*solid line*) and M101 outer field (*hashed*) Cepheids.

TABLE 4

RESULTS USING PERIOD RESIDUAL MINIMIZATION

A. WEAK I MAGNITUDE UNCERTAINTY RESTRICTIONS (0.4, 0.4, 1)

			Unweighted Photometry				Phase-Weighted Photometry			
Subset	N_V	N_I	μ_V	μ_I	$E(B-V)$	μ_0	μ_V	μ_I	$E(B-V)$	μ_0
All	29	29	10.59	10.67	0.04	29.29	10.57	10.67	0.03	29.32
Both	29	29	10.59	10.67	0.04	29.29	10.57	10.67	0.03	29.32
Chips 1,2,3	18	18	10.60	10.68	0.04	29.30	10.59	10.70	0.02	29.36
Chips 1,2,4	22	22	10.64	10.70	0.05	29.29	10.62	10.70	0.04	29.32
Chips 1,3,4	22	22	10.50	10.59	0.03	29.22	10.48	10.59	0.02	29.25
Chips 2,3,4	25	25	10.60	10.70	0.03	29.34	10.58	10.70	0.01	29.38
$\log P > 1.3$	19	19	10.77	10.79	0.09	29.32	10.75	10.80	0.06	29.37
$\log P < 1.5$	17	17	10.38	10.54	−0.02	29.27	10.37	10.55	−0.03	29.31
Large Amp.	15	15	10.51	10.66	−0.01	29.38	10.49	10.67	−0.03	29.43
Small Amp.	14	14	10.67	10.68	0.09	29.19	10.65	10.67	0.09	29.20

NOTE.—Derived reddenings reflect assumed LMC $E(B-V)_{\rm LMC} = 0.10$. For $E(B-V)_{\rm LMC} = 0.17$, add 0.07 to the values given above. PL relation slopes have been fixed at observed LMC values.

B. MODERATE I MAGNITUDE UNCERTAINTY RESTRICTIONS (0.3, 0.2, 4)

			Unweighted Photometry				Phase-Weighted Photometry			
Subset	N_V	N_I	μ_V	μ_I	$E(B-V)$	μ_0	μ_V	μ_I	$E(B-V)$	μ_0
All	29	27	10.59	10.69	0.03	29.34	10.57	10.70	0.00	29.39
Both	27	27	10.62	10.69	0.05	29.29	10.59	10.70	0.02	29.36
Chips 1,2,3	18	16	10.60	10.72	0.01	29.40	10.59	10.74	−0.01	29.46
	16	16	10.66	10.72	0.05	29.31	10.63	10.74	0.02	29.40
Chips 1,2,4	22	20	10.64	10.73	0.03	29.36	10.62	10.73	0.02	29.39
	20	20	10.68	10.73	0.06	29.30	10.67	10.73	0.05	29.32
Chips 1,3,4	22	20	10.50	10.62	0.01	29.29	10.48	10.62	0.00	29.32
	20	20	10.53	10.62	0.03	29.25	10.51	10.62	0.02	29.28
Chips 2,3,4	25	25	10.60	10.70	0.03	29.34	10.58	10.70	0.01	29.38
	25	25	10.60	10.70	0.03	29.34	10.58	10.70	0.01	29.38
$\log P > 1.3$	19	19	10.77	10.79	0.09	29.32	10.75	10.80	0.06	29.37
	19	19	10.77	10.79	0.09	29.32	10.75	10.80	0.06	29.37
$\log P < 1.5$	17	15	10.38	10.57	−0.04	29.35	10.37	10.57	−0.05	29.36
	15	15	10.41	10.57	−0.02	29.30	10.39	10.57	−0.03	29.33
Large Amp.	15	14	10.51	10.67	−0.02	29.40	10.49	10.68	−0.04	29.46
	14	14	10.52	10.67	−0.01	29.39	10.49	10.68	−0.04	29.46
Small Amp.	14	13	10.67	10.71	0.07	29.27	10.65	10.71	0.05	29.30
	13	13	10.72	10.71	0.11	29.19	10.70	10.71	0.09	29.23

NOTE.—Derived reddenings reflect assumed LMC $E(B-V)_{\rm LMC} = 0.10$. For $E(B-V)_{\rm LMC} = 0.17$, add 0.07 to the values given above. PL relation slopes have been fixed at observed LMC values.

C. STRONG I MAGNITUDE UNCERTAINTY RESTRICTIONS (0.2, 0.1, 4)

			Unweighted Photometry				Phase-Weighted Photometry			
Subset	N_V	N_I	μ_V	μ_I	$E(B-V)$	μ_0	μ_V	μ_I	$E(B-V)$	μ_0
All	29	19	10.59	10.76	−0.03	29.51	10.57	10.77	−0.05	29.56
Both	19	19	10.75	10.76	0.09	29.27	10.74	10.77	0.08	29.31
Chips 1,2,3	18	12	10.60	10.77	−0.03	29.52	10.59	10.80	−0.06	29.60
	12	12	10.75	10.77	0.09	29.30	10.73	10.80	0.05	29.40
Chips 1,2,4	22	16	10.64	10.80	−0.02	29.53	10.62	10.80	−0.03	29.56
	16	16	10.81	10.80	0.11	29.28	10.79	10.80	0.09	29.32
Chips 1,3,4	22	12	10.50	10.68	−0.03	29.44	10.48	10.69	−0.06	29.50
	12	12	10.69	10.68	0.11	29.17	10.69	10.69	0.10	29.19
Chips 2,3,4	25	17	10.60	10.78	−0.03	29.54	10.58	10.79	−0.06	29.59
	17	17	10.75	10.78	0.08	29.32	10.73	10.79	0.05	29.38
$\log P > 1.3$	19	17	10.77	10.82	0.06	29.39	10.75	10.83	0.04	29.45
	17	17	10.80	10.82	0.09	29.35	10.78	10.83	0.06	29.40
$\log P < 1.5$	17	7	10.38	10.60	−0.06	29.42	10.37	10.63	−0.09	29.51
	7	7	10.54	10.60	0.05	29.19	10.56	10.63	0.05	29.23
Large Amp.	15	9	10.51	10.77	−0.09	29.65	10.49	10.79	−0.12	29.73
	9	9	10.65	10.77	0.01	29.44	10.63	10.79	−0.02	29.52
Small Amp.	14	10	10.67	10.75	0.04	29.37	10.65	10.75	0.03	29.40
	10	10	10.85	10.75	0.17	29.10	10.84	10.75	0.17	29.12

NOTE.—Derived reddenings reflect assumed LMC $E(B-V)_{\rm LMC} = 0.10$. For $E(B-V)_{\rm LMC} = 0.17$, add 0.07 to the values given above. PL relation slopes have been fixed at observed LMC values.

TABLE 5

RESULTS FROM MAGNITUDE RESIDUAL MINIMIZATION

A. WEAK *I* MAGNITUDE UNCERTAINTY RESTRICTIONS (0.4, 0.4, 1)

			Unweighted Photometry						Phase-Weighted Photometry					
Subset	N_V	N_I	b_V	b_I	μ_V	μ_I	$E(B-V)$	μ_0	b_V	b_I	μ_V	μ_I	$E(B-V)$	μ_0
All	29	29	−2.76	−3.06	10.58	10.65	0.04	29.26	−2.79	−3.06	10.56	10.66	0.02	29.31
Both	29	29	−2.76	−3.06	10.58	10.65	0.04	29.26	−2.79	−3.06	10.56	10.66	0.02	29.31
Chips 1,2,3	18	18	−2.82	−3.09	10.57	10.65	0.04	29.28	−2.86	−3.11	10.55	10.67	0.01	29.34
Chips 1,2,4	22	22	−2.74	−3.00	10.60	10.67	0.05	29.26	−2.77	−2.99	10.59	10.67	0.05	29.28
Chips 1,3,4	22	22	−2.87	−3.20	10.55	10.61	0.05	29.20	−2.88	−3.18	10.53	10.61	0.04	29.23
Chips 2,3,4	25	25	−2.99	−3.22	10.59	10.68	0.03	29.32	−3.01	−3.21	10.56	10.68	0.01	29.36
$\log P > 1.3$	19	19	−3.04	−3.22	10.68	10.72	0.06	29.29	−3.04	−3.26	10.65	10.74	0.03	29.38
$\log P < 1.5$	1	17	−3.20	−3.39	10.47	10.57	0.02	29.23	−3.20	−3.36	10.46	10.59	0.01	29.27
Large Amp.	15	15	−3.20	−3.37	10.53	10.66	0.00	29.36	−3.24	−3.36	10.51	10.67	−0.02	29.41
Small Amp.	14	14	−2.77	−3.01	10.62	10.64	0.09	29.16	−2.77	−3.01	10.60	10.64	0.07	29.19

NOTE.—Derived reddenings reflect assumed LMC $E(B-V)_{LMC} = 0.10$. For $E(B-V)_{LMC} = 0.17$, add 0.07 to the values above.

B. MODERATE *I* MAGNITUDE UNCERTAINTY RESTRICTIONS (0.3, 0.2, 4)

			Unweighted Photometry						Phase-Weighted Photometry					
Subset	N_V	N_I	b_V	b_I	μ_V	μ_I	$E(B-V)$	μ_0	b_V	b_I	μ_V	μ_I	$E(B-V)$	μ_0
All	29	27	−2.76	−3.12	10.58	10.67	0.03	29.31	−2.79	−3.11	10.56	10.67	0.01	29.34
Both	27	27	−2.81	−3.12	10.59	10.67	0.04	29.28	−2.83	−3.11	10.57	10.67	0.02	29.33
Chips 1,2,3	18	16	−2.82	−3.17	10.57	10.68	0.01	29.35	−2.86	−3.20	10.55	10.70	−0.01	29.42
	16	16	−2.89	−3.17	10.59	10.68	0.04	29.31	−2.91	−3.20	10.57	10.70	0.00	29.39
Chips 1,2,4	22	20	−2.74	−3.06	10.60	10.69	0.04	29.32	−2.77	−3.06	10.59	10.69	0.03	29.33
	20	20	−2.80	−3.06	10.63	10.69	0.05	29.28	−2.83	−3.06	10.61	10.69	0.04	29.30
Chips 1,3,4	22	20	−2.87	−3.25	10.55	10.62	0.04	29.24	−2.88	−3.23	10.53	10.62	0.03	29.26
	20	20	−2.91	−3.25	10.56	10.62	0.05	29.22	−2.92	−3.23	10.54	10.62	0.04	29.25
Chips 2,3,4	25	25	−2.99	−3.22	10.59	10.68	0.03	29.32	−3.01	−3.21	10.56	10.68	0.01	29.36
	25	25	−2.99	−3.22	10.59	10.68	0.03	29.32	−3.01	−3.21	10.56	10.68	0.01	29.36
$\log P > 1.3$	19	19	−3.04	−3.22	10.68	10.72	0.06	29.29	−3.04	−3.26	10.65	10.74	0.03	29.38
	19	19	−3.04	−3.22	10.68	10.72	0.06	29.29	−3.04	−3.26	10.65	10.74	0.03	29.38
$\log P < 1.5$	17	15	−3.20	−3.43	10.47	10.59	0.01	29.27	−3.20	−3.39	10.46	10.60	−0.01	29.31
	15	15	−3.23	−3.43	10.49	10.59	0.02	29.25	−3.24	−3.39	10.47	10.60	0.00	29.30
Large Amp.	15	14	−3.20	−3.38	10.53	10.67	0.00	29.36	−3.24	−3.37	10.51	10.68	−0.03	29.43
	14	14	−3.20	−3.38	10.53	10.67	0.00	29.36	−3.23	−3.37	10.50	10.68	−0.03	29.44
Small Amp.	14	13	−2.77	−3.08	10.62	10.67	0.07	29.24	−2.77	−3.07	10.60	10.67	0.05	29.26
	13	13	−2.85	−3.08	10.66	10.67	0.09	29.19	−2.85	−3.07	10.64	10.67	0.08	29.22

NOTE.—Derived reddenings reflect assumed LMC $E(B-V)_{LMC} = 0.10$. For $E(B-V)_{LMC} = 0.17$, add 0.07 to the values above.

C. STRONG *I* MAGNITUDE UNCERTAINTY RESTRICTIONS (0.2, 0.1, 4)

			Unweighted Photometry						Phase-Weighted Photometry					
Subset	N_V	N_I	b_V	b_I	μ_V	μ_I	$E(B-V)$	μ_0	b_V	b_I	μ_V	μ_I	$E(B-V)$	μ_0
All	29	19	−2.76	−3.10	10.58	10.69	0.01	29.36	−2.79	−3.12	10.56	10.70	−0.01	29.42
Both	19	19	−3.00	−3.10	10.67	10.69	0.08	29.23	−3.03	−3.12	10.66	10.70	0.06	29.27
Chips 1,2,3	18	12	−2.82	−3.15	10.57	10.69	0.01	29.37	−2.86	−3.19	10.55	10.72	−0.03	29.47
	12	12	−2.94	−3.15	10.62	10.69	0.05	29.30	−2.99	−3.19	10.62	10.72	0.02	29.38
Chips 1,2,4	22	16	−2.74	−3.10	10.60	10.72	0.01	29.39	−2.77	−3.12	10.59	10.73	0.00	29.43
	16	16	−2.99	−3.10	10.71	10.72	0.09	29.24	−3.03	−3.12	10.70	10.73	0.08	29.28
Chips 1,3,4	22	12	−2.87	−3.19	10.55	10.64	0.03	29.28	−2.88	−3.19	10.53	10.65	0.01	29.33
	12	12	−3.07	−3.19	10.65	10.64	0.10	29.13	−3.08	−3.19	10.64	10.65	0.09	29.17
Chips 2,3,4	25	17	−2.99	−3.25	10.59	10.72	0.00	29.42	−3.01	−3.27	10.56	10.73	−0.03	29.49
	17	17	−3.25	−3.25	10.69	10.72	0.08	29.27	−3.28	−3.27	10.67	10.73	0.05	29.33
$\log P > 1.3$	19	17	−3.04	−3.27	10.68	10.75	0.04	29.37	−3.04	−3.31	10.65	10.77	0.01	29.46
	17	17	−3.06	−3.27	10.69	10.75	0.05	29.35	−3.09	−3.31	10.68	10.77	0.03	29.41
$\log P < 1.5$	17	7	−3.20	−3.35	10.47	10.62	−0.01	29.32	−3.20	−3.33	10.46	10.65	−0.04	29.41
	7	7	−3.32	−3.35	10.58	10.62	0.08	29.16	−3.32	−3.33	10.59	10.65	0.06	29.22
Large Amp.	15	9	−3.20	−3.41	10.53	10.74	−0.06	29.56	−3.24	−3.44	10.51	10.77	−0.09	29.64
	9	9	−3.31	−3.41	10.60	10.74	0.00	29.45	−3.35	−3.44	10.59	10.77	−0.03	29.52
Small Amp.	14	10	−2.77	−3.08	10.62	10.67	0.06	29.24	−2.77	−3.08	10.60	10.67	0.05	29.27
	10	10	−3.02	−3.08	10.75	10.67	0.16	29.06	−3.03	−3.08	10.74	10.67	0.15	29.07

NOTE.—Derived reddenings reflect assumed LMC $E(B-V)_{LMC} = 0.10$. For $E(B-V)_{LMC} = 0.17$, add 0.07 to the values above.

1992], M81 [Freedman et al. 1994a], and M100 [Freedman et al. 1994b; Ferrarese et al. 1995].)

7.2.2. *Systematic Effects—Sample Biases*

The LMC reference sample.—Much of the disagreement on the distance scale is due to systematic biases. We endeavored to minimize such potential biases in our results. For example, for the LMC Cepheids, we chose a sample with *both V* and *I* photometry, so that this comparison data set should not suffer from systematic effects affecting only one of the two filters. To test the effects of using different LMC samples in each filter, we also performed the unconstrained slide-fitting using the 47 Cepheids with *V* magnitudes from Madore (1985) within our period range. In the magnitude-residual fitting, the resulting distances and reddenings were almost always identical to those found with the set of 22 LMC Cepheids with *both V* and *I*. In a few of the M101 Cepheid subsets, the resulting true distance modulus changed by a hundredth of a magnitude. However, in the inverse-fitting, the *V* apparent modulus is systematically

0.08 mag longer. Since the I modulus does not change, the reddening-corrected distance modulus is 0.07 mag shorter. The best-fit V apparent PL relations in the two cases are identical, despite the shift of the larger set of LMC Cepheids to a greater M101 distance. The 1 σ width of the LMC V PL relation already accounts for zero-point errors on the order of 0.06 mag (from 0.29 mag/$N^{1/2}$), so a 0.08 mag shift caused by including 25 more LMC Cepheids in V is not surprising.

While the use of a set of Cepheids in the LMC that has both V and I measurements is desirable, as noted above, one issue that could arise concerns how they were chosen. The I set is a subset of the larger V set. If there was any selection bias in that subset of the larger V sample that was measured in I, this could potentially impact the final modulus.

The M101 Cepheid subsets.—A variety of checks was performed on the M101 sample by selecting various subsets of the M101 Cepheids and comparing the resulting distance moduli. These subsets allowed us to test the robustness of our reddening-corrected distance modulus. Tables 4A–4C list relative distance moduli (μ_V, μ_I), reddenings [$E(B-V)$], and true distance moduli (μ_0), for the different subsets using the unweighted and phase-weighted mean intensity magnitudes.

We also performed the same analysis using *magnitude* residual minimization with unrestricted slopes. In Tables 5A–5C, we include the resulting slopes (b_v, b_I), as well as relative distance moduli (μ_V, μ_I), reddenings [$E(B-V)$], and true distance moduli (μ_0). We opted to fit both the slope and intercept using this "traditional" method to identify how any luminosity selection effects may have biased the observed PL relations in slope *and* zero point. One can also test the accuracy of this presumably biased fitting method by comparing its results to the presumably unbiased, inverse fitting method.

For each of the different Cepheid subsets, we derived distances using those M101 Cepheids with *both* V and I mean photometry. We also varied the restrictive criteria that defined quality I photometry (see § 6.2). Two period groupings of the Cepheids were also fitted (log $P > 1.3$ and log $P < 1.5$). These subsets offered the largest changes in *relative* distance moduli. The fainter, short-period subset clearly showed evidence for a Malmquist-like bias, giving shorter estimates for the relative distance moduli. The resulting *true* distance modulus, however, remained essentially unaffected.[14] The changes in relative distance moduli, between the different period subgroupings, are probably not due to systematic differences in the period-luminosity relations for the fundamental and first overtone oscillation modes (see Bohm-Vitense 1994). The transition period is considered to be about 9 days, so it is unlikely that any of our short-period Cepheids systematically oscillate in the first harmonic (the shortest period in our sample is 13 days).

Contamination effects.—We also tested for contamination by unresolved neighboring stars and compared subsets of Cepheids with large and small amplitudes (we adopted an amplitude cut at about 1 mag). Contamination from unresolved neighbors would increase the measured brightness and could decrease observed light-curve amplitudes, if the neighbor is of comparable luminosity to the Cepheid (provided the Cepheid amplitude is not decreased to the point where it is unlikely to be found!). The small-amplitude subset should contain both intrinsically small-amplitude Cepheids, whose apparent magnitudes are not affected by neighbors, and large-amplitude Cepheids, whose variability is partially masked by the additional light of close neighbors. The large-amplitude subset should be mostly uncontaminated by neighbors. In V, the relative modulus between the small and large-smplitude subsets differed by up to +0.06 mag, in the sense that small-amplitude Cepheids appear more remote. However, serious contamination effects in the small-amplitude subset should have led to a *shorter* distance estimate, because these Cepheids would be spuriously brighter in the mean. This effect is likely to be present in both filters, approximately equally.

However, in I the effect of contamination was obscured by other uncertainties. For example, small-amplitude Cepheids with large I uncertainties gave an I relative modulus 0.09 mag *fainter* than the relative modulus of the large-amplitude subset. Since the amplitude-based subsets gave counterintuitive changes in the distance, this suggests that there are no substantial contamination effects in the overall Cepheid sample. As another check, in individual cases, visual inspection can be made of the typical environments of our Cepheids in the F555W image subsections shown in Figure 4.

The effects of incompleteness and selection biases.—The effects of incompleteness can be seen explicitly in Table 3, Tables 4A–4C, and Tables 5A–5C. Table 3 illustrates the effects of the I uncertainty restrictions on individual Cepheids. As larger magnitude errors are allowed, more Cepheids are included in the sample, with increasing mean magnitude uncertainties. Tables 4A–4C and 5A–5C illustrate how incompleteness affects the distance estimate. In particular, the Cepheid search was carried out in V, and the sample is intrinsically incomplete at the faint end. This resulted in up to a 0.39 mag difference between the long (log $P > 1.3$) and the short (log $P < 1.5$) period *relative* V distance moduli.

In I, the effects of incompleteness are spread across the broad color distribution. Subsets compared between the different I uncertainty restrictions lead to changes in the zero points and slopes in the apparent PL relations. In comparing PL relations derived from using tight limits on the I photometry quality, we see steeper slopes in the I PL relations than the slopes derived from subsets with less stringent limits on the I photometry quality. The results, as expected, are shorter relative I distance moduli. However, the reddening changes to compensate for these distance biases, and the true distance modulus remained generally unaffected to ± 0.05 mag in the magnitude residual minimization process. For a few subsets, larger differences were observed. However, the small samples within these subsets (as few as seven in one subset!) contribute large uncertainties to the relative distance moduli because of the intrinsic width of the PL relation.

The largest effect observed in the different I selection criteria is the impact that inconsistent V and I samples have on the distance and reddening determination. We argued earlier that we needed to use a consistent sample of LMC Cepheids in both filters. If we do not impose this restriction on the M101 Cepheids, e.g., by using the most restrictive criteria in selecting our I-band Cepheids, the distance esti-

[14] The reddening typically changed to compensate—without an independent check on the reddening, this is expected, though, as noted, the Cepheids themselves provide upper limits to the reddening.

mate can be severely impacted. As was the case for the LMC V-band Cepheid sample, the different M101 I-band samples can lead to different apparent distance moduli, on the order of $\sigma/N^{1/2}$. These changes translate to artificial reddening differences between the subsets. When we impose the strongest restrictions on the I sample, *and* only include those Cepheids measured in both V and I (19 Cepheids), the true distance modulus is 29.27 mag. In the more moderate and weak I selection criteria, the dual V and I Cepheid samples both lead to a reddening-corrected distance modulus of 29.29 mag. In other cases, strong I restrictions *and* smaller numbers of Cepheids change the I apparent distance modulus by up to $+0.07$ mag. With an unchanged V modulus, the subsets can lead to changes in the reddening-corrected distant modulus of $+0.17$ mag. However, when one restricts the M101 V sample to those present in the I constrained subset, the distance moduli are better behaved; both V and I relative distance moduli shift together. When this occurs, the reddening to the M101 Cepheids dictates the change in V modulus with respect to the I modulus offset. Therefore, the reddening of the M101 Cepheids is only meaningful when similar sets of Cepheids are used in both V and I.

Upon examination of the Cepheid subsets and I uncertainty effects, one clearly sees that the M101 sample suffers from magnitude selection effects. While clearly present, the biases are reassuringly small (at the level of $<|0.1|$ mag, based on a simple comparison of our least-squares fit slopes and the PL relation slopes from Madore & Freedman 1991). However, in spite of these different sample selection effects, the derived *true* distance modulus remained fairly constant for subsets and I error restrictions. Note, as well, that some subsets lead to negative estimates of the reddening. While physically meaningless, negative color excess, in this context, implies that the LMC Cepheid color excess was underestimated.

We feel that the current tests indicate that systematic errors have had a very small impact on our distance determination. As noted previously, the team is developing a suite of tests and simulations to explicitly study the effects of our selection processes on distance estimates, as part of its ongoing work. Artificial star experiments will serve as the primary test bed for incompleteness and other systematic biases. With our sample and simple tests using Cepheid subsets and photometry constraints, we have been able to measure the distance to M101 with a minimum of systematic biases.

7.2.3. *Systematic Effects—Flat-Fielding*

Systematic effects from flat-fielding errors were also considered. If the Cepheids resided on one part of a single CCD, then a relative distance modulus based solely on those Cepheids would systematically be offset by any large-scale flat-fielding error. However, two features of this particular data set naturally work against such a systematic effect. First, there are four distinct CCDs. Any systematic bias arising from preferential location would need to be repeated in all four CCDs, in locations consistent with the same flat-fielding errors, for some large fraction of our Cepheid sample. Second, and more importantly, our data were obtained at several different roll angles. This proved to be a useful feature of the distribution of roll angles (indeed the only one!).

The first set of observations had rotations of up to 20°. Any PL relation based on observations consistently in a large depression or enhancement in the flat field could indeed contain flat-fielding *systematic errors* arising from the flat-field structure consistent with the largest rotation angle. However, the second set of observations had a consistent roll angle around 90° from the first epoch. For example, CCD No. 1 objects from the early observations were placed in CCD No. 2 in the next set of observations. Mean CCD-to-CCD zero-point offsets come from stars all across the CCDs. Any star with a flat-fielding error in the first set observations would have an uncorrelated flat-fielding error in the second set of observations. Figure 6 of Phillips et al. (1994) shows that the flat-fielding errors for a given position are uncorrelated from one CCD to the next. The third set of roll angle offsets ranged from 0° to ~45°, leading to further decorrelation of flat-fielding errors. Third, our Cepheids were scattered around the field. Flat-field effects on the *mean* derived modulus would be beaten down by a further factor of up to $N^{1/2}$ from the number of Cepheids in the sample, assuming that the Cepheids are uniformly spatially distributed.

The F555W calibration, discussed in detail in Appendix A, was consistent for both the Medium Deep Survey flat-field corrected and uncorrected ALLFRAME magnitudes. The largest zero-point difference was 0.02 mag. As an *extreme* example, one Cepheid has *individual* data points with typical flat-field corrections of ± 0.08 mag. However, its *mean* magnitude changed by less than 0.01 mag. Again, the distribution of rotations helped alleviate flat-fielding errors.

In summary, even where large flat-field corrections have been applied, mean magnitudes derived from the full set of images show little change when the flat-field corrections were applied (the rms offset was ± 0.016 mag). For the CCDs with no distinct localization of secondary standards, the flat-fielding errors are a source of scatter in the individual observations of a single star. The distribution of roll angles helped minimize any systematic effects caused by errors in flat-fielding, not merely in the mean for the entire population of stars, but even *in the mean* for *individual* stars.

7.3. *The Error Budget of the True Distance Modulus*

An initial estimate of the final error can be seen by comparing the distance moduli from the different Cepheid subsets. Some of the subsets gave distance moduli that were noticeably larger or smaller (though only by $\lesssim|0.1|$ mag). Quantitatively, the error budget has been split into four parts: (1) the uncertainty in the LMC distance modulus, (2) the uncertainty in the ALLFRAME calibration, (3) the uncertainty in the zero point for long versus short exposure times, and (4) the uncertainties due to the widths of the V and I PL relations. Of these, (2) is the dominant uncertainty at ± 0.13 mag after propagation through the reddening curve. The contribution from (1) is not quite as large (± 0.10 mag), and the contributions from (3) and (4) are both small (± 0.03 mag), bringing the total uncertainty in the reddening-corrected distance modulus to ± 0.17 mag. Table 6 lists these factors in our error budget.

1. Reviews, such as those by Feast & Walker (1987), quote distances to the LMC from a variety of methods, including main sequence fitting, and Cepheid and RR Lyrae distance determinations. These distance moduli range from 18.1 to 18.7 mag. Schmidt et al. (1994) cite a distance to SN 1987A of 49 ± 4 kpc, or a modulus of 18.45 ± 0.16 mag. We

TABLE 6

THE ERROR BUDGET FOR THE TRUE DISTANCE MODULUS TO M101

Source of Uncertainty	Error (mag)	Error in True Distance Modulus (mag)
[A] LMC true distance modulus	±0.10	±0.10[a]
[B] F555W calibration	±0.06	...
[C] F814W/F785LP calibration	±0.04	...
[D] [B] and [C] are uncorrelated[b]	...	±0.13
[E] Long vs. short exposure-time correction	±0.03	±0.03[a]
[F] Cepheid V-band intrinsic width	±0.08	...
[G] Cepheid I-band intrinsic width	±0.06	...
[H] [F] and [G] are correlated[c]	...	±0.03[a]
Total (Quadrature Sum of [A], [D], [E], [H])	...	±0.17

[a] Systematic errors; see text.

[b] These uncorrelated uncertainties must be dereddened before being added in quadrature. A given systematic error, ϵ_V, in the V calibration leads to an error in the true distance modulus of $(1 - R_{VI})\epsilon_V$. From Cardelli et al. 1989, $R_{VI} = A_V/E(V-I) = 2.45$. Likewise, a systematic error in the I calibration, ϵ_I, will produce an error in the true distance modulus of $R_{VI}\epsilon_I$. Summed in quadrature, the total calibration error is $\sigma_D^2 = \epsilon_V^2(1 - R_{VI})^2 + \epsilon_I^2 R_{VI}^2$.

[c] The errors δ_V and δ_I, due to the V and I PL relation intrinsic widths, are treated as correlated (see Freedman et al. 1991, 1994b), since these errors are derived from nearly identical populations. When the two correlated errors, δ_V and δ_I, are propagated through the reddening curve, the total error in the true distance modulus is $\sigma_H^2 = [\delta_V(1 - R_{VI}) + \delta_I R_{VI}]^2$.

chose an uncertainty of 0.10 mag for our adopted LMC distance modulus of 18.50 mag (see item [A] in Table 6).

2. The uncertainties in the F555W and F814W/F785LP calibration were derived from Table A3 in Appendix A. We adopted uncertainties using the mean standard deviation in each of the four CCDs (using the dispersions between the calibration sources). We summed these initial estimates, in quadrature, with ±0.03 mag, our estimate for any unresolved differences between the calibrated WFPC2 ALLFRAME and DoPHOT systems. We corrected our WFPC2 magnitudes by approximately half of the trend observed in the globular clusters (as discussed in Appendix A, Stetson 1994c applied a correction ranging from −0.04 mag, at row 800, to 0 at row "0") and carried an additional uncertainty equal to the applied amplitude (±0.02 mag). Lastly, our F814W calibration is based on the assumption that the instrument zero point did not change with the decrease in operating temperature. We believe this is true to better than ±0.02 mag in the PC and WF3 CCDs. However, no measurements have been made in the other two CCDs to confirm this result. Therefore we added, in quadrature, another uncertainty of ±0.02 mag to the F814W calibration error estimate.

The F555W and F814W/F785LP calibration contributions to the error budget were determined to be ±0.06 and ±0.04 mag, respectively (see items [B] and [C] in Table 6). The contribution to the error budget from flat-fielding errors is assumed to be negligible, based on previous discussions. For the combined calibration contribution to the final error estimate, the F555W and F814W/F785LP calibrations were assumed to be uncorrelated. As shown in Table 6, their uncertainties were propagated through the reddening curve and summed in quadrature for a final contribution of

$$\sigma_u^2 = \epsilon_V^2(1 - R_{VI})^2 + \epsilon_I^2 R_{VI}^2 , \quad (16)$$

(see Table 6, item [D]) where $\sigma_u = \pm 0.13$ mag. $R_{VI} = A_V/E(V-I) = 2.45$ was determined from $A_I/A_V = 0.77 - 0.59/R_V$ (Cardelli et al. 1989).

3. The estimate of the calibration uncertainty, however, is not complete. Our calibration of the WFPC2 data includes a zero-point correction of 0.050 mag, determined from a comparison of long and short exposures of Galactic globular clusters. While it is likely that the Stetson (1994c) exposure-time correction is applicable to the high-background long exposures of M101, more observations are required to calibrate the effect and understand its source. Had our calibration ignored this correction, the true distance modulus would be 0.05 mag *shorter*, for a 2.5% shorter distance. This effect is small but still important. It is included as a potential systematic error of ±0.03 mag (Table 6, item [E]).

4. The final component of the error budget is due to the observed width of the PL relation. To estimate δ_V and δ_I, the errors in the V and I moduli due to the finite sampling of the intrinsic widths, the 1 σ intrinsic widths are combined with the number of Cepheids in the joint PL relations. The following expression arises because we are trying to measure the *difference* between two underlying fiducial PL relations with finite sampling in both.

$$\delta^2 = \sigma_{\rm width}^2 \left(\frac{N_{\rm LMC} N_{\rm M101}}{N_{\rm LMC} + N_{\rm M101}} \right)^{-1} . \quad (17)$$

The error budget contributions from the V and I PL relation dispersions were found to be $\delta_V = \pm 0.08$ and $\delta_I = \pm 0.06$ mag, and are listed as items [F] and [G] in Table 6. These errors, however, are correlated since they are derived from identical populations. After propagation through the reddening curve, the error contribution from sampling the V and I intrinsic widths was found to be

$$\sigma_c^2 = [\delta_V(1 - R_{VI}) + \delta_I R_{VI}]^2 , \quad (18)$$

where $\sigma_c = \pm 0.03$ mag (given as item [H] in Table 6). Note that the well-defined ratio of V and I 1 σ PL relation dispersions and the common sample in both V and I imply a simple correlation of the errors ($\delta_V \propto \delta_I$).

The total error in the M101 reddening-corrected distance modulus is a combination of the random and systematic

errors described above. The calibration uncertainties lead to a random error of ± 0.13 mag. The residual systematic uncertainties are ± 0.10, ± 0.03, and ± 0.03 mag, arising from errors in the LMC distance modulus, the WFPC2 exposure-time correction, and sampling of the PL relation width, respectively. This leads to a new M101 distance modulus of 29.34 mag ± 0.13 mag (random), ± 0.10, ± 0.03, and ± 0.03 mag (systematic); when combined in quadrature this equals 29.34 $\pm$ 0.17 mag.

8. DISCUSSION

De Vaucouleurs (1993) has emphasized the role that M101 plays in the extragalactic distance scale debate. Past distance estimates have clearly not converged to a value consistent with the typical quoted errors. To illustrate the full range of distances reported over the last 20 years, Table 10 of de Vaucouleurs (1993) shows distance moduli for M101 from 1973 to 1986, extending from an upper limit to the distance modulus of 28.4 mag (Humphreys et al. 1986) to 29.5 mag (the upper limit of the Cook et al. 1986 result), equivalent to a range of 5–8 Mpc in distance.

After finding 29 Cepheid variables in M101, we derived a true distance modulus of 29.34 $\pm$ 0.17 mag, corresponding to a distance of 7.4 $\pm$ 0.6 Mpc. We derived a mean reddening of $E(B-V) = 0.03$ mag for the Cepheid population. These values are based on an LMC distance modulus of 18.50 mag and a reddening of $E(B-V)_{\rm LMC} = 0.10$ mag. The color distribution of our Cepheid sample indicates that the *mean* reddening of the M101 Cepheids is probably $E(B-V) \lesssim 0.11$ mag, though likely to be $E(B-V) \sim 0.05$ mag. There are three primary contributions to our estimate of the error in the distance. The uncertainty in the LMC distance and the calibration uncertainty have approximately equal weight in our error budget. The natural widths of the PL relations form the third component, though with a smaller impact than the other two sources of error.

The new Cepheid distance agrees with the larger distances derived by Sandage & Tammann (1974) and Sandage (1983). In addition, the expanding photosphere distance determinations to M101, based on SN 1970G have favored the longer distance estimate, with a modulus of $\sim$29.35 mag ($D_{\rm EPM} = 7.4^{+1.0}_{-1.5}$ Mpc; Schmidt et al. 1994).

The recent Tully-Fisher distance modulus of 29.2 $\pm$ 0.5 mag from Pierce (1994), while extremely uncertain, is consistent with our Cepheid distance. Since M101 is nearly face-on, it is not itself useful as a Tully-Fisher calibrator. M101 is important, however, as a distance calibrator for the M101 group (Aaronson et al. 1982), which contains the infrared Tully-Fisher calibrating galaxies Ho IV, NGC 5204, and NGC 5585. (All these galaxies have galactocentric recession velocities between about 250 and 400 km s^{-1}.) Early Tully-Fisher line width analysis (Fisher & Tully 1975) assumed the Sandage & Tammann (1974) distance to the group (7.2 Mpc).

Cook et al. (1986) found a relative M101-LMC modulus of 10.8 with two Cepheids from KPNO 40 m CCD R-band images. Using an LMC distance of $\mu_0 = 18.50$, $E(B-V)_{\rm LMC} = 0.10$, and $A_R/A_V = 0.8686 - 0.3660/R_V$ (Cardelli et al. 1989), the *apparent* R distance modulus of 29.55 mag (shown on our reddening curve as an open square) leads to a true distance modulus of 29.47 mag, which is consistent with our new distance.

Alves & Cook (1995) added two Cepheids to the Cook et al. (1986) study and derived a shorter distance modulus, 29.08 $\pm$ 0.13 mag, to M101, assuming a distance modulus of 18.4 mag to the LMC. Their four Cepheids lie in the upper half of our V and I PL relations. The agreement is encouraging, given their small sample. After the difference in the LMC distance modulus is accounted for, their distance is within 1 σ of our result.

The abundance dependence of the PL relations remains an open issue. Past studies, such as in M31, did not find a significant effect (see Madore & Freedman 1991). However, Gould (1994) found a large effect, of up to $\Delta\mu = 0.88 \pm 0.16$ mag $\times \Delta$[Fe/H] (Δ[Fe/H] is the abundance difference between the galaxy and the LMC).

Fortunately, our new distance to M101 should not be affected by any uncertainty introduced by abundance differences. Zaritsky et al. (1994) measured abundances from H II regions and quote an [O/H] gradient of -0.14 dex/ρ_s (where $\rho_s = 2'.11$, the disk scale length). The outer field oxygen abundance is 12 + log O/H = 8.37 $\pm$ 0.15, versus 9.0 $\pm$ 0.15 for the inner field (Zaritsky et al. 1994). The abundance in the outer field is thus comparable to the LMC with $z/z_{\rm LMC} \approx 1.1$.

While not a factor here, abundance differences are an issue for other galaxies. M101 will provide a means to test the degree to which the distance modulus is abundance sensitive. The factor of 4–5 change in abundance between the M101 inner and outer fields will enable the Key Project to calibrate any effect, if present. Data from the inner regions of M101 will be used to compare with these new data to aid in solving for the PL relation's dependence on metal abundance.

M101 is clearly a large galaxy. At a distance of 7.4 Mpc, the disk scale length of 2'.1 corresponds to 4.8 kpc. M101's isophotal radius of 14'.4 (de Vaucouleurs et al. 1991) corresponds to 32 kpc. Sandage (1993) attempted to use the isophotal diameters of Sc galaxies as standard rods to derive H_0. The Freedman et al. (1994b) (and Ferrarese et al. 1995) distance to M100, an Sc galaxy in the Virgo cluster, however, implies a scale ratio of isophotal diameters for these two ScI galaxies of about $D_{25,\rm M101}/D_{25,\rm M100} \approx 2$.

9. SUMMARY

Despite the many problems intrinsic to the data set (the aberrated PSF, crowding, epoch-to-epoch rotations, and aliasing), 29 Cepheids have been found, including the recovery of two Cepheids previously discovered by Cook et al. (1986). These yielded an M101 distance modulus of 29.34 mag ± 0.13 mag (random), ± 0.10, ± 0.03, and ± 0.03 mag (systematic). These uncertainties, combined in quadrature, give 29.34 $\pm$ 0.17 mag (7.4 $\pm$ 0.6 Mpc). This new distance modulus is in good agreement with the previous Cepheid distance estimates, EPM distance estimates, and a recent Tully-Fisher reanalysis, yet provides a much more accurate value for the distance.

The M101 outer field data set contains data from two *HST* instruments, the WFC and WFPC2. The WFC and WFPC2 calibrations (Phillips et al. 1994; Holtzman et al. 1995b; Stetson 1994c) are clearly consistent to better than 5%. Freedman et al. (1994a), Stetson (1994c), and Hill et al. (1995) also show that the WFPC2 calibration is consistent with their ground-based calibration. Despite the agreement

in these sources, our calibration uncertainty makes up nearly half of the uncertainty in our distance to M101.

The continued use of *HST* to measure Cepheid distances to roughly 20 galaxies will allow us to set accurate zero points for these and other secondary distance indicators. Currently, the independent secondary distance indicators suffer from systematic differences that are poorly understood (Jacoby et al. 1992). New Cepheid-based distances will finally solve many of the discrepancies between the different techniques. The Key Project's continued use of WFPC2, with its secure calibration, ensures that the Key Project's goal of H_0 to 10% is within reach.

The work presented in this paper is based on observations with the NASA/ESA *Hubble Space Telescope*, obtained by the Space Telescope Science Institute, which is operated by AURA, Inc. under NASA Contract NAS 5-26555. Support for this work was provided in part by NASA through grant GO-2227-87A. The first author would also like to acknowledge the team's seemingly infinite patience. The team would also like to acknowledge the referee's valuable comments regarding sample biases and period-luminosity relation fitting. B. F. M. was supported in part by the NASA/IPAC Extragalactic Database (NED) and by the Jet Propulsion Laboratory.

APPENDIX A

CALIBRATION

The calibration of our data involves several steps and utilized several different calibration sources. Our primary calibration of the WFC observations is based on the calibration of our WFPC2 data. We have additional ground-based photometry from the Cook et al. (1986) and Alves & Cook (1995) Cepheid search as well, and these data provide for an additional check on our final calibration along with the Medium Deep Survey WFC instrument zero points.

The adopted calibration.—For the final calibration, we adopted the WFPC2-based calibration, because it is derived from observations of *several* globular clusters, with data from a variety of exposure times. Because of a possible exposure-time dependence of the WFPC2 zero point (Stetson 1994c, and explained earlier), we prefer to base the calibration of our WFPC2 observations on the combined data set of ω Cen, NGC 2419, and Pal 4 rather than on Holtzman et al. (1995b), whose WFPC2 calibration is based on observations of a single cluster, with constant, short exposure times for each filter. In the short-exposure regime, the Stetson (1994c) zero points agree to within ± 0.02 mag of the Holtzman et al. (1995b) zero points. However, our exposures are not in the "short-exposure regime" and Stetson (1994c) shows a $+0.050 \pm 0.007$ mag offset in the instrument zero point for long WFPC2 exposures (for $\gtrsim 1000$ s, there are too many counts for the short-exposure zero points to remain valid).

A1. CALIBRATION USING WFPC2 OBSERVATIONS AND ZERO POINTS

The inclusion of WFPC2 observations in the data set naturally provides an independent calibration of our photometric zero point. The uncertainties in the zero points given in the WFPC2 Status Report (Holtzman et al. 1995b) are expected to be quite small. Gilliland (1994) gives zero points derived from comparison of WFPC2 photometry with ground-based observations of M67. The zero points he derived are consistent with the Status Report zero points for F555W and F814W. The ground-based calibration for M100 (Hill et al. 1995) also confirms the WFPC2 Status Report zero points to ± 0.02 mag. Stetson (1994c) has determined V and I WFPC2 zero points using ground-based photometry in the globular clusters ω Cen, Pal 4, and NGC 2419. In the short-exposure limit, these globular cluster zero points also agree with the Status Report to better than ± 0.02 mag.

An STScI memo dated 1995 March 14 shows a history of observed counts for GRW + 70D5824 in several filters. According to the memo, based on data from Proposals 5563 and 6143, the cold zero points in F814W are essentially unchanged from the warm zero points (the PC CCD zero point changed by -0.02 ± 0.02 mag while the WF CCD No. 3 zero point changed by $+0.01 \pm 0.03$ mag). Figure 10 shows the count ratio history, for the PC and WF3 CCDs, in F814W. We therefore treat any residual F814W zero-point change as a ± 0.02 mag *uncertainty* in the F814W calibration.

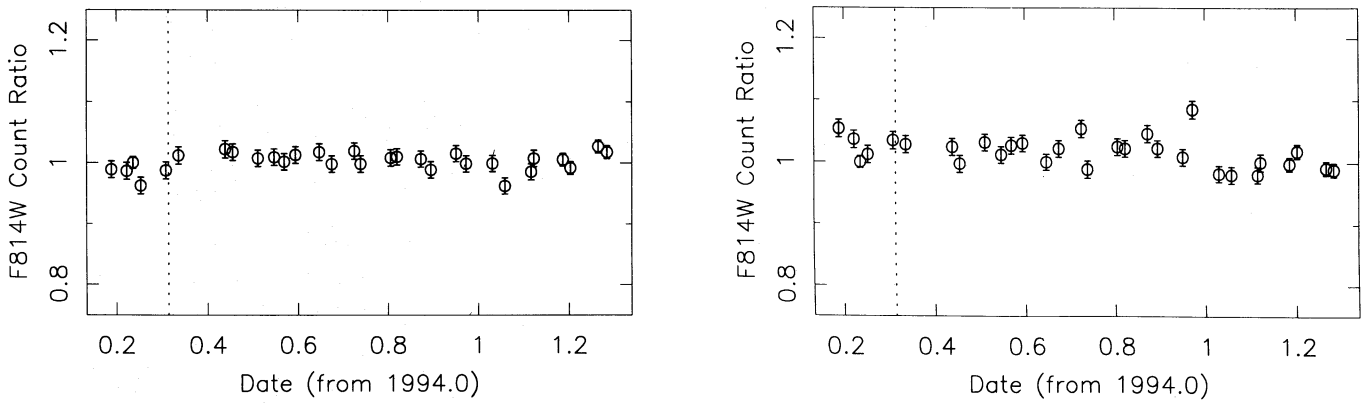

FIG. 10.—GRW + 70D5824 Count ratio histories for the WFPC2 PC and WF3 CCDs in F814W. Observations have been normalized by the observed counts from 1994 March 25. The change in operating temperature is signified by the dotted vertical line.

The WFPC2 instrumental system.—The WFPC2 ALLFRAME reduction included a photometric zero point of 25 mag (≡1 DN). The WFPC2 was chosen to have a radius of 1".0, i.e., the ALLFRAME magnitudes were integrated magnitudes inside a 1".0 radius aperture. Due to focus variations and telescope jitter, the ALLFRAME magnitudes are not strictly equivalent to aperture magnitudes through a 1".0 radius. Additional aperture corrections are needed. Furthermore, the Holtzman et al. (1995b) and Stetson (1994c) zero points are defined for 0".5 radius aperture magnitudes. We needed to correct our ALLFRAME magnitudes to the system of 0".5 radius aperture magnitudes.

Growth curve analysis on 100 of the brightest, isolated stars in the four WFPC2 F814W exposures and the seven F555W exposures was used to derive the appropriate aperture corrections in F814W and F555W. Using DAOGROW (Stetson 1990) to extrapolate model growth curves (fitted to observed curves obtained in each of the images), we found that corrections of -0.172 ± 0.009 mag (PC), $+0.023 \pm 0.002$ mag, $+0.010 \pm 0.005$ mag, and $+0.001 \pm 0.004$ mag were required for the four CCDs in F814W. In F555W, the aperture corrections were -0.022 ± 0.004 mag (PC), -0.031 ± 0.002 mag, -0.126 ± 0.004 mag, and -0.061 ± 0.008 mag, for the four respective CCDs. These aperture corrections are only valid for these exposures, the respective PSF-fit magnitudes derived from a particular set of PSFs, using specific fitting radii, and other parameters involved in the reduction.

Calibration of WFPC2 instrumental magnitudes.—Holtzman et al. (1995a) asserts that the WFPC2 flat fields have been normalized so that the four CCD photometric zero points were defined to be identical. However, the ratios of the gain states for each CCD are not identically a factor of 2 (Burrows et al. 1994; Hill et al. 1995; Stetson 1994c), so we have explicitly included the gain ratios from these references in the WFPC2 calibration.

These *HST* observations also unfortunately suffer from charge transfer problems and electron traps which deplete the wings of the stellar profiles. However, the peaks of the stellar profiles, which ALLFRAME uses to drive the stellar magnitudes, are not seriously affected. The charge-transfer effect can therefore be included as a spatially-dependent linear correction to the magnitudes, separate from the photometric zero point. From the calibration studies by Stetson (1994c) in the comparatively low-background cases of ω Cen, NGC 2419, and Pal 4, this correction has an approximate amplitude of -0.04 mag at row 800 and linearly drops to 0 at "row 0" (the charge transferred from a zeroth row would not be degraded by traps in the CCD substrate). However, in the high-background case, Hill et al. (1995) found that the warm/cold zero point difference did not appear to depend upon row number, implying that there was little or no charge transfer efficiency (CTE) gradient in the warm and cold data. The M101 outer field observations were corrected, conservatively, by *half* this ramp. We therefore carry a maximum error of ± 0.02 mag (see the error budget, § 7.3).

The V and I zero points include the grain ratio variations, renormalization of the pixel surface area,[15] and aperture corrections specific to the globular cluster exposures. These zero points have been adjusted to include aperture corrections appropriate for our M101 exposures.

The single F439W phase point was calibrated in the same fashion as the F814W observations. The appropriate photometric zero point, as taken from the Status Report, was used (20.069 mag ≡ 1 DN s^{-1} at gain = 14).

For a list of components in the WFPC2 ALLFRAME calibration, see Table A1. The listed WFPC2 instrument zero points, based on Stetson (1994c), have been converted to the Holtzman et al. (1995) Status Report system for easy comparison. The Stetson (1994c) instrumental system is defined by

$$m \equiv 25 - 2.5 \log (\text{DN within } 0''.5) - 2.5 \log t(\text{s}) - 0.02(y/800) , \quad \text{(A1)}$$

$$m = M + Z_M + a_M(V-I) + b_M(V-I)^2 , \quad \text{(A2)}$$

where m is the instrumental F555W (or F814W) magnitude and M is the standard V (or I) magnitude.

The Stetson (1994c) long-exposure zero points are, for F555W in the four respective CCDs, $Z_V = (0.967, 0.958, 0.950, 0.973)$ mag. In F814W, the four zero points are $Z_I = (1.861, 1.823, 1.842, 1.870)$ mag. The color term coefficients are $a_V = +0.052$, $b_V = -0.027$, $a_I = +0.063$, and $b_I = -0.025$. These coefficients are opposite in sign to those listed in Holtzman et al. (1995), because Stetson and Holtzman have used slightly different calibration equations; Holtzman et al. (1995) derived zero points using

$$M = m + Z_m + a_m(V-I) + b_m(V-I)^2 \quad \text{(A3)}$$

(where $a_m \equiv -a_M$ and $b_m \equiv -b_M$). The Stetson (1994c) rationale for defining his calibration equation as above is that the intrinsic properties are all contained on the right side of the equation, and therefore are separated from the observables and their measurement errors.

The photometric transformations were applied to *all* stars whose reported WFPC2 ALLFRAME magnitude errors were less than 0.3 mag, to bring their F555W, F814W, and F439W magnitudes onto the *BVI* system. The color terms in the transformations were iterated for each star, starting with the WFPC2 filter system colors as initial approximations to the standard colors. The color terms were not large, so only two or three iterations were required before the resulting standard magnitude converged to ± 0.001 mag.

Calibration of the WFC F555W ALLFRAME magnitudes.—The now-calibrated WFPC2 star list was used to provide a set of selected secondary standards for use in calibrating the WFC data. Bright, isolated stars were chosen in the WFPC2 exposures from the WFPC2 V photometry list and used to calibrate the mean WFC F555W ALLFRAME magnitudes. Since only a few WFPC2 exposures were used to calibrate the mean WFC ALLFRAME photometry, each secondary standard was checked for variability in the WFC observations.

[15] Holtzman's pipeline flat fields are normalized by the area of the *largest* pixel; Stetson has renormalized the pixel area map by the *median* pixel area. The difference is approximately 0.015 mag.

TABLE A1

CALIBRATION OF WFPC2 ALLFRAME PHOTOMETRY

Additive Term	Value	Correction (mag)
ALLFRAME zero point[a]	...	−25.000
Exposure time[b]	+2.5 log 1200	+7.698
WFPC2 zero point[c]	...	+21.744
Long exposure correction	...	+0.050
Instrument gain[d]	+2.5 log 1.965	+0.733
Image multiplication[e]	+2.5 log 4	+1.505
Aperture correction[f]	...	−0.022

[a] Zero-point equivalent to magnitude of 1 DN.
[b] F555W exposure time was 1200 s.
[c] Zero point ($\equiv 1$ DN s^{-1} at gain = 14) shown for F555W in the PC CCD. The *mean* F555W, F814W, and F439W zero points are, converted from Stetson 1994c, 21.730 mag, 20.845 mag, and, from Holtzman et al. 1995, 20.069 mag, respectively.
[d] Gain ratio is not exactly 2. Value shown is valid for PC CCD. Use 2.037, 2.022, 1.965 for the three WF CCDs.
[e] Images initially multiplied by four and stored as short integers.
[f] Aperture correction shown for F555W in the PC CCD.

TABLE A2

CALIBRATION OF WFC ALLFRAME PHOTOMETRY

Additive Term	Value	Correction (mag)
ALLFRAME zero point[a]	...	−25.00
Exposure time[b]	+2.5 log 1900	+8.20
MDS zero point[c]	...	+22.90
Image multiplication[d]	+2.5 log 4	+1.50
Aperture correction	...	−0.02
Contamination	...	−0.05

[a] Zero point equivalent to magnitude of 1 DN.
[b] F555W photometry normalized to first epoch (1900 s).
[c] Zero point ($\equiv 1$ DN s^{-1}) shown for WFC Chip 1 (F555W).
[d] Images initially multiplied by four and stored as short integers.

For F555W, we used 38 secondary standards in the PC CCD, plus 114, 236, and 160 secondary standards in the three WFC CCDs. The mean color for these secondary standards was approximately $(V-I) \approx 0.5$, so an additional mean color term of −0.01 mag is appropriate for the Cepheids. The resulting offsets and uncertainties are given in Table A3, in the column titled "WFPC2." The difference in the *mean* offsets for the MDS flat-field corrected and uncorrected WFC photometry was small ($\lesssim$0.01 mag); WFC flat-fielding errors did not affect the calibration.

The mean of the four CCD calibrations is nearly identical to the mean offset obtained with the MDS WFC zero points. Therefore, by using the mean calibration of the four CCDs and adding the CCD-to-CCD zero-point deviations from Phillips et al. (1994), we found results essentially identical to those obtained in § A2 (to within 0.01 mag). These offsets are shown in Table A3 under "Mean WFPC2." The errors listed were estimated by summing the reported MDS zero-point uncertainties in quadrature with the standard error of the mean WFPC2-based offsets and very closely approximate the MDS zero-point errors.

Inclusion of the WFC F785LP epoch.—The WFC F785LP ALLFRAME magnitudes were converted to the same system as the WFPC2 F814W ALLFRAME magnitudes using simple zero-point offsets based on differences in exposure time, instrument zero points, and aperture corrections. We used the difference in the WFC F785LP zero points from Phillips et al. (1994) and the WFPC2 F814W zero points from Holtzman et al. (1995b) to get them onto a common WFPC2 scale. The error incurred by the assumption of this zero-point difference is negligible for Cepheids, since their I photometry is principally derived from the F814W observations. Since the F814W color term given in the Status Report is small (0.000–0.038 mag for $0 \leq (V-I) \leq 1$), the assumption does not involve systematic color effects in placing the WFC F785LP magnitudes on to the WFPC F814W ($\approx$WFPC2 F814W) magnitude system. The effects of this assumption are seen in the derivation of mean I photometry, discussed in § 6. The large, mean color term applicable for Cepheids, $\sim$0.12 mag for $(V-I)$ (see Harris et al. 1991), was added to the Cepheid photometry *before* the determination of the mean I photometry. The full transformation of F785LP to F814W was easily derived:

$$\mathrm{F814W} = \mathrm{F785LP} + 0.1124(V-I) + 0.0072(V-I)^2 \,. \quad \text{(A4)}$$

Since we used a mean Cepheid color, the largest incurred error in the transformation should have been about $\pm$0.07 mag for the single F785LP epoch of an individual Cepheid. In most cases, this error was absorbed by the F814W data, since most of our sample was observed in the four F814W epochs.

A "mean epoch" versus the "reference epoch".—Since there were several F814W and F555W observations, we need to remove any systematic bias in the arbitrarily chosen reference epochs. The frame-to-frame magnitude offsets that register the observations onto one system (the reference epoch) are typically nonzero (i.e., due to changes in the PSF, contamination trends, etc.). Since the magnitudes at each epoch were registered onto a common system, defined by a reference epoch, we had to adjust to a system referred to the "mean" epoch. The arbitrarily chosen reference epoch suffers from arbitrary contamination or focus differences, so the mean of the epoch-to-epoch magnitude offsets were computed and the calibrations were adjusted to remove this bias. (For the intrinsic WFC calibration that was used by Phillips et al. 1994, the systematic bias in any given reference epoch is well understood—contamination and focus changes.)

A2. CALIBRATION USING THE MEDIUM DEEP SURVEY WFC ZERO POINTS

Phillips et al. (1994) provided accurate zero points and flat-field corrections for WFC photometry, adding that relative photometry "approaching 1%–2% is achievable with the WFC." While our data set involved large relative rotations and required a single ALLFRAME reduction on the full set of CCD images, the photometry solution could still be analyzed in four distinct sets, based on the quadrants of the reference WFC exposure (chosen by us to be the first exposure of the first epoch). Since the ALLFRAME photometry is registered to the reference (first) exposure, several corrections were needed to bring the ALLFRAME magnitudes, from individual epochs, onto the WFC instrumental system.

The ALLFRAME magnitudes are defined as $-2.5 \log \mathrm{DN} + 25.0$. To this must be added a number of corrections, which include the exposure time, intrinsic photometric zero point of the instrument, removal of the ALLFRAME photometric zero point (25 mag $\equiv$ 1 DN), and an aperture correction to convert the ALLFRAME magnitudes (with an effective aperture radius equal to the DAOPHOT PSF radius) to total magnitudes (from a large enough aperture to effectively include *all* counts from a star). The PSF radius, or effective aperture of the photometry, was 2.″5, so the aperture correction is quite small at -0.02 mag (as derived from the encircled energy curve shown in Fig. 4.5 of the Wide Field and Planetary Camera Instrument Handbook; see MacKenty et al. 1992).

Our reference epoch was taken approximately six months after the previous decontamination in 1992 August. We included an estimate for contamination based on Figure 11.1*a* of the WFC, which shows that the contamination correction is fairly constant at about $\lesssim -0.05$ mag by 180 days. There was no evidence of contamination features (so-called "measles") in either the F555W or F785LP data. One could choose an "average" epoch to be the reference point, by referencing the photometry to the mean of the epoch-to-epoch magnitude offsets (derived from direct star-by-star comparisons). The mean magnitude offset, however, was $+0.002$ mag, an inconsequential effect compared to other sources of scatter.

The individual components of our WFC calibration, based on the Medium Deep Survey zero points, are listed in Table A2. The calibration offsets derived from the additive terms discussed above, are listed later in Table A3, under the column titled "MDS."

A3. CALIBRATION USING GROUND-BASED SECONDARY STANDARDS

Our ground-based calibration data was taken at the KPNO 4 m telescope, using the Mould Cousins *BVRI* filter set at prime focus. Seeing was about 1.″–1.″2 (FWHM) (see Cook et al. 1986; Alves & Cook 1995). These observations form the basis of an extra consistency check on the previously discussed methods. Comparison of the ground-based photometry with the *HST* photometry was not straightforward, because crowding in the ground-based data was a severe problem. Only $\lesssim$10 resolved stars (single stars separated by roughly 12 pixels in the *HST* observations) could be found. We therefore used the DAOPHOT/ALLSTAR package to maximize the number of usable secondary standards. We chose bright, somewhat isolated stars in the *HST* observations, whose neighbors were unresolved from the ground, and carefully co-added their ALLFRAME-determined counts to form secondary "standards" (essentially clumps of stars that could then be used for a comparison with ground-based photometry). Seeing effects were explicitly included in this process.

Seeing effects.—The detailed construction was as follows. If the two brightest stars in a group were separated by less than the critical separation for the resolution of two stars, $0.375 \times \mathrm{FWHM}_{\mathrm{ground}}$($\approx$4.5 WFC pixels), then the count in the WFC images from those two stars would be summed directly. Counts from stars with distances from the local "center-of-light" greater than this critical separation would be down-weighted with a Gaussian-like kernel, with FWHM equal to that of the ground-based seeing (FWHM $\approx$ 12 WFC pixels, and $\sigma = \mathrm{FWHM}/2.35$). In essence, a group magnitude was defined as

$$m_{\mathrm{group}} = -2.5 \log \sum_{i=1}^{N_{\mathrm{group}}} 10^{-0.4 m_i} \times \begin{cases} 1 , & \text{if } |r| \le 4.5 \text{ pixels} , \\ \exp\left[-\dfrac{(|r| - 4.5)^2}{2\sigma^2} \right] , & \text{if } |r| > 4.5 \text{ pixels} . \end{cases} \tag{A5}$$

The centroid, from which to measure r, was defined as the flux-weighted center-of-light for the group of ALLFRAME-measured WFC (or WFPC2) stars, in the ground-based frame.

Thus, the *HST* observations were effectively convolved with a modified ground-based seeing profile (*after* determining the relative photometry for the stars in each "group"). The Gaussian-like kernel's flat-top conserves flux for unresolved pairs. The boundary between the flat-top and Gaussian wings, though not smooth, has the same limit from either side of the boundary. A potential difficulty arises, however, because unresolved, undetected stars are smeared and artificially increase the sky level as measured from the ground-based data. We tested for this effect, and it proved to be a generally small, but occasionally significant effect ($\pm$0.02 to $\pm$0.1 mag) for individual secondary standards compared to the rms scatter ($\pm$0.1 to $\pm$0.5 mag) in the ground-*HST* offsets. Overall, the typical magnitude uncertainties in the ground based photometry ranged from $\pm$0.1 mag at $V, I = 20$ mag to $\pm$0.3 mag at $V, I = 24$ mag.

The calibration derived from the KPNO data for F555W is shown in Table A3 in the column titled "Ground." Listings of the ground-based secondary standards are available upon request from the first author. The utility of these standards, however, is quite limited, as they are mostly groups of stars that were unresolved or marginally resolved from the ground in 1.″ to 1.″2 seeing. Thus, their photometry will be strongly dependent on seeing conditions.

$V-F555W$ color term.—The (F555W$-V$) color term has been ignored in the determination of these offsets. This color term, as determined by Harris et al. (1991), varies between 0 and $+0.05$ mag for $0 \le (B-V) \le 1$. For example, the mean $\langle B-V \rangle$ for Cepheids is 0.66, leading to an error of 0.04 mag in V *if* the mean $\langle B-V \rangle = 0$ for the secondary standards. However, the mean $\langle V-I \rangle$ of our ground-based secondary standards is $\langle V-I \rangle \approx 0.45$, corresponding to approximately $0.2 \lesssim \langle B-V \rangle \lesssim 0.3$. Thus, the additional color term we applied for Cepheids is only $\sim$0.02 mag, in the mean, for stars with similar colors to Cepheids. Given the color distribution of our Cepheids, any additional systematic effect is negligible.

Using the mean of the four CCD ground-based calibrations, with the CCD-to-CCD zero-point deviations from Phillips et al. (1994), we derived the "Mean Ground" offsets shown in Table A3. For stars with the colors of Cepheids, these reflect a 0.04 mag systematic offset, in the mean, between the ground-based and *HST*-derived offsets.

The ground-based $I-F814W$ comparison.—For ground-based I, the complete Holtzman et al. (1995b) transformation

$$\mathrm{F814W} = I + 0.067(V-I) - 0.025(V-I)^2 \tag{A6}$$

TABLE A3

CALIBRATION OF ALLFRAME PHOTOMETRY IN M101

CCCD	MDS	WFPC2	Mean WFPC2[b]	Ground[c,d]	Mean Ground[b,c,d]
WFC 1 F555W ALLFRAME Calibrating Offsets[a]					
1	7.53 ± 0.02	7.702 ± 0.051	7.522 ± 0.05	7.430 ± 0.110	7.466 ± 0.05
2	7.67 ± 0.04	7.698 ± 0.048	7.662 ± 0.06	7.674 ± 0.087	7.606 ± 0.06
3	7.67 ± 0.06	7.497 ± 0.034	7.662 ± 0.08	7.498 ± 0.111	7.606 ± 0.08
4	7.59 ± 0.04	7.531 ± 0.037	7.582 ± 0.06	7.602 ± 0.120	7.526 ± 0.06
WFPC2 F814W ALLFRAME Calibrating Offsets[e,f,g,h]					
1	...	5.640 ± 0.038	...	5.600 ± 0.050	...
2	...	5.830 ± 0.030	...	5.807 ± 0.039	...
3	...	5.817 ± 0.032	...	5.782 ± 0.044	...
4	...	5.787 ± 0.040	...	5.802 ± 0.093	...

[a] Valid for F555W photometry normalized to reference exposure (1900 s).
[b] "Mean" is defined as the mean of the 4 CCD zero points with CCD-to-CCD zero-point deviations from Phillips et al. 1994.
[c] Ground-based zero points were derived from V-F555W comparison.
[d] Using $V-$F555W, there is an additional mean color term of 0.02 mag for the Cepheids.
[e] Valid for F814W photometry normalized to reference exposure (1200 s).
[f] Gain ratio is not exactly 2 for each of the CCDs (Burrows et al. 1994).
[g] This calibration includes terms to correct ALLFRAME magnitudes to 0".5 radius aperture magnitudes.
[h] Ground-based zero points were derived after I transformed to F814W (Holtzman et al. 1995).

was used, since we have color information. The ground-based I magnitudes were first converted to F814W before direct comparison with the ALLFRAME secondary standards. The ground-based F814W ALLFRAME calibrating offsets are also shown in Table A3 under the column "Ground." The means of the individual CCD calibrations, derived from the Status Report and the ground-based observations, are listed in Table A3.

Systematic errors and biases.—Note that the *individual* CCD offsets show larger differences than expected from the random errors (listed as the offset uncertainties). One possible source of systematic difference between the ground-based and instrument calibrations is incompleteness in the inclusion process by which groups of stars were assembled from the *HST* images. Since most of the F555W observations were made with the WFC, the star list reflects poor resolution of tight groups into individual stars. Incompleteness in either the F555W or the F814W data may result in improper assignment of combined ALLFRAME magnitudes to the secondary standards; i.e., these magnitudes would be artificially too faint and lead to ground-based calibrating offsets that are too small (too bright). For example, if 50% of the faint half of the population was undetected, then we would miss about 25% of the flux in the combined ALLFRAME secondary standards, if stars were randomly distributed by luminosity in groups. If 20% of the faintest 20% (in a list of stars that we *should have* detected) went undetected, then the magnitude of our ALLFRAME secondary standard group would be deficient by 4%.

A4. COMPARING THE CALIBRATIONS

The final comparison of the different sets of derived ALLFRAME calibrating offsets and uncertainties is shown in Table A3. In the mean, the F555W calibrations agree well, with the exception of the ground-based calibration of CCD No. 1. For stars of Cepheid-like colors, the calibrations agree particularly well in the mean. In F814W, the calibrations agree exceptionally well in all four chips. One possible explanation for this behavior in CCD No. 1 in F555W is the highly nonuniform distribution of stars. Most of the stars are concentrated into one corner; the several H II regions and many bright stars are not well resolved and separated from each other. This field is covered by the PC CCD in the WFPC2 observations and is better resolved in the F814W observations. The WFC images do not resolve the individual, bright stars well and lead to a poor comparison with the ground-based image, while the improved resolution of the WFPC2 helps to provide accurate, unbiased, well-sampled star lists in the region. The calibration uncertainties are discussed in § 4 and in § 7.3 in the context of the error budget.

APPENDIX B

CEPHEID PHOTOMETRY

V and I epoch photometry and positions for the Cepheids are listed in Tables B1 and B2, respectively. Column one contains the Julian Date of the midpoint of each *individual* exposure. Note that each of the cosmic-ray split pairs are given individually in this tabulation. Column (2) shows which CCD the star can be found in for a given observation. Columns (3) and (4) show the (x, y) positions for the observations, while column (5) shows the calibrated F555W (or F814W) magnitudes with their reported ALLFRAME uncertainties. Only those data included in the light-curve analysis and mean photometry derivation are listed in Tables B1 and B2. Spurious observations have been excluded. The WFPC2 observations began on JD 2,449,404.

TABLE B1

V PHOTOMETRY

C1 P=58.5				
JD	CCD	x	y	V
2449049.0327	1	97.24	149.03	23.67 ± 0.12
2449049.0938	1	97.23	149.03	23.61 ± 0.10
2449057.4598	1	98.39	147.90	23.34 ± 0.10
2449064.0828	1	101.15	150.14	23.66 ± 0.10
2449064.1136	1	101.16	150.24	23.62 ± 0.13
2449069.2661	1	97.50	149.94	23.10 ± 0.38
2449069.3293	1	97.51	149.96	23.94 ± 0.26
2449131.6589	2	82.07	133.86	23.69 ± 0.10
2449131.7228	2	81.88	133.90	23.58 ± 0.12
2449141.6263	2	82.05	134.01	23.88 ± 0.12
2449141.6936	2	82.13	133.95	23.96 ± 0.12
2449146.1096	2	81.90	133.74	23.98 ± 0.14
2449146.1769	2	81.87	133.75	23.89 ± 0.12
2449156.8860	2	81.95	134.23	23.97 ± 0.11
2449156.9499	2	81.87	134.23	23.87 ± 0.12
2449160.7658	2	82.14	133.99	23.98 ± 0.08
2449160.8304	2	82.12	133.96	23.61 ± 0.34
2449163.2450	2	82.12	134.23	24.11 ± 0.12
2449163.3054	2	82.19	134.17	24.28 ± 0.12
2449251.6130	3	77.11	130.11	24.11 ± 0.22
2449251.6748	3	77.15	130.16	24.32 ± 0.12
2449295.2633	4	136.06	91.71	24.27 ± 0.17
2449295.3195	4	136.09	91.72	24.06 ± 0.13
2449307.7036	4	122.92	116.10	23.85 ± 0.12
2449307.7661	4	122.82	116.06	23.69 ± 0.10
2449429.6016	1	222.24	233.90	23.66 ± 0.08

C6 P=45.8				
JD	CCD	x	y	V
2449049.0327	2	199.91	263.23	23.37 ± 0.08
2449049.0938	2	199.90	263.22	23.49 ± 0.10
2449057.4598	2	198.71	262.30	23.58 ± 0.11
2449064.0828	2	200.90	259.73	23.60 ± 0.10
2449064.1136	2	200.91	259.90	23.74 ± 0.10
2449069.2661	2	200.71	263.35	23.73 ± 0.11
2449069.3293	2	200.74	263.33	23.82 ± 0.20
2449131.6589	3	179.33	271.94	23.58 ± 0.16
2449131.7228	3	179.38	272.14	23.83 ± 0.13
2449141.6263	3	179.44	271.57	23.94 ± 0.26
2449141.6936	3	179.38	271.48	23.90 ± 0.13
2449146.1096	3	179.20	272.26	23.85 ± 0.14
2449146.1769	3	179.21	272.30	23.77 ± 0.15
2449156.8860	3	179.68	271.72	23.87 ± 0.17
2449160.8304	3	179.57	271.77	23.60 ± 0.13
2449163.2450	3	179.77	271.59	23.64 ± 0.10
2449163.3054	3	179.71	271.48	23.69 ± 0.20
2449251.6130	4	180.59	272.23	23.60 ± 0.13
2449251.6748	4	180.65	272.24	23.48 ± 0.10
2449295.2633	1	333.49	109.52	23.47 ± 0.11
2449295.3195	1	333.46	109.46	23.10 ± 0.12
2449307.7036	1	312.83	169.14	23.18 ± 0.11
2449307.7661	1	312.78	169.15	23.23 ± 0.17
2449429.6016	2	201.87	256.05	23.32 ± 0.12

C19 P=43.0				
JD	CCD	x	y	V
2449049.0327	4	545.49	751.72	23.93 ± 0.19
2449049.0938	4	545.46	751.68	23.75 ± 0.13
2449057.4598	4	546.58	752.85	23.97 ± 0.11
2449064.0828	4	544.51	755.52	23.58 ± 0.17
2449064.1136	4	544.58	755.61	23.73 ± 0.17
2449069.2661	4	544.60	752.00	23.33 ± 0.07
2449069.3293	4	544.58	752.00	23.29 ± 0.07
2449131.6589	1	517.28	783.30	22.82 ± 0.29
2449131.7228	1	517.23	783.08	22.99 ± 0.18
2449141.6263	1	517.47	783.35	23.04 ± 0.13
2449141.6936	1	517.53	783.46	23.07 ± 0.12
2449146.1096	1	517.30	783.14	23.06 ± 0.08
2449146.1769	1	517.29	783.11	23.07 ± 0.07
2449156.8860	1	517.28	783.23	23.16 ± 0.07
2449156.9499	1	517.30	783.17	23.19 ± 0.06
2449160.7658	1	517.36	783.45	23.20 ± 0.07
2449160.8304	1	517.36	783.43	23.44 ± 0.11
2449163.2450	1	517.34	783.43	23.22 ± 0.22
2449163.3054	1	517.36	783.52	23.50 ± 0.28
2449429.6016	4	626.42	782.04	23.54 ± 0.09

C5 P=47.1				
JD	CCD	x	y	V
2449049.0327	2	730.21	199.07	23.45 ± 0.18
2449049.0938	2	730.20	199.06	23.51 ± 0.21
2449057.4598	2	729.01	198.21	23.42 ± 0.07
2449064.0828	2	731.12	195.62	23.44 ± 0.09
2449064.1136	2	731.09	195.67	23.53 ± 0.13
2449069.2661	2	730.96	199.29	23.82 ± 0.23
2449069.3293	2	731.00	199.27	23.78 ± 0.17
2449131.6589	3	712.04	233.49	23.81 ± 0.23
2449131.7228	3	712.09	233.66	24.03 ± 0.11
2449141.6263	3	712.20	233.14	23.87 ± 0.08
2449146.1769	3	711.96	233.80	24.25 ± 0.28
2449156.8860	3	712.36	233.26	24.32 ± 0.51
2449156.9499	3	712.38	233.27	23.58 ± 0.35
2449160.7658	3	712.28	233.27	23.84 ± 0.10
2449160.8304	3	712.26	233.31	23.59 ± 0.09
2449163.2450	3	712.42	233.15	23.49 ± 0.06
2449163.3054	3	712.38	233.03	23.65 ± 0.21
2449251.6130	4	717.19	229.27	23.73 ± 0.25
2449251.6748	4	717.19	229.35	23.44 ± 0.56
2449295.2633	4	342.64	700.29	23.20 ± 0.46
2449295.3195	4	342.70	700.25	23.14 ± 0.07
2449307.7036	4	199.68	754.17	23.10 ± 0.14
2449307.7661	4	199.55	754.20	23.37 ± 0.07
2449429.6016	2	744.53	187.40	23.36 ± 0.06

C7 P=43.0				
JD	CCD	x	y	V
2449049.0327	2	369.09	653.48	23.55 ± 0.10
2449049.0938	2	369.07	653.51	23.67 ± 0.11
2449057.4598	2	367.85	652.58	23.63 ± 0.12
2449064.0828	2	370.04	649.92	23.67 ± 0.15
2449064.1136	2	370.03	650.01	23.81 ± 0.07
2449069.2661	2	369.84	653.61	23.87 ± 0.10
2449069.3293	2	369.84	653.61	23.77 ± 0.09
2449131.6589	3	329.05	670.05	24.00 ± 0.14
2449131.7228	3	329.10	670.25	24.04 ± 0.12
2449141.6263	3	329.17	669.73	23.75 ± 0.30
2449141.6936	3	329.11	669.65	25.10 ± 0.62
2449146.1096	3	328.95	670.40	24.04 ± 0.12
2449146.1769	3	328.94	670.44	24.12 ± 0.13
2449156.8860	3	329.39	669.85	24.01 ± 0.10
2449156.9499	3	329.41	669.89	23.98 ± 0.11
2449160.7658	3	329.30	669.87	23.29 ± 0.16
2449160.8304	3	329.28	669.91	23.59 ± 0.09
2449163.2450	3	329.46	669.72	23.56 ± 0.08
2449163.3054	3	329.41	669.62	23.52 ± 0.11
2449295.2633	1	712.34	300.35	23.62 ± 0.22
2449295.3195	1	712.28	300.32	23.52 ± 0.23
2449307.7036	1	644.35	433.82	23.39 ± 0.12
2449307.7661	1	644.33	433.85	23.60 ± 0.07
2449429.6016	2	376.18	654.41	23.77 ± 0.10

C20 P=42.5				
JD	CCD	x	y	V
2449049.0327	4	137.54	199.71	23.70 ± 0.41
2449049.0938	4	137.52	199.69	23.90 ± 0.17
2449057.4598	4	138.72	200.84	24.01 ± 0.12
2449064.0828	4	136.69	203.58	24.42 ± 0.17
2449064.1136	4	136.69	203.83	24.00 ± 0.32
2449069.2661	4	136.75	200.00	24.09 ± 0.14
2449069.3293	4	136.70	200.01	24.12 ± 0.09
2449131.6589	1	148.45	205.88	24.33 ± 0.14
2449131.7228	1	148.36	205.70	24.08 ± 0.12
2449141.6263	1	148.61	205.92	24.38 ± 0.18
2449141.6936	1	148.67	206.01	24.65 ± 0.53
2449146.1096	1	148.42	205.70	24.58 ± 0.43
2449146.1769	1	148.39	205.66	24.60 ± 0.17
2449156.8860	1	148.42	205.80	24.70 ± 0.16
2449156.9499	1	148.42	205.74	24.08 ± 0.18
2449160.7658	1	148.52	206.01	24.30 ± 0.14
2449160.8304	1	148.52	205.99	24.26 ± 0.18
2449163.2450	1	148.50	206.01	23.91 ± 0.17
2449163.3054	1	148.54	206.11	23.84 ± 0.27
2449295.2633	3	204.79	66.85	23.88 ± 0.21
2449295.3195	3	204.81	66.91	23.91 ± 0.16
2449307.7036	3	190.77	104.96	23.67 ± 0.12
2449307.7661	3	190.78	104.86	23.76 ± 0.10
2449429.6016	4	201.71	223.44	24.15 ± 0.16

TABLE B1—*Continued*

C8 P=41.0				
JD	CCD	x	y	V
2449049.0327	2	301.46	198.03	24.38 ± 0.12
2449049.0938	2	301.46	198.02	24.26 ± 0.13
2449057.4598	2	300.27	197.12	24.50 ± 0.22
2449064.0828	2	302.44	194.56	24.46 ± 0.20
2449064.1136	2	302.45	194.71	24.04 ± 0.27
2449069.2661	2	302.26	198.18	24.21 ± 0.12
2449069.3293	2	302.29	198.16	24.11 ± 0.13
2449131.6589	3	283.95	211.71	23.87 ± 0.10
2449131.7228	3	284.00	211.91	23.81 ± 0.11
2449141.6263	3	284.07	211.34	23.94 ± 0.12
2449141.6936	3	284.01	211.26	23.88 ± 0.26
2449146.1096	3	283.83	212.02	23.54 ± 0.30
2449146.1769	3	283.83	212.06	23.31 ± 0.32
2449156.8860	3	284.29	211.49	23.67 ± 0.10
2449156.9499	3	284.29	211.50	23.45 ± 0.19
2449160.7658	3	284.21	211.50	23.58 ± 0.13
2449160.8304	3	284.19	211.54	23.49 ± 0.21
2449163.2450	3	284.38	211.37	23.63 ± 0.10
2449163.3054	3	284.33	211.25	23.80 ± 0.09
2449251.6130	4	286.24	211.12	23.73 ± 0.09
2449295.2633	4	63.45	374.85	23.88 ± 0.11
2449295.3195	4	63.48	374.85	23.95 ± 0.12
2449307.7036	1	371.85	64.25	23.73 ± 0.08
2449307.7661	1	371.79	64.25	24.03 ± 0.09

C9 P=38.0				
JD	CCD	x	y	V
2449049.0327	2	337.45	56.83	23.67 ± 0.08
2449049.0938	2	337.45	56.81	23.74 ± 0.08
2449057.4598	2	336.27	55.92	23.69 ± 0.08
2449064.0828	2	338.43	53.38	23.71 ± 0.11
2449064.1136	2	338.44	53.54	23.58 ± 0.11
2449069.2661	2	338.25	56.99	23.99 ± 0.10
2449069.3293	2	338.30	56.96	24.11 ± 0.10
2449131.6589	3	326.84	72.37	23.98 ± 0.08
2449141.6936	3	326.90	71.90	22.78 ± 0.09
2449146.1096	3	326.71	72.67	22.72 ± 0.10
2449146.1769	3	326.73	72.70	22.88 ± 0.07
2449156.8860	3	327.18	72.14	22.90 ± 0.09
2449156.9499	3	327.18	72.14	22.77 ± 0.25
2449160.7658	3	327.10	72.15	22.78 ± 0.14
2449160.8304	3	327.08	72.18	23.00 ± 0.10
2449163.2450	3	327.26	72.02	23.04 ± 0.08
2449163.3054	3	327.22	71.90	23.10 ± 0.07
2449251.6130	4	330.16	71.41	23.06 ± 0.11
2449251.6748	4	330.20	71.46	23.32 ± 0.08
2449295.2633	4	194.42	309.83	23.38 ± 0.10
2449295.3195	4	194.46	309.83	23.54 ± 0.10
2449307.7036	4	135.06	341.58	23.42 ± 0.07
2449307.7661	4	134.95	341.56	23.59 ± 0.11
2449429.6016	2	341.69	44.02	23.57 ± 0.10

C10 P=37.6				
JD	CCD	x	y	V
2449049.0327	2	346.21	738.88	23.65 ± 0.12
2449049.0938	2	346.19	738.91	23.79 ± 0.13
2449057.4598	2	344.96	737.97	23.60 ± 0.07
2449064.0828	2	347.16	735.30	23.78 ± 0.11
2449064.1136	2	347.15	735.39	23.72 ± 0.14
2449069.2661	2	346.95	739.00	23.77 ± 0.08
2449069.3293	2	346.95	739.00	23.81 ± 0.12
2449131.6589	3	302.00	754.27	23.75 ± 0.13
2449141.6936	3	302.06	753.88	23.94 ± 0.18
2449146.1096	3	301.90	754.63	23.83 ± 0.25
2449146.1769	3	301.89	754.67	23.94 ± 0.49
2449156.8860	3	302.34	754.08	24.15 ± 0.11
2449156.9499	3	302.36	754.12	24.17 ± 0.28
2449160.7658	3	302.25	754.10	24.05 ± 0.14
2449160.8304	3	302.23	754.14	24.14 ± 0.36
2449163.2450	3	302.42	753.95	24.36 ± 0.26
2449163.3054	3	302.36	753.85	24.12 ± 0.17
2449251.6130	4	301.60	753.52	24.17 ± 0.15
2449251.6748	4	301.65	753.51	24.51 ± 0.13
2449295.2633	1	749.37	380.35	24.54 ± 0.15
2449307.7661	1	664.10	519.77	24.29 ± 0.14
2449429.6016	2	353.22	741.75	23.58 ± 0.25

C21 P=33.5				
JD	CCD	x	y	V
2449049.0327	4	296.98	712.86	23.63 ± 0.13
2449049.0938	4	296.95	712.83	23.51 ± 0.12
2449064.0828	4	296.05	716.66	23.94 ± 0.12
2449064.1136	4	296.07	716.82	24.00 ± 0.12
2449069.2661	4	296.11	713.11	24.19 ± 0.19
2449069.3293	4	296.07	713.11	24.05 ± 0.09
2449131.6589	1	272.48	727.86	24.02 ± 0.11
2449131.7228	1	272.42	727.64	24.16 ± 0.22
2449141.6263	1	272.66	727.90	24.28 ± 0.17
2449141.6936	1	272.73	728.02	24.08 ± 0.13
2449146.1096	1	272.50	727.69	24.18 ± 0.13
2449146.1769	1	272.47	727.66	24.22 ± 0.24
2449156.8860	1	272.47	727.78	24.13 ± 0.41
2449156.9499	1	272.48	727.72	24.41 ± 0.38
2449160.7658	1	272.56	728.00	24.35 ± 0.16
2449160.8304	1	272.56	727.97	24.36 ± 0.16
2449163.2450	1	272.55	727.98	23.74 ± 0.23
2449163.3054	1	272.56	728.07	23.77 ± 0.11
2449251.6748	2	297.54	773.11	23.19 ± 0.10
2449295.2633	3	658.01	354.75	23.22 ± 0.09
2449295.3195	3	658.01	354.79	23.28 ± 0.06
2449307.7036	3	574.84	480.12	23.25 ± 0.06
2449307.7661	3	574.85	480.04	23.38 ± 0.08
2449429.6016	4	371.72	745.59	23.43 ± 0.08

C12 P=33.5				
JD	CCD	x	y	V
2449049.0327	3	356.29	200.10	22.96 ± 0.10
2449049.0938	3	356.32	200.07	22.94 ± 0.10
2449057.4598	3	355.33	201.07	22.73 ± 0.30
2449064.0828	3	352.88	198.66	22.91 ± 0.10
2449064.1136	3	352.89	199.00	23.26 ± 0.22
2449069.2661	3	356.32	198.94	23.33 ± 0.10
2449069.3293	3	356.31	198.92	23.21 ± 0.12
2449131.6589	4	343.88	235.59	23.51 ± 0.13
2449131.7228	4	344.06	235.50	23.49 ± 0.12
2449141.6263	4	343.92	235.79	23.23 ± 0.21
2449141.6936	4	343.83	235.86	23.24 ± 0.19
2449146.1096	4	344.00	235.54	23.41 ± 0.13
2449146.1769	4	344.02	235.53	23.47 ± 0.13
2449156.8860	4	344.02	235.59	23.43 ± 0.13
2449156.9499	4	344.06	235.58	23.48 ± 0.13
2449160.7658	4	343.92	235.71	23.70 ± 0.33
2449160.8304	4	343.91	235.69	23.53 ± 0.15
2449163.2450	4	343.95	235.70	23.56 ± 0.15
2449163.3054	4	343.84	235.74	23.84 ± 0.17
2449251.6130	1	375.45	221.91	23.90 ± 0.16
2449251.6748	1	375.41	221.88	23.70 ± 0.25
2449295.2633	1	124.31	410.36	23.59 ± 0.23
2449295.3195	1	124.31	410.32	23.32 ± 0.13
2449307.7036	1	46.07	420.64	23.24 ± 0.11
2449307.7661	1	46.02	420.69	22.81 ± 0.08
2449429.6016	3	365.10	254.32	22.85 ± 0.11

C13 P=32.0				
JD	CCD	x	y	V
2449049.0327	3	230.92	468.99	23.95 ± 0.10
2449049.0938	3	230.93	468.96	23.96 ± 0.12
2449057.4598	3	229.96	469.95	24.02 ± 0.12
2449064.0828	3	227.54	467.52	23.58 ± 0.20
2449064.1136	3	227.59	467.73	23.27 ± 0.08
2449069.2661	3	230.94	467.84	23.73 ± 0.09
2449069.3293	3	230.90	467.82	23.61 ± 0.08
2449131.6589	4	205.04	497.72	23.61 ± 0.10
2449131.7228	4	205.22	497.66	23.57 ± 0.09
2449141.6263	4	205.06	497.94	23.72 ± 0.10
2449141.6936	4	204.95	497.99	24.25 ± 0.41
2449146.1096	4	205.16	497.69	23.81 ± 0.09
2449146.1769	4	205.15	497.69	23.64 ± 0.20
2449156.8860	4	205.14	497.71	23.85 ± 0.12
2449156.9499	4	205.21	497.72	24.31 ± 0.24
2449160.7658	4	205.06	497.83	24.03 ± 0.12
2449160.8304	4	205.05	497.81	23.86 ± 0.13
2449163.2450	4	205.09	497.82	23.82 ± 0.13
2449163.3054	4	204.99	497.85	23.81 ± 0.08
2449251.6130	1	246.68	488.82	24.04 ± 0.13
2449251.6748	1	246.63	488.78	24.15 ± 0.11
2449429.6016	3	238.68	530.08	24.36 ± 0.13

TABLE B1—*Continued*

C22 P=27.3

JD	CCD	x	y	V
2449049.0327	4	307.15	453.01	24.22 ± 0.15
2449049.0938	4	307.13	452.98	24.08 ± 0.16
2449057.4598	4	308.29	454.14	23.95 ± 0.36
2449064.0828	4	306.24	456.85	24.52 ± 0.29
2449064.1136	4	306.27	457.02	24.30 ± 0.16
2449069.2661	4	306.31	453.29	24.46 ± 0.14
2449069.3293	4	306.27	453.29	24.54 ± 0.20
2449131.6589	1	300.18	469.65	24.30 ± 0.14
2449131.7228	1	300.11	469.45	24.54 ± 0.17
2449141.6263	1	300.36	469.70	22.85 ± 0.56
2449141.6936	1	300.42	469.80	24.43 ± 0.20
2449146.1096	1	300.18	469.48	23.75 ± 0.51
2449146.1769	1	300.16	469.45	24.19 ± 0.16
2449160.7658	1	300.26	469.79	23.68 ± 0.18
2449160.8304	1	300.26	469.77	23.63 ± 0.19
2449163.2450	1	300.24	469.78	23.65 ± 0.10
2449163.3054	1	300.27	469.88	23.85 ± 0.37
2449251.6130	2	326.15	516.02	23.65 ± 0.08
2449251.6748	2	326.11	516.06	23.62 ± 0.10
2449295.2633	3	497.91	150.30	23.82 ± 0.15
2449295.3195	3	497.92	150.35	23.98 ± 0.18
2449307.7036	3	460.29	247.01	23.88 ± 0.17
2449307.7661	3	460.31	246.92	24.28 ± 0.21
2449429.6016	4	378.36	479.73	24.33 ± 0.11

C14 P=25.0

JD	CCD	x	y	V
2449049.0327	3	642.09	401.70	24.55 ± 0.91
2449049.0938	3	642.12	401.66	25.00 ± 0.33
2449057.4598	3	641.10	402.71	23.91 ± 0.12
2449064.0828	3	638.63	400.25	23.70 ± 0.09
2449064.1136	3	638.59	400.52	24.04 ± 0.12
2449069.2661	3	642.09	400.59	23.90 ± 0.14
2449069.3293	3	642.07	400.57	24.06 ± 0.17
2449131.6589	4	619.32	451.30	23.92 ± 0.10
2449131.7228	4	619.49	451.21	23.89 ± 0.13
2449141.6263	4	619.36	451.51	24.13 ± 0.13
2449141.6936	4	619.28	451.57	24.22 ± 0.16
2449146.1096	4	619.46	451.26	24.18 ± 0.15
2449146.1769	4	619.48	451.24	24.53 ± 0.19
2449156.9499	4	619.50	451.29	24.82 ± 0.23
2449160.8304	4	619.35	451.40	24.75 ± 0.43
2449163.2450	4	619.38	451.40	24.71 ± 0.20
2449295.3195	1	150.98	759.24	24.75 ± 0.19
2449429.6016	3	659.06	458.87	24.57 ± 0.79

C24 P=23.5

JD	CCD	x	y	V
2449049.0327	4	72.63	240.46	24.61 ± 0.23
2449049.0938	4	72.61	240.43	24.35 ± 0.34
2449057.4598	4	73.81	241.57	24.77 ± 0.64
2449064.0828	4	71.79	244.32	24.35 ± 0.16
2449064.1136	4	71.77	244.57	24.40 ± 0.15
2449069.2661	4	71.85	240.73	24.30 ± 0.21
2449069.3293	4	71.79	240.73	24.71 ± 0.16
2449131.6589	1	81.06	242.10	24.82 ± 0.27
2449131.7228	1	80.98	241.92	24.09 ± 0.18
2449141.6263	1	81.22	242.14	24.09 ± 0.16
2449141.6936	1	81.29	242.24	23.76 ± 0.11
2449146.1096	1	81.04	241.92	23.97 ± 0.14
2449146.1769	1	81.01	241.88	23.64 ± 0.10
2449156.8860	1	81.04	242.02	23.63 ± 0.14
2449160.7658	1	81.14	242.23	24.27 ± 0.19
2449163.2450	1	81.12	242.23	23.81 ± 0.16
2449163.3054	1	81.15	242.32	24.00 ± 0.16
2449251.6748	2	106.90	287.69	24.30 ± 0.18
2449295.2633	3	181.55	139.76	24.17 ± 0.20
2449295.3195	3	181.57	139.81	23.62 ± 0.41
2449307.7036	3	153.04	171.54	24.18 ± 0.17
2449307.7661	3	153.06	171.45	24.28 ± 0.19
2449429.6016	4	136.21	265.94	24.37 ± 0.17

C23 P=25.6

JD	CCD	x	y	V
2449049.0327	4	187.71	501.00	24.95 ± 0.18
2449049.0938	4	187.68	500.97	24.62 ± 0.18
2449057.4598	4	188.84	502.12	24.84 ± 0.22
2449064.0828	4	186.82	504.83	24.86 ± 0.23
2449064.1136	4	186.82	505.04	24.93 ± 0.19
2449069.2661	4	186.88	501.26	25.21 ± 0.21
2449069.3293	4	186.83	501.26	24.87 ± 0.11
2449131.6589	1	178.01	509.43	25.12 ± 0.22
2449131.7228	1	177.94	509.23	24.96 ± 0.21
2449141.6263	1	178.18	509.47	25.27 ± 0.23
2449141.6936	1	178.25	509.58	24.95 ± 0.16
2449146.1096	1	178.01	509.26	24.58 ± 0.17
2449146.1769	1	177.98	509.22	24.54 ± 0.21
2449156.8860	1	178.00	509.35	23.89 ± 0.13
2449156.9499	1	178.00	509.29	24.03 ± 0.31
2449160.7658	1	178.09	509.57	23.85 ± 0.41
2449160.8304	1	178.09	509.54	23.96 ± 0.28
2449163.3054	1	178.10	509.65	24.17 ± 0.25
2449295.2633	3	437.73	263.92	24.53 ± 0.23
2449295.3195	3	437.73	263.97	24.41 ± 0.17
2449307.7661	3	378.08	345.76	24.38 ± 0.13
2449429.6016	4	257.17	530.36	24.16 ± 0.17

C11 P=23.7

JD	CCD	x	y	V
2449049.0327	2	406.06	183.49	24.94 ± 0.20
2449049.0938	2	406.05	183.48	24.35 ± 0.16
2449057.4598	2	404.86	182.59	24.53 ± 0.16
2449064.0828	2	407.02	180.03	24.90 ± 0.17
2449064.1136	2	407.02	180.16	24.82 ± 0.19
2449069.2661	2	406.84	183.66	23.82 ± 0.11
2449069.3293	2	406.88	183.64	23.69 ± 0.19
2449131.6589	3	389.11	202.25	23.71 ± 0.19
2449131.7228	3	389.16	202.44	23.91 ± 0.09
2449141.6263	3	389.24	201.88	23.93 ± 0.09
2449146.1096	3	388.99	202.55	24.21 ± 0.11
2449146.1769	3	389.00	202.58	24.05 ± 0.11
2449156.8860	3	389.45	202.02	24.11 ± 0.12
2449156.9499	3	389.45	202.03	23.75 ± 0.34
2449160.7658	3	389.36	202.04	24.41 ± 0.09
2449160.8304	3	389.35	202.07	24.17 ± 0.70
2449163.2450	3	389.52	201.90	24.42 ± 0.14
2449163.3054	3	389.48	201.78	24.76 ± 0.17
2449251.6130	4	392.18	200.76	24.34 ± 0.15
2449295.2633	4	142.82	444.58	24.59 ± 0.15
2449295.3195	4	142.85	444.56	24.57 ± 0.11
2449307.7036	4	56.65	462.91	24.66 ± 0.17
2449307.7661	4	56.53	462.90	24.47 ± 0.20
2449429.6016	2	412.17	173.53	24.04 ± 0.31

C15 P=23.4

JD	CCD	x	y	V
2449049.0327	3	318.10	185.21	24.47 ± 0.14
2449049.0938	3	318.13	185.18	24.16 ± 0.38
2449057.4598	3	317.14	186.18	24.23 ± 0.19
2449064.0828	3	314.70	183.77	24.38 ± 0.09
2449064.1136	3	314.71	184.11	24.50 ± 0.23
2449069.2661	3	318.13	184.04	24.53 ± 0.27
2449069.3293	3	318.12	184.02	23.48 ± 0.12
2449131.6589	4	306.47	218.79	23.52 ± 0.12
2449131.7228	4	306.65	218.71	23.82 ± 0.16
2449141.6263	4	306.50	218.99	23.97 ± 0.20
2449141.6936	4	306.41	219.06	23.80 ± 0.10
2449146.1096	4	306.58	218.74	23.81 ± 0.13
2449146.1769	4	306.60	218.73	23.88 ± 0.19
2449156.8860	4	306.60	218.79	24.04 ± 0.29
2449156.9499	4	306.64	218.79	23.91 ± 0.39
2449160.7658	4	306.50	218.92	24.56 ± 0.41
2449160.8304	4	306.49	218.90	24.01 ± 0.25
2449163.2450	4	306.53	218.90	24.09 ± 0.22
2449163.3054	4	306.42	218.94	24.24 ± 0.17
2449251.6130	1	337.51	206.54	24.16 ± 0.12
2449251.6748	1	337.46	206.51	24.31 ± 0.47
2449295.2633	1	111.45	371.43	24.33 ± 0.14
2449295.3195	1	111.45	371.39	24.12 ± 0.29
2449307.7036	1	41.51	379.89	24.49 ± 0.19
2449307.7661	1	41.46	379.93	24.39 ± 0.18
2449429.6016	3	326.09	239.58	24.65 ± 0.28

TABLE B1—*Continued*

C16 P=22.8

JD	CCD	x	y	V
2449049.0327	3	743.64	608.43	25.12 ± 0.27
2449049.0938	3	743.66	608.38	24.79 ± 0.29
2449057.4598	3	742.65	609.45	24.57 ± 0.17
2449064.0828	3	740.18	606.96	24.61 ± 0.17
2449064.1136	3	740.11	607.14	24.37 ± 0.17
2449069.2661	3	743.63	607.34	24.79 ± 0.25
2449069.3293	3	743.58	607.33	24.06 ± 0.13
2449131.6589	4	710.38	662.82	23.98 ± 0.10
2449131.7228	4	710.55	662.74	24.08 ± 0.14
2449141.6263	4	710.41	663.04	24.43 ± 0.16
2449141.6936	4	710.33	663.10	24.47 ± 0.19
2449146.1096	4	710.54	662.79	24.42 ± 0.15
2449146.1769	4	710.54	662.78	24.43 ± 0.54
2449156.8860	4	710.51	662.81	24.63 ± 0.17
2449156.9499	4	710.56	662.81	24.53 ± 0.14
2449160.7658	4	710.42	662.93	24.77 ± 0.18
2449160.8304	4	710.41	662.93	24.74 ± 0.23
2449163.2450	4	710.44	662.91	25.01 ± 0.29
2449163.3054	4	710.34	662.95	24.97 ± 0.22
2449251.6130	1	756.87	634.79	24.67 ± 0.18
2449251.6748	1	756.83	634.74	24.92 ± 0.25
2449429.6016	3	764.57	669.93	24.85 ± 0.30

C2 P=18.2

JD	CCD	x	y	V
2449049.0327	1	217.48	344.10	24.28 ± 0.24
2449049.0938	1	217.43	344.08	24.43 ± 0.25
2449057.4598	1	218.59	342.98	23.92 ± 0.08
2449064.0828	1	221.31	345.13	23.99 ± 0.13
2449064.1136	1	221.34	345.30	24.09 ± 0.25
2449069.2661	1	217.68	344.98	23.99 ± 0.35
2449069.3293	1	217.69	345.01	23.78 ± 0.10
2449131.6589	2	194.23	334.25	23.93 ± 0.13
2449131.7228	2	194.06	334.30	23.85 ± 0.09
2449141.6263	2	194.21	334.40	23.67 ± 0.09
2449141.6936	2	194.29	334.37	23.95 ± 0.19
2449146.1096	2	194.06	334.17	23.90 ± 0.19
2449146.1769	2	194.05	334.18	23.44 ± 0.45
2449156.8860	2	194.12	334.61	23.91 ± 0.10
2449156.9499	2	194.04	334.61	24.21 ± 0.17
2449160.7658	2	194.28	334.37	24.07 ± 0.12
2449160.8304	2	194.27	334.36	24.18 ± 0.13
2449163.2450	2	194.27	334.60	24.40 ± 0.20
2449163.3054	2	194.35	334.55	24.44 ± 0.24
2449251.6130	3	200.12	323.87	24.13 ± 0.10
2449251.6748	3	200.15	323.93	24.31 ± 0.13
2449295.2633	4	355.41	159.89	24.54 ± 0.51
2449295.3195	4	355.47	159.88	24.40 ± 0.31
2449307.7036	4	323.82	227.77	24.30 ± 0.16
2449307.7661	4	323.73	227.74	24.31 ± 0.08
2449429.6016	1	498.95	663.08	24.26 ± 0.44

C27 P=17.2

JD	CCD	x	y	V
2449049.0327	4	433.81	35.42	24.27 ± 0.20
2449049.0938	4	433.81	35.40	24.29 ± 0.25
2449057.4598	4	435.01	36.58	23.81 ± 0.31
2449064.0828	4	432.94	39.32	23.76 ± 0.25
2449064.1136	4	432.99	39.51	24.19 ± 0.22
2449069.2661	4	433.03	35.78	24.49 ± 0.36
2449069.3293	4	432.99	35.79	24.28 ± 0.19
2449131.6589	1	454.55	62.15	24.26 ± 0.14
2449131.7228	1	454.46	61.98	24.31 ± 0.17
2449141.6263	1	454.73	62.19	24.11 ± 0.17
2449141.6936	1	454.75	62.27	24.26 ± 0.24
2449146.1096	1	454.51	61.97	24.21 ± 0.17
2449146.1769	1	454.50	61.93	24.06 ± 0.12
2449156.9499	1	454.54	62.02	23.44 ± 0.06
2449160.7658	1	454.61	62.27	23.44 ± 0.10
2449160.8304	1	454.61	62.28	23.87 ± 0.13
2449163.2450	1	454.58	62.30	23.46 ± 0.16
2449163.3054	1	454.64	62.39	23.75 ± 0.15
2449251.6130	2	482.21	111.18	23.74 ± 0.13
2449295.3195	2	295.45	331.24	23.99 ± 0.11
2449307.7036	2	225.92	379.74	23.85 ± 0.15
2449307.7661	2	226.08	379.71	24.09 ± 0.21
2449429.6016	4	502.26	51.04	24.04 ± 0.34

C25 P=19.4

JD	CCD	x	y	V
2449049.0938	4	304.63	501.27	24.57 ± 0.18
2449057.4598	4	305.78	502.42	24.66 ± 0.11
2449064.0828	4	303.74	505.13	24.74 ± 0.15
2449064.1136	4	303.77	505.30	24.37 ± 0.27
2449069.2661	4	303.81	501.57	24.54 ± 0.16
2449069.3293	4	303.77	501.58	23.82 ± 0.09
2449131.6589	1	294.43	517.60	23.84 ± 0.09
2449131.7228	1	294.36	517.39	23.78 ± 0.17
2449141.6263	1	294.60	517.64	23.68 ± 0.50
2449141.6936	1	294.66	517.74	23.96 ± 0.11
2449146.1769	1	294.41	517.39	24.16 ± 0.10
2449156.8860	1	294.42	517.52	24.45 ± 0.20
2449160.7658	1	294.51	517.73	24.55 ± 0.26
2449160.8304	1	294.51	517.71	25.16 ± 0.29
2449163.2450	1	294.48	517.72	24.50 ± 0.23
2449163.3054	1	294.51	517.82	24.27 ± 0.27
2449251.6748	2	320.19	563.79	24.42 ± 0.17
2449295.3195	3	527.21	188.74	24.45 ± 0.17
2449307.7036	3	481.04	290.62	24.47 ± 0.19
2449307.7661	3	481.06	290.53	24.47 ± 0.14
2449429.6016	4	376.48	529.10	24.42 ± 0.13

C26 P=17.7

JD	CCD	x	y	V
2449049.0327	4	31.18	301.62	24.43 ± 0.16
2449049.0938	4	31.15	301.60	24.31 ± 0.40
2449057.4598	4	32.34	302.73	24.19 ± 0.12
2449064.0828	4	30.33	305.48	24.34 ± 0.19
2449064.1136	4	30.31	305.74	24.47 ± 0.17
2449069.2661	4	30.38	301.88	24.57 ± 0.22
2449069.3293	4	30.32	301.88	24.40 ± 0.16
2449131.6589	1	35.65	300.25	24.30 ± 0.15
2449131.7228	1	35.56	300.07	24.56 ± 0.19
2449141.6263	1	35.80	300.29	24.58 ± 0.19
2449146.1769	1	35.59	300.03	24.69 ± 0.18
2449156.8860	1	35.62	300.17	24.62 ± 0.18
2449156.9499	1	35.61	300.10	25.02 ± 0.23
2449160.7658	1	35.73	300.38	24.80 ± 0.19
2449160.8304	1	35.72	300.36	24.65 ± 0.17
2449163.2450	1	35.71	300.37	24.60 ± 0.10
2449163.3054	1	35.73	300.47	25.08 ± 0.30
2449251.6130	2	61.17	345.30	25.29 ± 0.43
2449251.6748	2	61.15	345.29	25.01 ± 0.21
2449295.2633	3	189.41	213.09	24.71 ± 0.20
2449295.3195	3	189.43	213.14	25.25 ± 0.43
2449307.7036	3	145.65	244.95	24.94 ± 0.66

C28 P=16.7

JD	CCD	x	y	V
2449049.0327	4	535.17	572.41	24.92 ± 0.29
2449049.0938	4	535.15	572.38	24.81 ± 0.19
2449064.1136	4	534.28	576.35	24.84 ± 0.22
2449069.2661	4	534.30	572.71	25.10 ± 0.27
2449069.3293	4	534.28	572.72	25.21 ± 0.30
2449131.6589	1	519.13	603.97	25.08 ± 0.21
2449131.7228	1	519.07	603.75	25.82 ± 0.39
2449141.6263	1	519.33	604.01	24.79 ± 0.33
2449141.6936	1	519.37	604.11	25.33 ± 0.26
2449146.1096	1	519.14	603.80	25.23 ± 0.19
2449156.9499	1	519.15	603.84	25.18 ± 0.25
2449163.2450	1	519.18	604.10	24.80 ± 0.20
2449163.3054	1	519.22	604.19	25.11 ± 0.21
2449251.6748	2	545.42	651.53	24.99 ± 0.20
2449295.2633	3	749.14	94.10	25.32 ± 0.33
2449429.6016	4	613.13	598.64	24.91 ± 0.17

TABLE B1—*Continued*

C3 P=16.7

JD	CCD	x	y	V
2449049.0327	1	355.75	461.29	24.83 ± 0.18
2449049.0938	1	355.67	461.26	24.86 ± 0.15
2449064.0828	1	359.52	462.26	24.58 ± 0.32
2449064.1136	1	359.54	462.48	25.23 ± 0.13
2449069.2661	1	355.90	462.17	25.13 ± 0.13
2449069.3293	1	355.92	462.19	25.43 ± 0.22
2449131.6589	2	327.69	457.49	25.20 ± 0.25
2449131.7228	2	327.53	457.54	25.18 ± 0.18
2449141.6263	2	327.67	457.64	25.03 ± 0.15
2449141.6936	2	327.75	457.62	24.95 ± 0.19
2449146.1096	2	327.53	457.43	25.23 ± 0.19
2449146.1769	2	327.54	457.45	25.39 ± 0.23
2449156.8860	2	327.58	457.83	24.36 ± 0.08
2449156.9499	2	327.52	457.83	24.29 ± 0.13
2449160.7658	2	327.73	457.61	23.99 ± 0.16
2449160.8304	2	327.73	457.59	24.19 ± 0.14
2449163.2450	2	327.72	457.83	24.36 ± 0.09
2449163.3054	2	327.81	457.78	24.43 ± 0.13
2449251.6130	3	340.12	439.43	24.40 ± 0.14
2449251.6748	3	340.14	439.49	24.21 ± 0.25
2449295.2633	4	536.74	157.30	24.82 ± 0.16
2449295.3195	4	536.82	157.29	24.41 ± 0.37
2449307.7036	4	502.07	262.39	24.55 ± 0.10
2449307.7661	4	501.99	262.37	24.51 ± 0.13

C4 P=14.3

JD	CCD	x	y	V
2449049.0327	1	426.18	135.88	24.55 ± 0.17
2449049.0938	1	426.16	135.89	24.64 ± 0.21
2449057.4598	1	427.30	134.79	24.76 ± 0.24
2449064.0828	1	430.00	136.98	24.48 ± 0.18
2449064.1136	1	429.98	137.08	24.60 ± 0.18
2449069.2661	1	426.43	136.85	25.82 ± 1.43
2449069.3293	1	426.44	136.86	24.56 ± 0.18
2449131.6589	2	411.80	134.92	25.17 ± 0.32
2449131.7228	2	411.62	134.95	24.73 ± 0.19
2449141.6263	2	411.79	135.07	25.08 ± 0.19
2449141.6936	2	411.89	135.00	25.19 ± 0.39
2449146.1096	2	411.67	134.81	25.02 ± 0.27
2449146.1769	2	411.63	134.81	24.69 ± 0.15
2449156.8860	2	411.68	135.28	24.26 ± 0.11
2449156.9499	2	411.62	135.26	24.55 ± 0.14
2449160.7658	2	411.89	135.07	24.59 ± 0.17
2449160.8304	2	411.86	135.03	24.09 ± 0.11
2449163.2450	2	411.85	135.29	24.22 ± 0.24
2449163.3054	2	411.93	135.23	24.23 ± 0.16
2449251.6130	3	406.20	112.74	24.53 ± 0.14
2449251.6748	3	406.24	112.77	24.40 ± 0.16
2449295.2633	3	192.00	383.84	24.51 ± 0.13
2449295.3195	3	192.01	383.86	24.27 ± 0.09
2449307.7036	3	113.08	412.63	24.40 ± 0.13
2449307.7661	3	113.10	412.55	24.25 ± 0.51

C18 P=13.0

JD	CCD	x	y	V
2449049.0327	3	77.90	120.12	25.53 ± 0.49
2449049.0938	3	77.93	120.10	25.46 ± 0.41
2449057.4598	3	76.96	121.06	25.72 ± 0.37
2449064.0828	3	74.54	118.69	25.55 ± 0.34
2449069.2661	3	77.95	118.92	25.73 ± 0.44
2449069.3293	3	77.95	118.89	24.80 ± 0.17
2449131.6589	4	69.72	141.68	25.60 ± 0.39
2449131.7228	4	69.91	141.60	25.15 ± 0.50
2449141.6263	4	69.75	141.88	25.66 ± 0.53
2449141.6936	4	69.65	141.95	25.13 ± 0.24
2449146.1096	4	69.82	141.63	24.76 ± 0.21
2449146.1769	4	69.83	141.62	24.79 ± 0.19
2449156.8860	4	69.84	141.68	24.49 ± 0.19
2449156.9499	4	69.89	141.67	24.70 ± 0.18
2449160.7658	4	69.75	141.81	24.49 ± 0.19
2449160.8304	4	69.74	141.77	24.78 ± 0.22
2449163.2450	4	69.79	141.79	25.03 ± 0.33
2449163.3054	4	69.67	141.83	25.01 ± 0.29
2449251.6130	1	98.50	138.39	24.68 ± 0.31
2449251.6748	1	98.45	138.36	25.41 ± 0.30
2449295.2633	2	131.45	47.34	24.95 ± 0.27
2449307.7661	2	123.80	68.10	25.28 ± 0.44
2449429.6016	3	80.07	174.09	25.60 ± 0.60

C17 P=16.5

JD	CCD	x	y	V
2449049.0327	3	387.27	265.40	24.81 ± 0.18
2449049.0938	3	387.29	265.37	25.30 ± 0.46
2449057.4598	3	386.30	266.38	24.89 ± 0.29
2449064.0828	3	383.86	263.96	24.97 ± 0.26
2449064.1136	3	383.86	264.27	24.67 ± 0.19
2449069.2661	3	387.29	264.25	24.24 ± 0.17
2449069.3293	3	387.28	264.23	24.35 ± 0.15
2449131.6589	4	371.55	302.35	24.41 ± 0.24
2449131.7228	4	371.73	302.27	24.40 ± 0.17
2449141.6263	4	371.58	302.56	23.89 ± 0.15
2449141.6936	4	371.49	302.62	24.08 ± 0.13
2449146.1096	4	371.67	302.31	24.13 ± 0.16
2449146.1769	4	371.68	302.29	24.14 ± 0.29
2449156.8860	4	371.68	302.35	24.25 ± 0.14
2449156.9499	4	371.73	302.34	24.72 ± 0.17
2449160.7658	4	371.58	302.47	24.75 ± 0.23
2449163.2450	4	371.61	302.46	24.53 ± 0.21
2449163.3054	4	371.50	302.50	24.49 ± 0.17
2449251.6130	1	405.52	287.54	24.87 ± 0.28
2449251.6748	1	405.48	287.50	24.39 ± 0.17
2449295.2633	1	93.68	475.91	24.50 ± 0.62
2449295.3195	1	93.69	475.88	24.68 ± 0.27
2449307.7036	2	465.05	49.33	25.15 ± 0.32
2449307.7661	2	464.93	49.38	24.96 ± 0.48
2449429.6016	3	397.17	320.97	24.54 ± 0.23

C29 P=14.0

JD	CCD	x	y	V
2449049.0327	4	61.29	181.50	24.70 ± 0.17
2449049.0938	4	61.27	181.47	24.95 ± 0.30
2449057.4598	4	62.47	182.61	25.16 ± 0.26
2449064.1136	4	60.44	185.63	25.36 ± 0.50
2449069.2661	4	60.51	181.78	25.36 ± 0.46
2449069.3293	4	60.45	181.78	25.00 ± 0.25
2449131.6589	1	73.76	182.60	25.80 ± 0.40
2449131.7228	1	73.67	182.42	25.29 ± 0.29
2449141.6936	1	73.98	182.73	25.73 ± 0.41
2449146.1096	1	73.73	182.41	25.27 ± 0.32
2449156.8860	1	73.73	182.52	25.30 ± 0.35
2449156.9499	1	73.72	182.45	25.90 ± 0.39
2449160.7658	1	73.84	182.72	23.27 ± 0.88
2449160.8304	1	73.83	182.71	25.18 ± 0.35
2449163.3054	1	73.85	182.82	24.76 ± 0.21
2449251.6748	2	99.74	228.35	24.68 ± 0.22
2449295.2633	3	134.80	102.18	24.43 ± 0.20
2449295.3195	3	134.83	102.23	24.25 ± 0.40
2449307.7661	3	115.07	125.03	25.12 ± 0.38
2449429.6016	4	124.00	205.96	24.93 ± 0.32

TABLE B2

I PHOTOMETRY

C1 P=58.5				
JD	CCD	x	y	I
2449161.1644	2	79.26	131.77	22.15 ± 0.04
2449161.2318	2	79.29	131.80	22.50 ± 0.07
2449404.6849	1	222.77	233.04	22.63 ± 0.09
2449429.5467	1	222.38	233.98	22.49 ± 0.07
2449434.5655	1	222.41	235.16	22.68 ± 0.13

C6 P=45.8				
JD	CCD	x	y	I
2449161.1644	3	177.36	274.66	22.85 ± 0.12
2449161.2318	3	177.37	274.60	22.66 ± 0.08
2449404.6849	2	201.73	255.44	23.03 ± 0.12
2449429.5467	2	201.91	256.05	22.90 ± 0.31
2449434.5655	2	202.41	256.05	22.35 ± 0.09
2449446.4370	2	201.34	256.84	22.34 ± 0.10

C19 P=43.0				
JD	CCD	x	y	I
2449161.2318	1	519.53	780.18	22.66 ± 0.18
2449404.6849	4	626.65	782.85	22.56 ± 0.10
2449429.5467	4	626.33	781.91	22.47 ± 0.08
2449434.5655	4	625.74	781.99	22.36 ± 0.15
2449446.4370	4	626.93	781.06	22.51 ± 0.18

C8 P=41.0				
JD	CCD	x	y	I
2449161.1644	3	281.89	214.47	23.06 ± 0.07
2449161.2318	3	281.89	214.43	22.79 ± 0.08
2449404.6849	2	305.15	188.46	22.75 ± 0.09
2449429.5467	2	305.33	189.06	22.77 ± 0.10
2449434.5655	2	305.83	189.06	23.24 ± 0.14
2449446.4370	2	304.75	189.84	23.13 ± 0.28

C10 P=37.6				
JD	CCD	x	y	I
2449161.1644	3	299.93	756.61	22.90 ± 0.08
2449161.2318	3	299.92	756.54	22.65 ± 0.09
2449404.6849	2	353.02	740.85	22.74 ± 0.10
2449434.5655	2	353.68	741.57	23.38 ± 0.16
2449446.4370	2	352.69	742.27	23.41 ± 0.14

C12 P=33.5				
JD	CCD	x	y	I
2449161.1644	4	346.77	238.06	22.95 ± 0.16
2449161.2318	4	346.74	238.11	22.95 ± 0.11
2449404.6849	3	364.69	254.90	22.52 ± 0.08
2449429.5467	3	365.02	254.38	22.73 ± 0.09
2449434.5655	3	365.02	253.83	22.79 ± 0.12
2449446.4370	3	365.90	254.92	22.84 ± 0.12

C22 P=27.3				
JD	CCD	x	y	I
2449161.1644	1	302.61	466.70	23.14 ± 0.08
2449161.2318	1	302.62	466.74	23.34 ± 0.15
2449404.6849	4	378.71	480.71	23.34 ± 0.16
2449429.5467	4	378.38	479.74	23.17 ± 0.11
2449434.5655	4	377.79	479.78	22.97 ± 0.12
2449446.4370	4	378.96	478.92	23.10 ± 0.11

C14 P=25.0				
JD	CCD	x	y	I
2449161.1644	4	621.94	453.59	23.22 ± 0.08
2449161.2318	4	621.94	453.59	23.12 ± 0.11
2449404.6849	3	658.48	459.35	23.38 ± 0.10
2449429.5467	3	658.84	458.83	23.23 ± 0.22
2449434.5655	3	658.87	458.33	23.48 ± 0.18
2449446.4370	3	659.72	459.34	23.76 ± 0.14

C24 P=23.5				
JD	CCD	x	y	I
2449161.1644	1	83.69	239.31	23.82 ± 0.16
2449161.2318	1	83.71	239.33	23.84 ± 0.15
2449404.6849	4	136.67	267.03	23.40 ± 0.15
2449429.5467	4	136.33	266.04	23.55 ± 0.16
2449434.5655	4	135.74	266.05	23.44 ± 0.16
2449446.4370	4	136.90	265.26	23.73 ± 0.11

C5 P=47.1				
JD	CCD	x	y	I
2449161.1644	3	709.64	236.20	22.55 ± 0.07
2449161.2318	3	709.57	236.23	22.74 ± 0.08
2449404.6849	2	744.09	186.87	23.27 ± 0.09
2449429.5467	2	744.27	187.46	23.21 ± 0.08
2449434.5655	2	744.79	187.48	22.45 ± 0.09
2449446.4370	2	743.68	188.19	22.36 ± 0.09

C7 P=43.0				
JD	CCD	x	y	I
2449161.1644	3	326.96	672.45	22.85 ± 0.10
2449161.2318	3	326.95	672.39	22.81 ± 0.13
2449404.6849	2	375.96	653.57	23.03 ± 0.13
2449429.5467	2	376.15	654.23	23.08 ± 0.13
2449434.5655	2	376.63	654.27	22.61 ± 0.10
2449446.4370	2	375.62	654.98	22.60 ± 0.09

C20 P=42.5				
JD	CCD	x	y	I
2449161.1644	1	151.00	203.13	23.10 ± 0.08
2449161.2318	1	151.02	203.15	23.27 ± 0.13
2449404.6849	4	202.14	224.56	22.93 ± 0.22
2449446.4370	4	202.36	222.78	22.94 ± 0.10

C9 P=38.0				
JD	CCD	x	y	I
2449161.1644	3	324.75	75.23	22.52 ± 0.12
2449161.2318	3	324.74	75.21	22.88 ± 0.08
2449404.6849	2	341.47	43.54	22.45 ± 0.06
2449429.5467	2	341.64	44.13	22.28 ± 0.07
2449434.5655	2	342.17	44.12	22.78 ± 0.12

C21 P=33.5				
JD	CCD	x	y	I
2449161.1644	1	274.95	724.68	23.25 ± 0.14
2449161.2318	1	274.98	724.74	23.25 ± 0.12
2449404.6849	4	372.08	746.42	23.01 ± 0.06
2449429.5467	4	371.76	745.48	22.90 ± 0.10
2449446.4370	4	372.37	744.64	22.48 ± 0.08

C13 P=32.0				
JD	CCD	x	y	I
2449161.1644	4	208.04	500.05	22.44 ± 0.08
2449161.2318	4	208.02	500.05	22.41 ± 0.12
2449404.6849	3	238.35	530.52	22.64 ± 0.08
2449429.5467	3	238.66	530.00	22.75 ± 0.09
2449434.5655	3	238.63	529.47	23.01 ± 0.14
2449446.4370	3	239.56	530.54	22.86 ± 0.11

C23 P=25.6				
JD	CCD	x	y	I
2449161.1644	1	180.56	506.42	23.40 ± 0.09
2449161.2318	1	180.59	506.47	24.28 ± 0.25
2449404.6849	4	257.58	531.31	24.15 ± 0.21
2449429.5467	4	257.24	530.34	23.37 ± 0.08
2449434.5655	4	256.64	530.38	23.22 ± 0.11
2449446.4370	4	257.84	529.53	23.23 ± 0.18

C11 P=23.7				
JD	CCD	x	y	I
2449161.1644	3	386.97	205.00	23.57 ± 0.13
2449161.2318	3	386.95	204.99	23.68 ± 0.13
2449404.6849	2	411.92	172.98	23.76 ± 0.10
2449429.5467	2	412.10	173.58	23.67 ± 0.19
2449434.5655	2	412.61	173.58	23.63 ± 0.37
2449446.4370	2	411.51	174.34	23.13 ± 0.08

C15 P=23.4				
JD	CCD	x	y	I
2449161.1644	4	309.39	221.28	22.67 ± 0.14
2449161.2318	4	309.36	221.33	22.77 ± 0.11
2449404.6849	3	325.70	240.17	22.90 ± 0.13
2449429.5467	3	326.02	239.65	23.55 ± 0.18
2449446.4370	3	326.90	240.19	23.40 ± 0.17

TABLE B2—*Continued*

JD	CCD	x	y	I
C16 P=22.8				
2449161.1644	4	712.91	664.97	23.41 ± 0.10
2449161.2318	4	712.92	664.93	23.46 ± 0.12
2449404.6849	3	763.93	670.31	23.69 ± 0.12
2449429.5467	3	764.31	669.78	23.74 ± 0.17
2449434.5655	3	764.33	669.32	23.85 ± 0.31
2449446.4370	3	765.19	670.28	23.78 ± 0.24
C2 P=18.2				
2449161.2318	2	191.36	332.06	23.33 ± 0.10
2449404.6849	1	499.34	661.91	23.17 ± 0.10
2449429.5467	1	498.96	662.90	23.33 ± 0.10
2449434.5655	1	498.96	664.06	23.27 ± 0.28
2449446.4370	1	497.36	661.49	23.34 ± 0.14
C27 P=17.2				
2449161.1644	1	456.79	59.58	23.61 ± 0.14
2449404.6849	4	502.53	52.28	23.70 ± 0.15
2449429.5467	4	502.19	51.25	23.49 ± 0.16
C3 P=16.7				
2449161.1644	2	324.70	455.19	23.63 ± 0.16
C4 P=14.3				
2449161.1644	2	408.77	132.88	23.45 ± 0.16
2449161.2318	2	408.80	132.86	23.90 ± 0.29
C18 P=13.0				
2449161.1644	4	72.87	144.25	24.21 ± 0.13
2449161.2318	4	72.82	144.32	24.19 ± 0.16
2449404.6849	3	79.82	174.71	24.46 ± 0.21
2449446.4370	3	81.01	174.76	24.63 ± 0.16
C25 P=19.4				
2449161.1644	1	296.86	514.60	23.14 ± 0.20
2449161.2318	1	296.88	514.64	22.92 ± 0.19
2449404.6849	4	376.83	530.05	23.02 ± 0.21
2449429.5467	4	376.50	529.09	23.57 ± 0.18
2449446.4370	4	377.08	528.27	23.11 ± 0.27
C26 P=17.7				
2449161.1644	1	38.32	297.40	23.55 ± 0.14
2449161.2318	1	38.35	297.43	24.12 ± 0.27
2449404.6849	4	95.29	329.99	23.78 ± 0.19
2449429.5467	4	94.96	329.01	23.66 ± 0.19
2449434.5655	4	94.35	329.02	23.92 ± 0.15
2449446.4370	4	95.54	328.22	24.01 ± 0.12
C28 P=16.7				
2449161.1644	1	521.35	600.94	23.61 ± 0.10
2449161.2318	1	521.36	600.98	23.74 ± 0.12
2449404.6849	4	613.36	599.57	23.42 ± 0.18
2449429.5467	4	613.04	598.60	23.47 ± 0.14
2449434.5655	4	612.46	598.66	23.57 ± 0.11
2449446.4370	4	613.62	597.76	23.75 ± 0.12
C17 P=16.5				
2449161.1644	4	374.40	304.77	23.85 ± 0.14
2449161.2318	4	374.38	304.81	23.78 ± 0.13
2449404.6849	3	396.74	321.52	23.39 ± 0.11
2449429.5467	3	397.07	321.00	23.48 ± 0.11
2449434.5655	3	397.08	320.46	24.33 ± 0.25
2449446.4370	3	397.95	321.53	23.99 ± 0.24
C29 P=14.0				
2449161.1644	1	76.39	179.85	24.46 ± 0.39
2449161.2318	1	76.41	179.87	23.97 ± 0.24
2449429.5467	4	124.13	206.09	25.01 ± 0.27
2449434.5655	4	123.54	206.08	24.92 ± 0.29
2449446.4370	4	124.69	205.31	24.87 ± 0.25

APPENDIX C

UNCLASSIFIED VARIABLE STARS

Several objects, which are not Cepheids, were found to be variable (from the cross-correlation of DoPHOT and ALLFRAME variable candidate lists). Further analysis of the light curves, and image blinking, convinced us of their variability. However, many of these objects did not have well-defined periods, or, even if potentially periodic, could not be easily classified as Cepheid variables or eclipsing variables. In addition to the analysis of their light curves, some had unusual $(V-I)$ colors (for Cepheids). This category is a melange of objects with unusual periods, light curves, and colors.

Table C1 lists the finder chart coordinates with mean V, I, and B magnitudes, when applicable.

TABLE C1

PROPERTIES OF UNCLASSIFIED VARIABLE STARS

CCD[a]	x^a	y^a	$\langle V\rangle$	σ_V	$\langle I\rangle$	σ_I	$\langle B\rangle$	σ_B
1.....	366.4	521.7	23.54	0.06	21.07	0.08	25.88	0.62
1.....	81.1	98.4	24.74	0.36	23.44	0.06	...	...
1.....	160.7	449.3	23.18[b]	0.54	20.88	0.15	25.15	0.24
1.....	430.6	790.5	24.51[c]	0.07	24.77	0.16	24.94	0.18
1.....	476.7	782.8	25.22[d]	0.11	26.00	0.33	26.10	0.37
2.....	54.8	267.1	23.68	0.03	21.75	0.04	26.70	0.71
2.....	252.7	300.0	23.59[e]	0.16	21.43	0.11	...	...
2.....	385.0	330.6	24.68	0.06	25.14	0.31	.....	
2.....	585.6	176.3	24.34[f]	0.04	23.85	0.14	...	...
3.....	251.6	200.8	24.40	0.04	23.22	0.02	26.49	0.61
4.....	301.5	494.5	24.18	0.04	24.03	0.05	...	...

[a] Positions applicable for epochs shown in finder charts.
[b] Low-level variable with many discrepant points, $P \approx 60$ days.
[c] $P \approx 15.8$ days, but extremely blue for Cepheid.
[d] $P \approx 15.4$ days, also extremely blue for Cepheid.
[e] Possible eclipsing binary.
[f] Too few observations to specify period, but definitely variable.

REFERENCES

Aaronson, M., Huchra, J., Mould, J. R., Schechter, P. L., & Tully, R. B. 1982, ApJ, 258, 64
Alves, D. R., & Cook, K. H. 1995, AJ, 110, 192
Bessell, M. S. 1991, A&A, 242, L17
Bohm-Vitense, E. 1994, AJ, 107, 673
Bottinelli, L., Gougenheim, L., Paturel, G., & de Vaucouleurs, G. 1985, A&AS, 59, 43
Burrows, C. J., et al. 1994, Wide Field and Planetary Camera 2 Instrumental Handbook, ed. C. J. Burrows (Baltimore: STScI)
Burstein, D., & Heiles, C. 1984, ApJS, 54, 33
Cardelli, J. A., Clayton, G. C., & Mathis, J. S. 1989, ApJ, 345, 245
Cohen, J. G. 1993, BAAS, 25, 818
Cook, K. H., Aaronson, M., & Illingworth, G. 1986, ApJ, 301, L45
de Vaucouleurs, G. 1975, in Galaxies and the Universe, ed. A. Sandage, M. Sandage, & J. Kristian (Chicago: Univ. Chicago)
de Vaucouleurs, G. 1993, ApJ, 415, 10
de Vaucouleurs, G., de Vaucouleurs, A., Corwin, H. G., & Bottinelli, L. 1991, Third Reference Catalog of Bright Galaxies (New York: Springer)
Eastman, R. G., Schmidt, B. P., & Kirshner, R. P., 1994, in preparation
Elmegreen, B. G., Elmegreen, D. M., & Montenegro, L. 1992, ApJS, 79, 37
Feast, M., & Walker, A. R. 1987, ARA&A, 25, 345
Ferrarese, L., et al. 1996, ApJ, in press
Fisher, J. R., & Tully, R. B. 1975, A&A, 44, 151
Freedman, W. L. 1988, ApJ, 326, 691
Freedman, W. L., et al. 1994a, ApJ, 427, 628
Freedman, W. L., et al. 1994b, Nature, 371, 757
Freedman, W. L., & Madore, B. F. 1990, ApJ, 365, 186
Freedman, W. L., Madore, B. F., Hawley, S. L., Horowitz, I. K., Mould, J. R., Navarrete, M., & Sallmen, S. 1992, ApJ, 396, 80
Freedman, W. L., Wilson, C. D., & Madore, B. F. 1991, ApJ, 372, 455
Fukugita, M., Hogan, C. J., & Peebles, P. J. E. 1993, Nature, 366, 309
Gascoigne, S. C. B. 1969, MNRAS, 146, 1
Gilliland, R. L. 1994, preprint
Gould, A. 1994, ApJ, 426, 542
Harris, H. C., Baum, W. A., Hunter, D. A., & Kreidl, T. J. 1991, AJ, 101, 677
Hill, R., et al. 1996, ApJ, in preparation
Holtzman, J. A., et al. 1995a, PASP, 107, 156
———. 1995b, PASP, 107, 1065
Hughes, S. M., et al. 1994, ApJ, 428, 143
Humphreys, R. M., Aaronson, M., Lebofsky, M., McAlary, C. W., Strom, S. E., & Capps, R. W. 1986, AJ, 91, 808
Jaakkola, T., & Le Denmat, G., 1976, MNRAS, 176, 307
Jacoby, G. H., et al. 1992, PASP, 104, 599
Kennicutt, R. C., Freedman, W. L., & Mould, J. R. 1995, AJ, 110, 1476
Lafler, J., & Kinman, T. D. 1965, ApJS, 11, 216
Lauer, T. R. 1989, PASP, 101, 445
MacKenty, J. W., et al. 1992, WF/PC Instrument Handbook (Baltimore: STScI)
Madore, B. F. 1985, in IAU Colloq. 82, Cepheids: Theory and Observations, ed. B. F. Madore (Cambridge: Cambridge Univ. Press), 166
Madore, B. F., & Freedman, W. L. 1991, PASP, 103, 933
Martin, W. L., Warren, P. R., & Feast, M. W. 1979, MNRAS, 188, 139
Mould, J. R., et al. 1995, ApJ, 449, 413
Phillips, A. C., Forbes, D. A., Bershady, M. A., Illingworth, G. D., & Koo, D. C. 1994, AJ, 107, 1904
Pierce, M. J. 1994, ApJ, 430, 53
Saha, A., & Hoessel, J. G. 1990, AJ, 99, 97
Saha, A., Labhardt, L., Schwengeler, H., Macchetto, F. D., Panagia, N., Sandage, A., & Tammann, G. A. 1994, ApJ, 425, 14
Sandage, A. R. 1983, AJ, 88, 1569
Sandage, A. R. 1993, ApJ, 402, 3
Sandage, A. R., & Tammann, G. A. 1974, ApJ, 194, 223
———. 1976, ApJ, 210, 7
Schechter, P. L., Mateo, M., & Saha, A. 1993, PASP, 105, 1342
Schmidt, B. P., Kirshner, R. P., & Eastman, R. G. 1992, ApJ, 395, 366
Schmidt, B. P., Kirshner, R. P., Eastman, R. G., Phillips, M. M., Suntzeff, N. B., Hamuy, M., Maza, J., & Aviles, R. 1994, ApJ, 432, 42
Shields, R., & Searle, L. 1978, ApJ, 222, 821
Scowen, P. A., Dufour, R. J., & Hester, J. J. 1992, AJ, 104, 93
Stellingwerf, R. F. 1978, ApJ, 224, 953
Stetson, P. B. 1987, PASP, 99, 101
———. 1990, PASP, 102, 932
———. 1994a, PASP, 106, 250
———. 1994b, private communication
———. 1994c, private communication
Welch, D. L., & Stetson, P. B. 1993, AJ, 105, 1813
Westerlund, B. E. 1990, A&A Rev., 2, 29
Zaritsky, D., Elston, R., & Hill, J. M. 1990, AJ, 99, 1108
Zaritsky, D., Kennicutt, R. C., & Huchra, J. F. 1994, ApJ, 420, 87